Central role of sphingolipids on the intracellular survival of *Neisseria gonorrhoeae* in epithelial cells

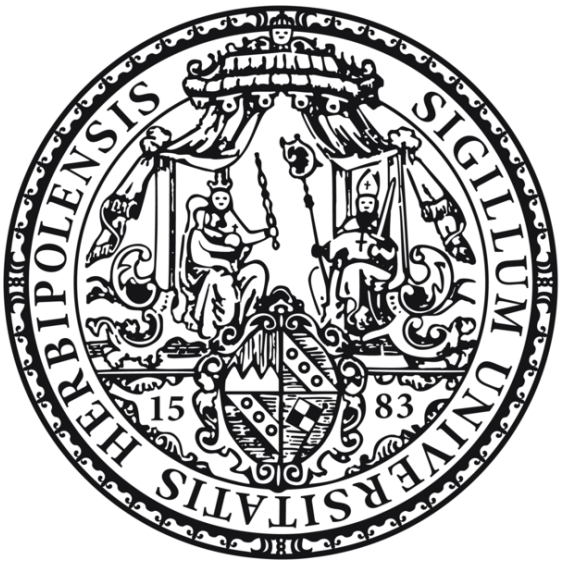

DISSERTATION

zur Erlangung des

naturwissenschaftlichen Doktorgrades

der Julius-Maximilians-Universität

vorgelegt von

Franziska Solger

aus Hof/Saale

Würzburg, 2021

Eingereicht am:

Mitglieder der Prüfungskommission

Vorsitzender:

Erstgutachter: Prof. Dr. Thomas Rudel

Zweitgutachter: Prof. Dr. Alexandra Schubert-Unkmeir

Tag des Promotionskolloquiums:

Doktorurkunde ausgehändigt am:

It`s hard to light a candle,

easy to curse the dark instead.

Nightwish

- Last Ride of the Day -

Table of contents

Table of contents

Table of contents

Abstract

Neisseria gonorrhoeae are Gram-negative bacteria with diplococcal shape. As an obligate human pathogen, it is the causative agent of gonorrhoea, a sexually transmitted disease. Gonococci colonize a variety of mucosal tissues, mainly the urogenital tract in men and women. Occasionally *N. gonorrhoeae* invades the bloodstream, leading to disseminated gonococcal infection. These bacteria possess a repertoire of virulence factors, which expression patterns can be adapted to the environmental conditions of the host. Through the accumulation of antibiotic resistances and in absence of vaccines, some neisserial strains have the potential to spread globally and represent a major public health threat. Therefore, it is necessary to understand the exact molecular mechanisms underlying the successful infection and progression of gonococci within their host. This deeper understanding of neisserial infection and survival mechanisms is needed for the development of new therapeutic agents.

In this work, the role of host-cell sphingolipids on the intracellular survival of *N. gonorrhoeae* was investigated. It was shown that different classes of sphingolipids strongly interact with invasive gonococci in epithelial cells. Therefore, novel and highly specific clickable sphingolipid analogues were applied to study these interactions with this pathogen. The formation of intra- and extracellular sphingosine vesicles, which were able to target gonococci, was observed. This direct interaction led to the uptake and incorporation of sphingosine into the neisserial membrane. Together with *in vitro* results, sphingosine was identified as a potential bactericidal reagent as part of the host cell defence. By using different classes of sphingolipids and their clickable analogues, essential structural features, which seem to trigger the bacterial uptake, were detected. Furthermore, effects of key enzymes of the sphingolipid signalling pathway were tested in a neutrophil infection model.

In conclusion, the combination of click chemistry and infection biology made it possible to shed some light on the dynamic interplay between cellular sphingosine and *N. gonorrhoeae*. Thereby, a possible “catch-and-kill” mechanism could have been observed.

Zusammenfassung

Neisseria gonorrhoeae ist ein Gram-negatives Bakterium, welches als Diplokokke vorkommt. Als ein ausschließliches Humanpathogen sind Neisserien der Erreger für die sexuell übertragbare Infektionskrankheit Gonorrhö. Gonokokken besiedeln eine Vielzahl von Schleimhäuten, jedoch hauptsächlich den Urogenitaltrakt bei Männern und Frauen. Gelegentlich kann *N. gonorrhoeae* in die Blutbahn invadieren, was zu einer disseminierten Infektion führen kann. Diese Bakterien verfügen über ein Repertoire an Virulenzfaktoren, deren Expressionskombination den Umgebungsbedingungen des Wirts angepasst werden können. Durch die Anhäufung von Antibiotikaresistenzen und durch das Fehlen eines Impfstoffes, besteht die Gefahr, dass spezielle Neisserienstämme sich weltweit verbreiten und daher eine ernstzunehmende Bedrohung des Menschen sind. Daher ist es notwendig die zugrundeliegenden molekularen Mechanismen der erfolgreichen Infektion und Ausbreitung der Gonokokken im Wirt genauestens zu verstehen. Das detaillierte Wissen über die Neisserieninfektion und Überlebensmechanismen ist nötig für die Entwicklung neuer Therapieansätze.

In dieser Arbeit wurde der Effekt von Sphingolipiden der Wirtszelle auf das intrazelluläre Überleben von *N. gonorrhoeae* untersucht. Es konnte gezeigt werden, dass unterschiedliche Klassen von Sphingolipiden stark mit invasiven Gonokokken in Epithelzellen interagieren. Um dies zu tun, wurden neue und hochspezifische clickbare Sphingolipidanaloge eingesetzt, um deren Interaktionen mit diesem Pathogen zu studieren. Die Formation von intra- als auch extrazellulären Sphingosinvesikeln, welche Gonokokken gezielt erreichten, konnte beobachtet werden. Diese direkte Interaktion führte zu einer Aufnahme und Einbau des Sphingosins in die Neisserienmembran. Zusammen mit *in vitro* Ergebnissen, konnte Sphingosin als potenzieller und antibakterieller Bestandteil des zellulären Abwehrsystems identifiziert werden. Weiterhin wurde durch die Verwendung unterschiedlicher Sphingolipidklassen und deren clickbaren Analoge wichtige Strukturen erkannt, die die bakterielle Aufnahme auslösen. Des Weiteren wurden die Auswirkungen von Schlüsselenzymen des Sphingolipidsignalwegs in einem Infektionsmodell mit Neutrophilen getestet.

Abschließend ist zu sagen, dass die Kombination aus Click Chemie und Infektionsbiologie es ermöglicht hat, die dynamischen Wechselwirkungen zwischen zellulären Sphingosin und *N.*

gonorrhoeae zu beleuchten. Dadurch konnte ein möglicher „catch-and-kill”-Mechanismus entdeckt werden.

1 Introduction

1.1 *Neisseria gonorrhoeae*

1.1.1 Genus *Neisseria* and pathogenesis of *N. gonorrhoeae*

The genus *Neisseria* belongs to the family of *Neisseriaceae* together with other genera such as *Kingella* and *Eikenella* (Adeolu and Gupta, 2013). All *Neisseria* (*N.*) species have in common that they are aerobic, Gram-negative, oxidase-positive β-proteobacteria and occur mostly as diplococci (Fig. 1.1) with the exceptions of *N. elongata*, *N. weaveri*, *N. bacilliformis* and *N. shayeganii* (Bennett et al., 2013). Until now, roughly 30 different *Neisseria* species have been identified, isolated from humans and animals (Humbert and Christodoulides, 2019). The phylogenetic relationship between these species is not clearly solved yet. Genomes of *Neisseria* are quite diverse due to the ability of horizontal gene transfer. The uptake of genetic material from different sources is enabled throughout the whole life cycle (Biswas et al., 1977). Most *Neisseria* are specialized to colonize a variety of mucosa surfaces in humans without causing any pathology. Therefore, these species are encountered as part of the normal microbiota. But two species are outstanding, the exclusively human pathogens *N. meningitidis* and *N. gonorrhoeae*. They show great similarities of their genomes but are specialized to different infection sites. The natural habitat for *N. meningitidis* is the nasopharynx and 10-15% of the general population carry this bacterium as commensal (Cartwright et al., 1987; Unemo et al., 2019). Occasionally, *N. meningitidis* invades the bloodstream and crosses the blood-brain-barrier to cause septicemia and/or meningitis (Coureuil et al., 2013). *N. gonorrhoeae* is the cause of the sexually transmitted infection (STI) gonorrhoea. This *Neisseria* specie can infect a variety of mucosal tissues, including endo-/ectocervix (Edwards et al., 2000), urethra, rectum, pharynx and conjunctiva (Britigan et al., 1985). The most common infection site is the urogenital

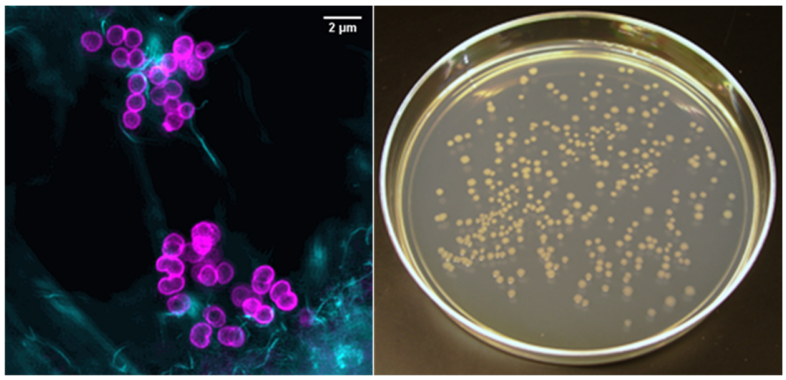

Figure 1.1 ***Neisseria gonorrhoeae.***
Super resolution microscopy picture of immunolabelled *N. gonorrhoeae* shows the typical diplococcal shape with an average size of 2 µm (left; magenta: *N. gonorrhoeae*, cyan: actin cytoskeleton). Single colonies grown on GC agar plate for approximately 24 hours (right).
The microscopy picture was taken by Dr. Tobias C. Kunz.

tract, resulting in urethritis in men and cervicitis in women. Especially in women, a large proportion shows asymptomatic infections which is hardly diagnosed in early stages. Therefore, complications of gonorrhoea are developed including pelvic inflammatory disease (PID), chronic pelvic pain, ectopic pregnancy and infertility (Quillin and Seifert, 2018). In both sexes as well as in adults and neonates (Unemo et al., 2019), the rare outcome of disseminated gonococcal infection (DGI) can occur when *N. gonorrhoeae* invades the bloodstream with serious consequences like endocarditis (Olayemi et al., 2017; Neto et al., 2021) and arthritis (Rice, 2005). Furthermore, infected women can suffer complications during pregnancy or transmit bacteria to their new-borns during birth causing ophthalmia neonatorum (neonatal conjunctivitis) (Morrow and Abbott, 1998). An infection with *N. gonorrhoeae* promotes the transmission and acquisition of other STIs, for example *Chlamydia* (*C.*) *trachomatis* (Leonard et al., 2019) and HIV (Jarvis and Chang, 2012).

1.1.2 Epidemiology, treatment opportunities and antibiotic crisis

Since there is no gonococcal vaccine available and as the second most frequent STI, gonorrhoea is a major public health threat globally with an estimated incidence rate of 86.9 million adults (15-49 years of age) per year (Rowley et al., 2019). But the prevalence differs strongly among certain populations and in geographical distribution, determined by sexual orientation, socioeconomics, demographics, education and medical care (Kirkcaldy et al., 2019). The only medical available "treatment" to this point is prevention, diagnosis and antibiotic therapy. In the last decades, individual countries noted a drastic increase in cases of infection with *N. gonorrhoeae* (ECDC, 2019; Kirkcaldy et al., 2019). Multifactorial reasons have been identified to cause this increase, including already known ones as mixing sexual partners, ethnical background or gender (Unemo et al., 2019). But also new factors have been observed to amplify the infection dynamics, for example increased number of sexual partners due to electronic connectivity or changes in sexual behaviour in the post-retroviral era (Kojima et al., 2016; Unemo et al., 2019). Moreover, *N. gonorrhoeae* has developed to a new superbug by acquiring antimicrobial resistance (AMR) to all recommended antibiotic treatments of gonorrhoea (Tapsall, 2009; Unemo and Shafer, 2014; Suay-García and Pérez-Gracia, 2018) (Fig. 1.1). Since gonococci are naturally competent for transformation throughout their whole life cycle, they can acquire chromosomally encoded AMR determinants leading to genetic mosaicism by horizontal gene transfer or homologous

recombination from commensal *Neisseria* species (spp.) or other bacteria (Wadsworth et al., 2018) besides the evolutionary occurring mutations. Most of the AMR are chromosomally, only the *tetM* (Morse et al., 1986) and *bla*$_{TEM}$ (Phillips, 1976) genes are known to be plasmid-encoded, resulting in high resistances against tetracycline and penicillin, respectively. Most of the accumulated AMR determinants do not impair the biological fitness of gonococci (Warner et al., 2008; Kunz et al.,

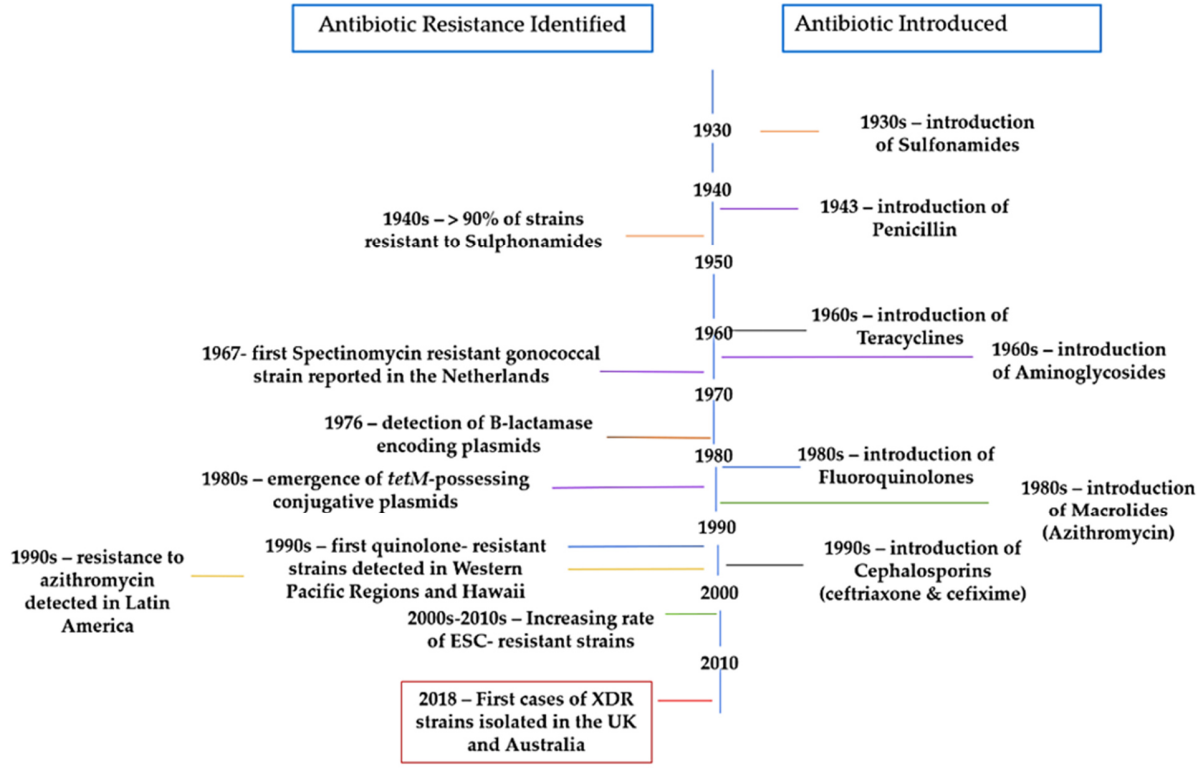

Figure 1.2 Timeline of recommended therapy for gonorrhea and acquired AMR in *N. gonorrhoeae*.
Timescale shows the introductions of antibiotic therapies and the first identification of resistance. Combination of therapy and respective resistance is indicated by the same color code (XDR: extreme drug resistant; modified according to Suay-García and Pérez-Gracia, 2018).

2012; Unemo and Shafer, 2014). Today`s suggested first-line treatment by the WHO is the dual therapy of ceftriaxone plus azithromycin. Gonococci show a decreased susceptibility towards azithromycin, which can be traced back to changes in the *m*ultiple *t*ransferable *r*esistance (*mtr*) efflux pump locus acquired by transformation (Rouquette-Loughlin et al., 2018; Wadsworth et al., 2018). In 2018 the first strain with high-level azithromycin and ceftriaxone resistance was identified (Eyre et al., 2018). Until now, more strains with this resistance combination have been isolated (Eyre et al., 2019; Jennison et al., 2019) with the potential to disseminate worldwide (Fig. 1.1). These findings of extremely drug resistant (XDR) and multi drug resistant (MDR) neisserial

strains clearly demonstrate the need for new antimicrobials (Jacobsson et al., 2020) or therapy approaches.

1.1.3 Virulence factors and $PorB_{IA}$-mediated invasion

For successful attachment and invasion into the host cell, *N. gonorrhoeae* expresses an arsenal of virulence factors, including type IV pili, opacity-associated (opa) proteins, lipooligosaccharides (LOS) and porin (PorB) (Fig. 1.3). As a mucosal colonizer the first step of infection is the adherence to the epithelial cell surface by type IV pili. Further functions of pili are twitching motility, DNA uptake by transformation, the involvement in phase and antigenic variation and the resistance to polymorphonuclear leukocyte (PMN)-mediated killing (Stohl et al., 2013). Especially the antigenic

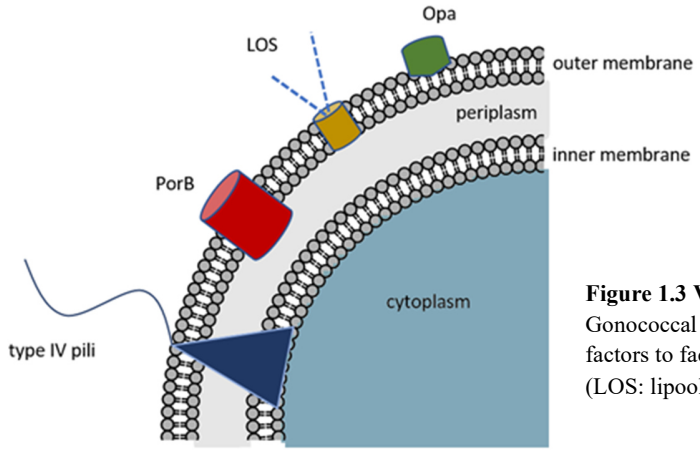

Figure 1.3 Virulence factors of *N. gonorrhoeae*.
Gonococcal cutout to depict surface structures as virulence factors to facilitate the attachment and invasion into the host cell (LOS: lipooligosaccharides, opa: opacity-associated).

variation of the pilus subunits is essential to avoid the recognition by the immune system of the host cell (Heckels, 1989). After the initial cell contact, pili are retracted to gain proximity between the gonococcus and its target. For closer interactions, the outer membrane Opa proteins bind to a variety of cell surface receptors, which can be found on different cell and tissue types. The most important receptor for Opa proteins is the carcinoembryonic antigen cell adhesion molecule (CEACAM) family (Dehio et al., 1998). The expression of up to 12 *opa* genes is phase-variable (Hauck and Meyer, 2003) and play an important role in the invasiveness of gonococci (Makino et al., 1991). The surface factor LOS facilitates the colonization as well but also promotes the invasion (Song et al., 2000). Furthermore through variation of LOS structures by length, carbohydrate content and sialylation, gonococci are resistant to human serum killing (Hill et al., 2016). The major outer membrane protein PorB can be divided into the two serotypes $PorB_{IA}$ and $PorB_{IB}$ (Sandstrom et al., 1982), being predominantly associated with DGI and local infections of the urogenital tract,

respectively (Cannon et al., 1983; Britigan et al., 1985). Besides the physiological function to supply with nutrients from the host cell, neisserial porins modulate the intracellular survival for example by interference with phagosome maturation (Mosleh et al., 1998; Hill et al., 2016). Also, $PorB_{IA}$ binds to the scavenger receptor expressed on endothelial cells (SREC-I) (Rechner et al., 2007) to promote invasion under low-phosphate conditions, which mimics the physiological conditions in human serum (van Putten et al., 1998; Kühlewein et al., 2006). This invasion mechanism is independent of Opa- and type IV pilus-expression (Faulstich et al., 2013). The $PorB_{IA}$-binding triggers the re-localization of SREC-I to plasma membrane microdomains, called membrane rafts. Such membrane rafts are highly dynamic platforms, which are often enriched with cholesterol and sphingolipids (Bieberich, 2018). The re-localization starts a signaling cascade with activation and recruitment of phosphoinositide 3-kinase (PI3K) and phospholipase Cγ1 (PLCγ1) to phosphorylate the integral membrane protein caveolin-1. Phosphorylated caveolin-1 leads to the recruitment of protein kinase D1 (PKD1), which gets phosphorylated and activates Rac-1, resulting in cytoskeletal rearrangements to take up gonococci (Faulstich et al., 2013). This process involves the turnover of sphingolipids, to be more precisely the turnover of sphingomyelin (SM) to ceramide (cer) through the enzymatic activity of the neutral sphingomyelinase (nSMase) (Faulstich et al., 2015). The sphingolipid metabolism is depicted in the following section.

1.2 Sphingolipids

1.2.1 Chemical structure and metabolism

As already mentioned above, sphingolipids are important components of lipid rafts, which serve as platforms for cell signaling (Simons and Ikonen, 1997) and entry points for different pathogens (Hanada, 2005). The structural blueprint of sphingolipids contains a hydrophobic sphingoid base (amino-alcohol) backbone (i.e. 2*S*,3*R*,4E-2-aminooctadec-4-ene-1,3-diol containing of 18 carbon atoms; normally sphingosine, sphinganine or phytosphingosine) with an amide-linkage to a fatty acid resulting in an *N*-acyl chain (Futerman and Hannun, 2004) (Fig. 1.4 A). These fatty acids can vary in chain length, degree of saturation and the number of bound hydroxyl groups to the α or ω carbon atom (Chen et al., 2010). The simplest sphingolipid is ceramide (cer), where additionally to the *N*-acyl chain the polar head group is functionalized further to a hydroxyl group at position C1 (Fig. 1.4 A).

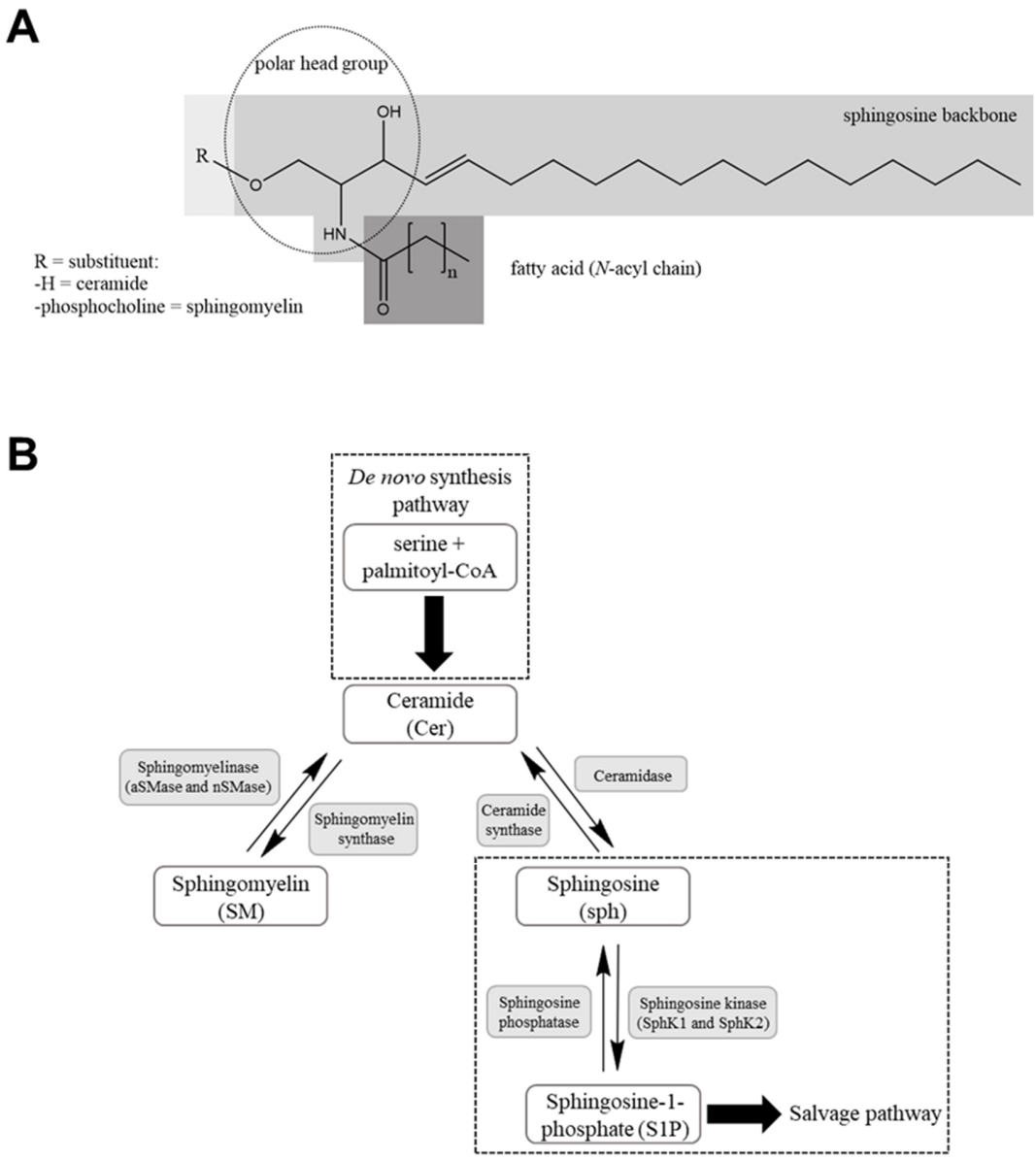

Figure 1.4 Chemical structure and metabolism of sphingolipids.
A) Universal structure of sphingolipids consisting of sphingoid backbone (here sphingosine), amide-linked fatty acid and polar head group. The polar head group can be further functionalized with an ester-linkage at the C1 atom (R). B) Simplified overview of the sphingolipid metabolism with the key lipids (white boxes) and enzymes (grey boxes).

This position can also be ester-linked to phosphate (sphingosine-1-phosphate: S1P) or phosphocholine (sphingomyelin: SM). In the cases of S1P and SM the sphingoid backbone is not amide-linked. Simpler sphingolipids can also be precursor molecules or breakdown products for more complex ones (Gault et al., 2010), catalyzed by the activity of multiple enzymes. This complexity of structural modifications and therefore also biological properties indicates the

heterogeneity of this lipid class. They are not only components of membranes but are also important bioactive molecules for a variety of cell processes. The major molecule for cell signalling is ceramide, which serves as a metabolic branch point (Pralhada Rao et al., 2013) (Fig. 1.4 B). Ceramide itself is involved in diverse signalling pathways including cell growth, differentiation, senescence and apoptosis (Bartke and Hannun, 2009). As indicated in the cut-out of the sphingolipid metabolism (Fig. 1.4 B), ceramide can be metabolized through different pathways: *de novo* synthesis starting with the condensation of the amino acid serine with palmitoyl-coenzyme A (CoA) through the enzymatic activity of serine palmitoyltransferase (SPT), hydrolysis of SM by the acid or neutral SMase (aSMase or nSMase) and through the salvage pathway. Besides ceramide, sphingosine-1-phosphate (S1P) was identified as a crucial regulator for proliferation (Olivera and Spiegel, 1993) and anti-apoptotic signalling (Cuvillier et al., 1996). S1P is an intermediate product of the salvage pathway and generated by the phosphorylation of sphingosine (sph) through one of two ATP-dependent sphingosine kinase isoenzymes, sphingosine kinase 1 and 2 (SphK1 and 2). Sphingosine is obtained through the hydrolysis of ceramide by ceramidase, which negatively regulates proliferation and promotes apoptosis (Cuvillier, 2002). The signalling of S1P counteracts the functions of ceramide and sphingosine, therefore the cellular fate is strictly determined by the balance of these sphingolipid levels (Spiegel and Milstien, 2003).

1.2.2 Sphingolipids in bacterial infections

Sphingolipids are not only crucial for the cellular signalling, but also important during the infection process of many bacteria. Most of the bacteria are not able to synthesize sphingolipids on their own but developed different mechanisms to utilize host cell sphingolipids to increase the virulence. Some classes of sphingolipids serve as membrane receptors for a variety of pathogens, for example *Escherichia coli*, *Pseudomonas aeruginosa* or *Bordetella pertussis* (Hanada, 2005). As mentioned above, lipid rafts can function as binding and entry platforms by the activation of sphingolipid signalling. Not only the $PorB_{IA}$-mediated invasion of *N. gonorrhoeae* (section 1.1.3) facilitates the sphingolipid signalling by activation of nSMase (Faulstich et al., 2015). It was also shown that aSMase is involved in the Opa-dependent invasion mechanism of gonococci (Grassmé et al., 1997; Hauck et al., 2000). The closely related pathogen *N. meningitidis* induces the activation of aSMase as well to increase ceramide levels on the host cell surface for internalization, either mediated by the binding of the meningococcal invasin Opc (Simonis et al., 2014) or type IV pili (Peters et al.,

2019). Bacteria do not only manipulate the sphingolipid signalling for their invasion but are also crucial for the intracellular survival. One example is the pathogenic genus *Chlamydia* which are obligate intracellular bacteria and therefore highly dependent on their host cell for nutrition supply. *Chlamydia* forms a membrane-bound vacuole (called inclusion) in which their unique biphasic development cycle occurs. The inclusion membrane of *C. trachomatis* is formed with host-derived SM (Hackstadt et al., 1995), which is essential for membrane inclusion stability and the reactivation after persistency (Robertson et al., 2009). Since SM appears to be crucial, *C. trachomatis* developed a mechanism to provide their supply of sphingolipids. Therefore, *Chlamydia* recruits host cell proteins of the sphingolipid metabolism to their inclusion, building its own SM biosynthetic factory (Elwell et al., 2011). These proteins are for example ceramide transfer protein (CERT), vesicle-associated membrane protein-associated protein A (VAP-A) and sphingomyelin synthases (SMS), which enables the conversion of ceramide to SM in close proximity to the inclusion. Another study using knockout cell lines showed that host cell SMS are not essential for the chlamydial proliferation in contrast to CERT and conclude that *C. trachomatis* developed an unrecognized host SMS-independent mechanism for the conversion of SM from ceramide (Tachida et al., 2020). Other *Chlamydia* species developed similar hijacking strategies (Wolf and Hackstadt, 2001; Koch-Edelmann et al., 2017; Banhart et al., 2019). These are only a few examples of pathogens using host-cell sphingolipids for their own benefit. On the other hand, host sphingolipids can also be part of the immune response upon infection.

1.2.3 Antimicrobial activity of sphingolipids

There is evidence that sphingolipid signaling regulates the trafficking and functioning of immune cells to the sites of infection and inflammation (Maceyka and Spiegel, 2014). An ambivalent function has aSMase and ceramide, which are used by bacteria for example to facilitate internalization but are also part of the inflammatory response (Li et al., 2019). However, antimicrobial effects of sphingoid bases have been tested on a variety of pathogenic organisms (Fischer, 2020). Sphinganine (dihydrosphingosine) and sphingosine were identified as potent antimicrobial agents against Gram-positive and -negative bacteria (Bibel et al., 1992; Fischer et al., 2012). In another study focusing on pathogenic *Neisseria*, additionally to sphingosine the toxic effect of short-chain C6 and the long-chain C16 ceramide as well as clickable ceramide analogs were determined (Becam et al., 2017). Not only sphingosine is taken up but also ceramides,

interestingly with a toxic effect only for the C6 ceramide. The level of toxicity of single sphingoid bases is highly specific for the species and depends also on the isomeric form of the sphingolipid (Bibel et al., 1992). How sphingoid bases efficiently kill bacteria is not elucidated yet, but in the case of sphingosine there is evidence for ultrastructural damage of the cell wall (Fischer et al., 2013) probably mediated by the binding to cardiolipin in the plasma membrane of bacteria (Verhaegh et al., 2020). All these studies were only conducted in a few bacterial species and since the specificity of sphingoid bases is well known, these experiments need to be extended to more organisms. Furthermore, methods have to be refined and developed to gain more details of this mechanism. One promising technique providing new insights into the interplay of host cell sphingolipids and bacteria is the application of click chemistry in infection biology (Götz et al., 2020; Solger et al., 2020; Peters et al., 2021).

1.3 Click chemistry

The term “click chemistry” was introduced in 2001, describing a toolbox of selective chemical reactions to join functional groups together (“click”) which must fulfil certain criteria (Kolb et al., 2001). The functional groups can be introduced on any synthetic molecule (for example dyes for visualization purposes) and are bioorthogonal, meaning these do not occur in nature and are therefore highly selective with low background signal. Another advantage is the rapid and quantitative labelling. Biomolecule labelling and clicking requires mild (neutral pH) and aqueous solvent conditions. The most common click reactions, which fit the mentioned criteria are copper-catalysed azide-alkyne click chemistry reaction (CuAAC), strain-promoted azide-alkyne click chemistry reaction (SPAAC) and inverse electron demand Diels-Alder ligation (IEDDA) (Fig. 1.5). As the name CuAAC already indicates, this Huisgen 1,3-dipolar cycloaddition is driven by Cu(I) ions to form a stable triazole conjugate from the small azido- and alkyne-group which are introduced on the substrates. The main drawback of this click reaction is the usage of copper, which is toxic for living cells. The biocompatibility can be restored by adding Cu(I) chelating ligands (Besanceney-Webler et al., 2011). An enhancement of this click reaction is SPAAC, a [3+2]-cycloaddition between an azide and a strained cyclooctyne instead of an terminal alkyne (Agard et al., 2004). The reaction between a cycloalkyne and azide is spontaneous and the instability of the cyclic alkynes increases with the ring size (Dommerholt et al., 2016). By using a cyclooctyne

derivate fast reactivity due to decreased activation energy and high stability in aqueous media is ensured, no metal catalyst is needed and therefore, this reaction can be easily applied in living systems. Cyclooctyne derivates have been developed differing in their kinetic and hydrophilic properties, with the most abundant cyclooctyne derivates being dibenzocyclooctyne (DIBO) and dibenzylcyclooctyne (DBCO). Besides the two azide-alkyne cycloaddition reactions, tetrazine ligation based on inverse electron demand Diels-Alder reactivity is emerging (Blackman et al., 2008). IEDDA describes the Diels–Alder [4+2]-cycloaddition between a diene (e.g. 1,2,4,5-tetrazines) and a dienophile (here alkene) forming a stable pyridazine product (Zeng et al., 2013). As SPAAC, this clicking reaction is highly selective and non-cytotoxic. The major advantage of IEDDA is superfast kinetics of all known click chemistry reactions, which is provided by large reactive groups (Oliveira et al., 2017). These groups could implicate cellular processes under certain circumstances and show increased hydrophobicity. To overcome these possible disadvantages, the development of smaller, hydrophilic and stable dienophiles is needed.

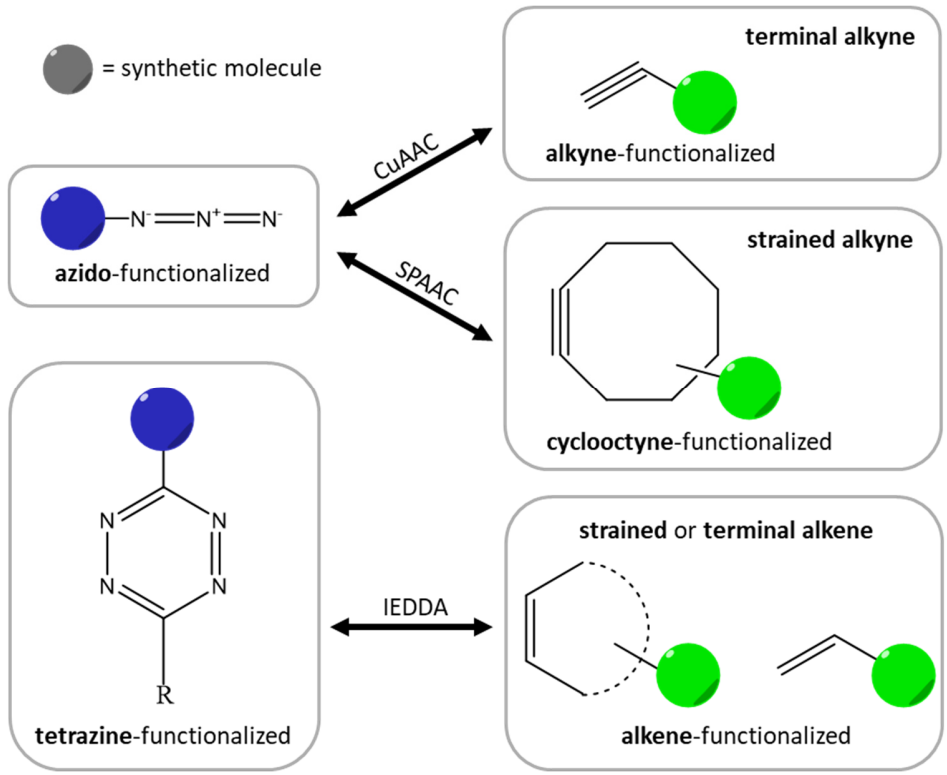

Figure 1.5 Most common click chemistry reactions for mild, aqueous conditions.
In general click chemistry reactions are categorized in copper (Cu(I))-catalysed (CuAAC) and copper-free (SPAAC and IEDDA). CuAAC and SPAAC have the cycloaddition of the functional groups azide and alkyne in common, whereas IEDDA is the ligation of a diene (tetrazine) with a dienophile (alkene).

As outlined above, bioorthogonal chemistry is a powerful tool for a variety of applications. All available reactions so far have their limitations, but the flexibility of this technique is striking and provides numerous possibilities of adjustment.

1.4 Aim of the study

Previous studies identified nSMase (Faulstich et al., 2015; Wu et al., 2018) and aSMase (Li et al., 2019) as key enzymes for bacteria to facilitate their internalization via ceramide-enriched platforms. In the case of *N. gonorrhoeae*, the $PorB_{IA}$-dependent invasion mechanism in epithelial cells is well established and triggers the activation of nSMase (Faulstich et al., 2015).

Further downstream sphingolipid signalling of the host cell and its effect on intracellular gonococci remains unclear. Therefore, this present study aims to elucidate the role of different host-cell derived sphingolipids on the intracellular survival of gonococci. By using click chemistry the interplay between these lipids and invasive bacteria was observed and examined.

2 Material and Methods

2.1 Materials

2.1.1 Bacterial strains

Neisserial phenotypes were checked by colony morphology. The strains used in this study are shown in Table 2.1.

Table 2.1 Neisserial strains used in this study. Arrowheads indicate 5′end (> or <) and 5′ to 3′ orientation (>) of genes.

Strain	Relevant phenotype	Genotype and orientation of gene in the PorB locus	Source
24871	$PorB_{IA}$, $Pili^-$, Opa^-	Clinical isolate	(Zeth et al., 2013)
FA1090	$PorB_{IB}$, $Pili^-$, Opa^-	Clinical serum-resistant, genital isolate from a patient with DGI	(Connell et al., 1988)
F3	$PorB_{IA}$, $Pili^+$, Opa^-	cat<$porB_{IA}$< >ermC	(Haas et al., 1987)
N924	$PorB_{IB}$, $Pili^-$, Opa^-	ΔPilE1/2, cat<$porB_{IA}$< >ermC	(Bauer, 1997)
N927	$PorB_{IA}$, $Pili^-$, Opa^-	ΔPilE1/2, cat<$porB_{IA}$< >ermC	(Bauer, 1997)
GFP-N927	$PorB_{IA}$, $Pili^-$, Opa^-, GFP	ΔPilE1/2, cat<$porB_{IA}$< >ermC pMKGFP	(Rechner et al., 2007)
RFP-N927	$PorB_{IA}$, $Pili^-$, Opa^-, RFP	ΔPilE1/2, cat<$porB_{IA}$< >ermC	V. Kozjak-Pavlovic
N931	$PorB_{IB}$, $Pili^-$, Opa^{50}	ΔPilE1/2, cat<$porB_{IB}$< >ermC pTH6a (opa_{50})	(Bauer, 1997)
VP1	$PorB_{IA}$, $Pili^-$, Opa^-	Clinical isolate	(Makino et al., 1991)

The chemo-competent *E. coli* strain DH5α was used for amplification of plasmids.

2.1.2 Cell lines and culture media

The cell lines used in this study are shown in Table 2.2 with the respective medium.

Table 2.2 Cell lines used in this study.

Cell line	Origin	Media	Source/Reference
Chang	Human conjunctiva epithelial cells	RPMI 1640, 10% FCS	ATCC CCL-20.2
Rab5-YFP Chang	Human conjunctiva epithelial cells	RPMI 1640, 10% FCS	E. Meier
Rab7-YFP Chang	Human conjunctiva epithelial cells	RPMI 1640, 10% FCS	E. Meier

LAMP1-YFP Chang	Human conjunctiva epithelial cells	RPMI 1640, 10% FCS	E. Meier
End1/E6E7	Human epithelial cervix cells	DMEM/F12, 10% FCS	(Fichorova et al., 1997)

The CRSPR/Cas9 knockout experiments were performed in Chang cells.

2.1.3 Plasmids

Plasmids used in this study are enlisted in Table 2.3.

Table 2.3 List of used plasmids

Plasmid	Properties	Source
pSpCas9(BB)-2A-GFP (PX458)	CRISPR/Cas9 plasmid Addgene plasmid 48138	(Ran et al., 2013)
SphK1-Cas9	CRISPR/Cas9 plasmid with insertion of gRNAs SphK1	This study
SphK2-Cas9	CRISPR/Cas9 plasmid with insertion of gRNAs SphK2	This study

2.1.4 Oligonucleotides

Oligonucleotides used in this study are shown the following Tables 2.4-2.6. All oligonucleotides were synthesized by Sigma-Aldrich.

Table 2.4 sgRNA sequences for CRISPR/Cas9 used in this study

Labeling	Sequence 5' to 3'
SphK1gRNAFOR	CACCGGGTTCAGCAGCACCAGCA
SphK1gRNAREV	AAACCGTGCTGGTGCTGCTGAAC
SphK2gRNAFOR	CACCGGGTAGGAGCCAAACTCGC
SphK2gRNAREV	AAACTGGCGAGTTTGGCTCCTAC

Table 2.5 Oligonucleotides for checking CRISPR/Cas9 deletions used in this study

Labeling	Sequence 5' to 3'
SphK1_Check_fwd	CAGCACCGATAAGGAGC
SphK1_Check_rev	AGACATGACCACCAGAGC
SphK2_Check_fwd	GCATCCTCAAGGTCTGC
SphK2_Check_rev	CTGTGTATCACTCCTAACG
U6-fwd	GAGGGCCTATTTCCCATGATTCC

Table 2.6 Primers for qRT-PCR used in this study

Labeling	Sequence 5' to 3'
SphK1_neuqRT_for	CATTATGCTGGCTATGAGCAG
SphK1_neuqRT_rev	ATCAGCAATGAAGCCCCAGG
SphK2_neuqRT_for	CATCCAGACAGAACGACAGAAC
SphK2_neuqRT_rev	CAGGCATCTTCACAGCTTCCTC
GAPDH-qRT for	GAAATCCCATCACCATCTTCCAGG
GAPDH-qRT rev	GAGCCCCAGCCTTCTCCATG

2.1.5 Antibodies

Primary and secondary antibodies are shown in Tables 2.7 and 2.8 with the dilution factor depending on the application.

Table 2.7 Primary antibodies with dilution factors for immunofluorescence (IF), structured illumination microscopy (SIM) and expansion microscopy (ExM)

Antibody	Origin	Dilution and application	Manufacturer
N. gonorrhoeae	polyclonal rabbit	1:200, IF 1:100, SIM 1:100, ExM	US Biological N0600-02
N. gonorrhoeae	monoclonal mouse IgG_1	1:100, SIM 1:100, ExM	Antibodies-online ABIN110874

Table 2.8 Secondary antibodies with dilution factors for immunofluorescence (IF), structured illumination microscopy (SIM) and expansion microscopy (ExM)

Antibody	Origin	Dilution and application	Manufacturer
anti-mouse Alexa555	goat	1:300, SIM 1:300, ExM	Thermo Scientific
anti-rabbit Alexa488	goat	1:300, SIM 1:300, ExM	Thermo Scientific
anti-rabbit Atto647	goat	1:300, SIM 1:300, ExM	Sigma-Aldrich
anti-rabbit Cy2™ conjugate	goat	1:100, IF 1:150, SIM	Dianova
anti-rabbit Cy5™ conjugate	goat	1:100, IF 1:150, SIM	Dianova

2.1.6 Clickable analogues and dyes

All clickable analogues, which were used in this study, are shown in Table 2.9. All analogues were synthesized at the organic chemistry department (AG Seibel) at University of Würzburg.

Dyes used for click chemistry experiments and for flow cytometry are shown in Tables 2.10 and 2.11, respectively.

Table 2.9 Clickable sphingolipid analogues

Analogue	Abbreviations	Modification	Properties
1-azido-sphingosine	1-N_3-Sph	Exchange of the hydroxyl group at C1 position with azido group	each dissolved in DMSO stocks 10 mM
ω-azido-sphingosine	ω-azido-sph, ω-N_3-Sph	Introduction of azido group at the alkene chain of the sphingosine backbone	
1-azido-sphinganine	1-N_3-Spg	Exchange of the hydroxyl group at C1 position with azido group	
ω-azido-sphinganine	ω-N_3-Spg	Introduction of azido group at the alkene chain of the sphinganine backbone	
1-azido-C6-ceramide	1-N_3-C6 cer	Exchange of the hydroxyl group at C1 position with azido group	
18-azido-C6-ceramide	18-N_3-C6 cer	Introduction of azido group at the alkene chain of the sphingosine backbone	
ω-azido-C6-ceramide	ω-N_3-C6 cer	Introduction of azido group at the ω-position of the fatty acid chain	
1-azido-C16-ceramide	1-N_3-C16 cer	Exchange of the hydroxyl group at C1 position with azido group	
18-azido-C16-ceramide	18-N_3-C16 cer	Introduction of azido group at the alkene chain of the sphingosine backbone	
α-azido-C16-ceramide	α-N_3-C16 cer	Introduction of azido group at the α-position of the fatty acid chain	
ω-azido-C16-ceramide	ω-N_3-C16 cer	Introduction of azido group at the ω-position of the fatty acid chain	

Table 2.10 Dyes used for staining the actin cytoskeleton and click chemistry experiments

Dye	Dilution factor or final concentration	Properties	Manufacturer
Alexa Fluor® (AF) 488-DBCO	5 µM final	dissolved in DMSO, stock 5 mM	Jena Bioscience
MFP™DY-555-Phalloidin	1:100, ExM 1:250, IF 1:150, SIM	dissolved in MeOH, 6 U/µl	MoBiTec
Alexa Fluor™ 647 Phalloidin	1:150, SIM		Invitrogen
DBCO-PEG$_4$-ATTO-425	5 µM final	dissolved in DMSO, stock 10 mM	Jena Bioscience
DyLight™ 650-4xPEG NHS Ester	0,48 µg final	dissolved in DMSO, stock 10 mg/ml	Thermo Scientific
Click-iT™ Alexa Fluor™ 488 DIBO Alkyne	5 µM final	dissolved in DMSO, stock 10 mM	Thermo Scientific
Click-iT™ Alexa Fluor™ 594 DIBO Alkyne	5 µM final	dissolved in DMSO, stock 10 mM	Thermo Scientific
Click-iT™ Alexa Fluor™ 647 DIBO Alkyne	5 µM final	dissolved in DMSO, stock 10 mM	Thermo Scientific
silicon-rhodamine (SiR)-lysosome	0.5 µM final		spirochrome

Table 2.11 Dyes used for flow cytometry

Dye	Dilution factor or final concentration	Manufacturer
7-aminoactinomycin D (7AAD)	1:100	BD Pharming
APC-Annexin V	1:100	BD Pharming
Propidium Iodide (PI)	1:100	Immunochemistry Technologies (ICT)

2.1.7 Kits

Kits used in this study are shown in Table 2.12.

Table 2.12 Commercial kits

Kit	Manufacturer
GeneJET™ Gel Extraction Kit	Fermentas
miRNeasy Micro Kit	Qiagen
NucleoSpin® Plasmid	Macherey Nagel
NucleoSpin® Tissue Mini Kit	Macherey Nagel
pGEM®-T and pGEM®-T Easy Vector Systems	Promega
PureYield™ Plasmid Midiprep System	Promega
RevertAid™ Premium First Strand cDNA Synthesis Kit	Fermentas
RNase-Free DNase Set	Qiagen

2.1.8 Buffers, solutions and media

All buffers and solutions used in this study are listed in Tables 2.13-2.15.

Table 2.13 Cell culture media and solutions

Medium/solution	Manufacturer/composition
DMEM/F12	Gibco
DPBS	Gibco
Fetal calf serum (FCS)	PAA, PAN-Biotech
Freezing medium	FCS, 10% DMSO (v/v)
Medium 199 (M199) Modified	Sigma-Aldrich
Opti-MEM®	Gibco
PVA	Sigma-Aldrich
RPMI 1640	Gibco
TrypLETM Express	Gibco

Table 2.14 Bacteria culture and infection media

Medium/solution	Manufacturer/composition
GC agar	36.23 g GC agar base in 1 l ddH_2O supplemented with 1% vitamin after autoclaving
Graver-Wade medium	according to (Wade and Graver, 2007): M199 modified cell culture medium in 1 l H_2O 37 mM glucose 17 mM ammonium bicarbonate 4.9 mM sodium acetate trihydrate

	3.4 mM L-glutamine 919 µM spermidine 383 µM L-arginine 245 µM hypoxanthin (dissolved in 1 M NaOH) 298 µM uracil (dissolved in 1 M NaOH) 252 µM oxaloacetate 99 µM thiamine hydrochloride 39 µM L-ornithine 10 µM nicotinamide adenine dinucleotide 13 mM sodium dl-lactate (2.5 ml of a 60% w/w syrup) in 500 ml ddH_2O adjusted to pH 6.8, sterile filtrated
HEPES medium **(phosphate-free infection medium)**	50 ml solution I 10 ml solution II 200 µl solution III 3 ml solution IV/V 5 ml solution VI 50 ml solution VII 50 ml solution VIII in 500 ml of distilled water pH adjusted to 7.3, sterile filtrated
HEPES solution I	0.1% (w/v) L-alanine 0.15% (w/v) L-arginine 0.0025% (w/v) L-asparagine 0.025% (w/v) glycine 0.018% (w/v) L-histidine 0.05% (w/v) L-lysine 0.015% (w/v) L-methionine 0.05% (w/v) proline 0.05% (w/v) L-serine 0.05% (w/v) L-threonine 0.061% (w/v) L-cysteine 0.036% (w/v) L-cystine 0.05% (w/v) L-glutamine 0.046% (w/v) GSH 0.0032 (w/v) hypoxanthine 0.008% (w/v) uracil 0.004% (w/v) D-biotin in 18% 1 N NaOH and 82 % ddH_2O adjusted to pH 7.2

HEPES solution II	37.5% (w/v) glucose
HEPES solution III	1% (w/v) $Fe(NO_3)_3$ x $9H_2O$
HEPES solution IV/V	0.33% (w/v) NAD 0.33% (w/v) cocarboxylase 0.33% (w/v) thiamine 0.33% (w/v) calcium pantothenate 0.188% (w/v) $CaCl_2$ x 2 H_2O 4.17% (w/v) sodium lactate 15.33% (w/v) glycerol 3.33% (w/v) oxaloacetate
HEPES solution VI	5% (w/v) $MgCl_2$ x 7 H_2O
HEPES solution VII	5% (w/v) NaCl 3.4% (w/v) sodium acetate
HEPES solution VIII	2.38% (w/v) Hepes
LB agar	10 g/l tryptone 5 g/l yeast extract 10 g/l NaCl 15 g/l agar
LB medium	10 g/l tryptone 5 g/l yeast extract 10 g/l NaCl
***Neisseria* growth medium (PPM+)**	1% vitamin mix 0.5% $NaHCO_3$ (8.4%) in PPM
Proteose Peptone medium (PPM)	15 g proteose peptone No. 5 5 g NaCl 0.5 g soluble starch 1 g KH_2PO_4 4 g K_2HPO_4 dissolved in 1 l dH_2O adjusted to pH 7.2, autoclaved
Stocking medium *E. coli*	50% glycerol 2.9% NaCl
Stocking medium *N. gonorrhoeae*	25% glycerol 75% PPM
Vitamin mix	combine vitamin mix solution I and II add dH_2O up to 2 l
Vitamin mix solution I	200 g D(+)-glucose 20 g L-glutamine 0.026 g 4-aminobenzoic acid

	0.2 g cocarboxylase 0.04 g iron(III)nitrate nonahydrate 0.006 g thiamine hydrochloride (vitamin B1) 0.5 g NAD 0.02 g vitamin B12 52 g L-cysteine hydro-chloride monohydrate add 1 l dH_2O
Vitamin mix solution II	2.2 g L-cystine 0.3 g L-arginine mono-hydrochloride 1 g uracil 0.06 g guanine-hydrochloride 2 g adenine-hemisulfate add 600 ml dH_2O 30 ml 32% HCl

Table 2.15 Buffers for IF, click chemistry and 4x ExM

Buffer	Composition
Blocking solution for IF	1x PBS 1% (w/v) bovine serum albumin (BSA)
Permeabilization solution	1x PBS 0.1% (v/v) Triton X-100
Mounting medium	35 g glycerol 12 g Mowiol 30 ml dH_2O 60 ml 0.2 M Tris/HCl pH 8.5
Clicking buffer	1 mM sodium ascorbate 5 µM clickable dye in Hepes medium
Monomer solution for ExM	8.625% sodium acrylate 2.5% acrylamide 0.15% N,N‘-methylenebisacrylamide 2 M NaCl and 1x PBS for polymerization 0.2% (w/v) APS and TEMED were added
Digestion buffer for ExM	50 mM Tris pH 8.0 1 mM ethylenediaminetetraacetic acid dipotassium salt dihydrate (EDTA) 0.5% Triton X-100 0.8 M guanidine HCl 8 U/ml protease K 1 mg/ml lysozyme

2.1.9 Chemicals and enzymes

All used chemicals, including antibiotics and enzymes, are shown in the Tables 2.16-2.18.

Table 2.16 Antibiotics used in this study

Antibiotic	Final concentration	Manufacturer
Ampicillin	10 µg/ml in dH_2O	Sigma-Aldrich
Gentamicin	150 µg/ml in Hepes medium	Sigma-Aldrich
Kanamycin	15 µg/ml	Roth
Penicillin	100 U/ml	Sigma-Aldrich
Streptomycin	100 µg/ml	Sigma-Aldrich

Table 2.17 Enzymes used in this study

Enzymes	Manufacturer
BbsI	Thermo Scientific
DNase I	Thermo Scientific
Lysozyme	Sigma-Aldrich
Protease K	Sigma-Aldrich
Restriction enzymes	Thermo Scientific, New England BioLabs
SphK1 (human)	Sigma-Aldrich
T4 DNA ligase	Fermentas
T4 DNA polymerase	Fermentas
Taq DNA polymerase	Genaxxon

Table 2.18 Chemicals used in this study

Chemicals	Manufacturer
Acrylamide	Sigma-Aldrich
Adenosine triphosphate (ATP)	Sigma-Aldrich
Albumin Fraktion V (BSA)	Roth
Ammonium bicarbonate	Sigma-Aldrich
Ammonium persulfate (APS)	Merck, Sigma-Aldrich
C6 ceramide	Avanti Polar Lipids
C16 ceramide	Avanti Polar Lipids
C16-d_{31}-sphingomyelin	Avanti Polar Lipids
Chloroform	Sigma-Aldrich
DAPI	Sigma-Aldrich
D-erythro-sphinganine	Avanti Polar Lipids
D-erythro-sphingosine	Santa Cruz
Dimethyl sulfoxide (DMSO)	Roth

Ethylenediaminetetraacetic acid dipotassium salt dihydrate (EDTA)	Sigma-Aldrich
Ficoll	VWR
GC Agar Base	Oxoid
GeneRuler™ 1 kb DNA ladder	Thermo Scientific
Glucose	Sigma-Aldrich
Glutaraldehyde (GA)	Sigma-Aldrich
Guanidine HCl	Sigma-Aldrich
HDGreen Plus	Intas
HEPES KOH pH 7.4	Sigma-Aldrich
Hypoxanthine	Sigma-Aldrich
Isopropyl-β-D-thiogalactopyranosid (IPTG)	Roth
K-acetate	Sigma-Aldrich
L-arginine	Sigma-Aldrich
L-glutamine	Sigma-Aldrich
L-ornithine monohydrochloride	Sigma-Aldrich
Lipofectamine™ 2000	Invitrogen
Loading dye 6x	Thermo Scientific
Mg-acetate	Sigma-Aldrich
N,N′-methylenbisacrylamide	Sigma-Aldrich
Nicotinamide adenine dinucleotide (NAD)	Sigma-Aldrich
Oxaloacetate	Sigma-Aldrich
Palmitic acid	Cortecnet
Paraformaldehyde (PFA)	Morphisto
PerfeCTa® SYBR® Green FastMix™, ROX	Quantabio
Poly-D-Lysine (PDL)	Merck
Saponin	Sigma-Aldrich
Sodium acetate trihydrate	Sigma-Aldrich
Sodium acrylate	Sigma-Aldrich
Sodium D-L-acetate	Sigma-Aldrich
(+)-Sodium L-ascorbate	Sigma-Aldrich
Soluble starch	Riedel-deHaen
Spermidine	Sigma-Aldrich
Sphingosine-d_7 (Sph-d_7)	Avanti Polar Lipids
Tetramethylethylenediamine (TEMED)	Fluka Analytica
Thiamine hydrochloride	Sigma-Aldrich
TRIzol™	Thermo Scientific
Trypan Blue solution	Thermo Scientific
Uracil	Sigma-Aldrich

Viromer Red	Biozym
X-Gal	Sigma-Aldrich

All other used chemicals were purchased from Roth, Sigma-Aldrich, Serva or Merck Chemicals if not stated otherwise.

2.1.10 Inhibitors

The used inhibitors with their respective target(s) are listed in Table 2.19.

Table 2.19 Inhibitors used in this study

Inhibitor	Target	Properties	Manufacturer
Amitriptyline	aSM	dissolved in H_2O, stock 10 mM	Sigma-Aldrich
GW4869	nSM	dissolved in DMSO, stock 4 mM	Sigma-Aldrich
5C	SphK1	dissolved in DMSO, stock 4 mM	Santa Cruz Biotechnology
K145	SphK2	dissolved in DMSO, stock 10 mM	Sigma-Aldrich
SKI-II	SphK1 and 2	dissolved in DMSO, stock 4 mM	abcam

2.1.11 Technical equipment

Technical equipment used in this study are shown in Table 2.20.

Table 2.20 Technical equipment

Equipment	Manufacturer
1260 Infinity high performance liquid chromatography (HPLC)	Agilent Technologies
6530 quadrupole-time-of-flight mass spectrometer (QTOF MS)	Agilent Technologies
Autoclave VX 150	Systec
Binocular SMZ-168	Motic
DMIL light microscope	Leica
electric balance ABS-80-4	Kern
electric balance EW 1500-2M	Kern
ELYRA S.1 SR-SIM	Zeiss
FACSAriaIII	BD
Hera Cell 240i incubator	Thermo Scientific
Hera Safe sterile bench	Thermo Scientific
Magnetic stirrer	Hartenstein
Megafuge 1.0R centrifuge	Heraeus
MiniStar microcentrifuge	VWR
Minitron Incubator Shaker	Infors HT
NanoDrop 1000 spectrophotometer	Peqlab Biotechnology
Operetta LCS™	Perkin Elmer
OptimaTM L-80-XP Ultracentrifuge	Beckman Coulter
pH-meter InoLab pH 720 with SenTix Electrode	WTW
Positive electrospray ionization (ESI+) mode	Agilent Technologies
See-saw rocker SSL4	Stuart
Spectrophotometer Ultrospec™ 3100 pro	Amersham Bioscience
Step One Plus RT PCR system	Applied Biosystems
TCS SP5 confocal microscope	Leica
TCS SPE confocal microscope	Leica
Thermal cycler 2720	Applied Biosystems
Thermo mixer comfort	Thermo Scientific
Vortex Genie 2	Bender & Hobein AG

2.1.12 Consumables and glassware

Consumables and glassware used in this study are listed in Table 2.21.

Table 2.21 Consumables and glassware used in this study

Equipment	Manufacturer
µ-Plate 24 Well Black	ibidi
µ-Slide 8 Well ibiTreat	ibidi
Centrifuge Tubes Falcon® (15 ml and 50 ml, polypropylene)	Corning
Cell culture flasks (25 cm^2 and 75 cm^2, polystyrene)	Corning
Cover glasses with one chamber (8,6 cm^2)	Merck
Cover glasses (round, 12 and 15 mm)	VWR
Cotton swabs (single sterile)	Hartenstein
CryoPure Tube (1.6 ml, polypropylene)	Sarstedt
Erlenmeyer flasks DURAN® narrow neck	Duran Group
Falcon® Polystyrene Test Tube (Cell Strainer Snap Cap, sterile)	Corning
Glass bottles Duran® graduated (1 l, 500 ml, 250 ml, 100 ml)	Duran Group
Inoculation loops (1 µl10 µl, sterile, polystyrene)	Sarstedt
Microtiter plates Costar® (6, 12, 24, 48 and 96 wells, cell culture grade, clear, TC-treated, sterile)	Corning
Pasteur pipettes (glass, length 230 mm)	Hartenstein
PCR SoftTubes (0.2 ml)	Biozym
Petri Dishes (92x16 mm, with cams, polystyrene)	Sarstedt
Pipette tips (20 µl, 200 µl and 1000 µl, transparent, polypropylene)	Sarstedt
Pipette tips (200 µl, yellow, polypropylene)	Sarstedt
RNase-free Microfuge tubes (1.5 ml, polypropylene, sterile)	Thermo
Semi-micro cuvette (1.6 ml, polystyrene)	Sarstedt
Serological Pipettes CELLSTAR® (1 ml, 5 ml, 10 ml and 25 ml, polystyrene)	Greiner Bio-One
Syringes BD Plastipak™ (1 ml, 5 ml and 10 ml, luer-lock, sterile)	Becton Dickinson
Syringe filter Filtropur (0.22 µm pore size, PES membrane, luer-lock, sterile)	Sarstedt
Vacuum Filter/Storage Bottle System (0.22 µm pore size, Cellulose acetate membrane, sterile)	Corning

2.1.13 Software

Software used for this study is listed in Table 2.22.

Table 2.22 Software

Software	Manufacturer
Argus X1 gel documentation software	Biostep GmbH
ChemDraw 20.0	Perkin Elmer
EndNote X9	Thomson Reuters
FACSDiva™	BD
Flowing 2	Perttu Terho (University of Turku)
Harmony® High Content Imaging and Analysis Software	Perkin Elmer
ImageJ	Wayne Rasband (NIH)
LabImage Chemostar	Intas
LAS AF confocal microscopy software	Leica microsystems
NCBI blast	http://blast.ncbi.nlm.nih.gov
ND-100 V3.7.1	NanoDrop Technologies, Inc. Wilmington
Office 365	Microsoft
Prism9	GraphPad
SnapGene Viewer 2.7.1	SnapGene
Fluorescence SpectraViewer	Online tool, Thermo Scientific
StepOne™ v2.3	Thermo Scientific
Windows 7, 10	Microsoft
ZEISS ZEN Imaging Software	Zeiss

2.2 Methods

2.2.1 Bacterial culture techniques

2.2.1.1 *E. coli*

Cultivation

E. coli were grown on LB agar plates or as liquid culture in LB medium at 190 rpm and 37°C overnight. For selection, transformed bacteria were grown on LB agar plates or in LB medium supplemented with the according antibiotic.

Transformation using heat-shock

An aliquot of 100 µl chemo-competent *E. coli* DH5α was thawed on ice. After thawing, 15 µl of the ligated vector were added to the competent bacteria and additionally incubated for 30 minutes on ice. *E. coli* were heat-shocked by incubation for 90 seconds at 42°C, immediately followed by an incubation step for 2 minutes on ice. Afterwards, 1 ml of LB medium was added and the suspension was incubated for 45 minutes at 37°C and 190 rpm. The transformed bacteria were plated on selective LB agar plates supplemented with the respective antibiotic and incubated overnight at 37 °C.

2.2.1.2 *N. gonorrhoeae*

Cultivation

N. gonorrhoeae strains were cultivated on gonococci (GC) agar plates supplemented with 1% vitamin mix at 37°C and 5% CO_2. After thawing *Neisseria* were streaked once more after 24 hours to select for Opa- and pili-negative colonies by using binocular microscopy. For liquid cultures, bacteria were collected approximately 16 hours after streaking.

Preparation liquid culture for infection and growth curves

All infections were done with bacteria grown in liquid cultures, which were performed in proteose peptone medium (PPM) supplemented with 1% vitamin mix and 0.5% sodium bicarbonate 8.4% solution (PPM+) at 37°C and 120 rpm by inoculation from GC agar plate. After growing for about 2.5 hours, the PPM+ medium was changed to phosphate-free Hepes medium by centrifugation with

4000 rpm for 5 minutes before infecting. To calculate the number of bacteria respective to the defined multiplicity of infection (MOI) for the different experimental set-ups, the optical density (OD) of this suspension was measured and aligned to a standardized neisserial growth curve.

Growth curve experiments were carried out by inoculating a liquid culture with a starting OD_{550nm} 0.15 and were grown until they reached OD_{550nm} 0.5-0.6. The preculture was then diluted to OD_{550nm} 0.1 and supplemented with the substances to be tested and DMSO as solvent control. In addition, a positive control with 15 µg/ml kanamycin was included to each growth curve experiment. Bacterial growth was measured every hour.

2.2.2 Cell culture methods

2.2.2.1 Cultivation

The used cell lines were cultured in their respective medium (see Table 2.2) supplemented with 10% fetal calf serum (FCS) at 37°C and 5% CO_2 in a humidified atmosphere. All cells were grown in cell culture flasks up to a confluency of about 80-90% before seeding or splitting. The detachment of the cells was performed by washing once with phosphate buffer saline (PBS) and adding trypsin for about 5 minutes at 37°C and 5% CO_2. To inactivate the detachment process, cells were resuspended in medium containing 10% FCS. Cells were cultured for 4-6 weeks.

2.2.2.2 Cryopreservation

Cells were cultured in 75 cm^2 flasks, washed with PBS and treated with trypsin for detaching the cells. After detachment, cells were resuspended in medium supplemented with 10% FCS and centrifuged at 800 g for 5 minutes. The supernatant was discarded and the cell pellet was resuspended in FCS supplemented with 10% DMSO. The suspension was transferred to cryovials and gradually frozen to -80°C. For long time storage, cells were kept in liquid nitrogen.

To thaw cryopreserved cells, the cryovial was incubated at 37°C in a water bath and the cells were resuspended in the respective pre-warmed cell culture medium. To remove residual DMSO, the cells were centrifuged at 800 g for 5 minutes, resuspended in medium and transferred into cell culture flask.

2.2.3 DNA methods

2.2.3.1 Plasmid isolation

Plasmids from *E. coli* were isolated with the NucleoSpin® Plasmid Kit or for larger amounts with the PureYield™ Plasmid Midiprep System according to manufacturers` protocol. The isolated plasmid DNA was eluted in sterile water, concentration measured and stored at -20°C.

2.2.3.2 Genomic DNA isolation

Genomic DNA from human cells was isolated with the NucleoSpin® Tissue Mini Kit according to manufacturer`s instructions. The DNA was eluted in sterile water. The quality and quantity of the isolated genomic DNA was assessed via NanoDrop spectrophotometer and stored at -20°C.

2.2.3.3 Polymerase chain reaction (PCR)

PCR was performed with Taq polymerase and $MgCl_2$-containing buffer E according to manufacturer´s protocol. The reaction was conducted with 200 µM of each dNTP (dATP, dTTP, dCTP and dGTP), 200 µM primer (forward and reverse) and 2.5 units (U) polymerase. The PCR started with an initial denaturation step at 94°C for 2 minutes, followed by 30 cycles of denaturation (94°C, 20 seconds), annealing (60°C, 30 seconds) and extension (72°C, 3 minutes 30 seconds). Final step was the extension at 72°C for 10 minutes. PCR products were stored at 4°C. The annealing temperature T_m (melting temperature) was determined with T_m Calculator (www.thermofisher.com/tmcalculator).

For analysis, the PCR products were mixed with 6x loading dye and separated via electrophoresis with a 1% agarose gel (1x TAE buffer) supplemented with 0.005% HD Green at 120 V for approximately 1 hour. The gel was visualized with UV light and if necessary, the PCR products were purified with the GeneJET™ Gel Extraction Kit for following experiments.

2.2.4 RNA methods

2.2.4.1 RNA isolation and DNA digestion

RNA was isolated from cells which were detached and lysed with TRIzol™ for 5 minutes at room temperature. To that suspension chloroform was added and centrifuged for 15 minutes with 12000g at 4°C. The aqueous phase was transferred and mixed with 100% EtOH for RNA precipitation. The

purification of the RNA was performed with the miRNeasy Micro Kit according to manufacturer´s instructions including the additional step for DNA digestion by using RNase-Free DNase Set. The quality and quantity of the isolated RNA was measured with UV-Vis spectrophotometer Nanodrop. RNA was stored at -20°C.

2.2.4.2 Reverse Transcription

The isolated RNA was used as template to generate complementary DNA (cDNA) with the RevertAid™ Premium First Strand cDNA Synthesis Kit. The reverse transcription was carried out by mixing 1000 ng RNA with random hexamer primers, 5x reaction buffer, RNase inhibitor, dNTPs and reverse transcriptase, followed by an incubation at 42°C for 1 hour. The reaction was stopped by heating up to 70°C for 5 minutes and cDNA was stored at -20°C.

2.2.4.3 Quantitative real-time PCR (qRT-PCR)

Quantitative real-time PCR (qRT-PCR) was performed on the Step One Plus RT PCR system. Therefore, the cDNA was diluted 1:10 and 5 µl were mixed with PerfeCTa® SYBR® Green FastMix™ and 100 nM qRT-primers (see Table 2.6) in a total reaction volume of 20 µl. The samples were done in technical triplicates. The reaction was performed with an initial holding stage at 95°C for 10 minutes followed by 40 cycles at 95 °C for 15 seconds and 60 °C for 1 minute. The expression levels of the gene-of-interest were normalized to them of the house-keeping gene GAPDH. The relative gene expression was analyzed according to the $2^{-\Delta\Delta C}{}_T$ method (Livak and Schmittgen, 2001).

2.2.5 CRISPR/Cas9

Vector DNA was digested with the restriction enzyme BbsI according to the manufacturer´s protocol with an increase of the incubation time to 3 hours. The success of the digestion was checked via agarose gel electrophoresis (see 2.2.3.3). The cut vector was purified with the GeneJET™ Gel Extraction Kit followed by ligation with annealed gRNAs as insert. Gene-specific sgRNAs were designed with the online tool CRISPOR (crispor.tefor.net) by PD Dr. Vera Kozjak-Pavlovic.

The sgRNAs (Table 2.4) were annealed by incubating 0.2 mM of each oligonucleotide with the annealing buffer (100 mM K-acetate, 30 mM HEPES KOH pH 7.4, 2 mM Mg-acetate) for 4 minutes at 94°C, followed by 10 minutes at 70°C. With the following formula the required masses of vector and insert were calculated: mass of insert (ng) = molar ratio vector/insert · mass of vector (ng) · ratio insert to vector length, with the used molar ratio vector/insert 1:4. The ligation was performed with T4 DNA ligase and 10x T4 DNA buffer at 16°C overnight.

The success of the transformation of the ligated plasmid in DH5α was tested by colony-PCR. Therefore, single clones were selected and put on fresh agar plates with the respective antibiotic for selection. Five single clones were lysed together at 95°C for 5 minutes followed by an incubation on ice and centrifugation for 1 minute at 12000g. The supernatant was used as a template for PCR and electrophoresis. The samples, which showed a DNA fragment with the right size, were chosen to test the single clones similarly. Positive single clones were put in liquid culture supplemented with antibiotics for plasmid isolation to check the right insertion of sgRNA by Sanger sequencing with primer U6-fwd (SeqLab, Göttingen).

Chang cells were transfected with Lipofectamine™ 2000 according to manufacturer´s protocol. Briefly, Chang cells with a low passage number were seeded into 12-well plates and grown to a confluency of about 70%. 1 µg pSp-Cas9(BB)-2A-GFP-sgRNA and Lipofectamine were mixed with OptiMEM and incubated 20 minutes at room temperature. During this incubation time, cells were washed with PBS and the cell culture medium was exchanged for OptiMEM. The transfection solution containing the plasmid was added dropwise to the well. Cells were incubated in a humidified atmosphere for 4-6 hours before the medium was exchanged for cell culture medium supplemented with antibiotics. After 36 more hours of incubation at 37°C and 5% CO_2, cells were detached, collected and GFP-positive cells were single sorted into 96-well plates. Single cell clones were grown for approximately 3 weeks for preparation of cryostocks and isolation of DNA. The DNA was used for subcloning with pGEM®-T and pGEM®-T Easy Vector Systems into DH5α. Positive *E. coli* were sequenced (SeqLab, Göttingen) to verify the alterations/deletions in the targeted gene sequence. Furthermore, the knockout approaches were checked for mRNA-expression levels of the respective gene by qRT-PCR.

2.2.6 Neutrophil isolation

Ficoll-Hypaque density gradient was used to isolate neutrophils from human venous blood. 10 ml heparinized blood was layered on 15 ml Ficoll-Paque and was centrifuged at 1000 rpm for 30 min at 20°C without brake. The upper layers were aspirated and the two lowest layers, containing granulocytes and red blood cells (RBCs), were mixed 3-4 times at a ratio 1:3 with 1% polyvinyl alcohol in 0.85% saline (PVA). The mixture was incubated for 45 minutes at room temperature. From that PVA gradient, the upper faint red layer was transferred in a new tube and centrifuged at 1000 rpm for 5 minutes with break. Residual RBCs were lysed by resolving the pellet in 16 ml H_2O and incubating for 30 seconds at room temperature. Immediately after this incubation, 4 ml 5x PBS were added and the neutrophils were collected by centrifugation at 1000 rpm for 5 minutes with break. The supernatant was discarded and the white neutrophil pellet was resuspended in 1x Hank's Balanced Salt Solution (HBSS) and stored at room temperature until use in further experiments. The vitality of the freshly isolated neutrophils was verified with Trypan blue staining.

2.2.7 Infection protocols

2.2.7.1 Gentamicin protection assay

Cells were seeded into 24-well plates and grown to a confluency of about 70%. Before infecting the cells, the medium wash changed to Hepes medium to provide phosphate-free conditions and the cells were incubated for about 20 minutes before inhibitor treatment with 5C, K145 or SKI-II for 2 hours. The inhibitors remained the whole infection time in the medium. Infection was performed at an MOI of 50 for 1 hour at 37°C and 5% CO_2 with solvent or inhibitor present. The infection was stopped by washing the cells three times with Hepes medium. The total quantity of adherent and invasive bacteria was assessed by lysing the cells with saponin for about 7 minutes. For Chang and End1/E6E7 cells different saponin concentrations showed the best lysis efficiency, 1% and 1.5% saponin respectively. The bacteria suspensions were serial diluted 10^{-1} to 10^{-3} and 25 µl of each dilution step was plated on a GC agar plate. The plates were incubated overnight and colony forming units (CFUs) were counted 24 hours after plating. To quantify exclusively intracellular *Neisseria*, the infection was followed by an incubation step with 150 µg/ml gentamicin for 2 hours, followed by saponin lysis as described earlier. The dilutions series had the range 10^{0} to 10^{-2}. All samples of the gentamicin protection assays were performed in technical triplicates.

2.2.7.2 Differential Immunofluorescence staining

To discriminate between intracellular and extracellular *Neisseria*, differential immunofluorescence staining was performed. The immunolabeling was analyzed either manually or by using an Operetta High-Content Imaging System for automated counting. Depending on the counting method, cells were seeded either on 12 mm^2 cover slips in 12-well plates or in µ-Plate 24 Well Black plates, respectively, and grown to a confluency of 70 – 80%. The immunolabeling procedure was the same for both methods. The infection with *Neisseria* with an MOI 10 was carried out as previously described (see gentamicin protection assay). To stop the infection, cells were washed three times with PBS. The samples were fixed by incubation with 4% paraformaldehyde (PFA) for 15 minutes in the dark at room temperature, followed by washing three times with PBS. Then they were subsequently blocked with 1% bovine serum albumin (BSA) in PBS for 45 minutes at room temperature. All following antibody immunolabeling steps were performed at room temperature and in the dark. The used antibodies and dyes for the whole differential immunofluorescence staining were diluted in 1% BSA in PBS. After blocking, the cells were incubated in a 1:200 dilution of the primary polyclonal rabbit anti-gonococcal antibody for 1 hour to detect the extracellular *Neisseria*. To remove residual primary antibody, the cells were washed twice with PBS and once with 1% BSA in PBS. Afterwards, the Cy5-conjugated secondary anti-rabbit antibody (1:100) was applied for 1 hour. The cells were washed again three times with PBS and permeabilized with 0.1% Triton-X in PBS for 15 minutes. After another washing step, the blocking with 1% BSA in PBS for 45 minutes was repeated. To immunolabel both extra- and intracellular bacteria the anti-gonococcal primary antibody (1:200) was applied a second time for 1 hour, followed by washing steps. The staining was completed by adding the Cy2-conjugated secondary anti-rabbit antibody (1:100) together with the dyes for actin cytoskeleton (Alexa Fluor® 555 Phalloidin, 1:100) and the DNA (DAPI, 1:3000) for 45 minutes. Finally, the wells were washed again three times. For manually counting the cover slips were embedded in mowiol mounting medium on object slides, dried overnight and analyzed by confocal microscopy (63x oil immersion objective) with a Leica TCS SPE. The samples for Operetta automated counting (20x objective, NA=0.45) were stored in 4% PFA at 4°C until they were measured and analyzed with Harmony Software. Samples for manually counting were performed as technical duplicates, the Operetta samples were done in technical triplicates.

Operetta was performed by Kerstin Paprotka and the members of the Core Facility Functional Genomics, University Würzburg.

2.2.7.3 Neutrophil survival assay

Each sample was prepared with $5x10^5$ freshly isolated neutrophils in RPMI (see 2.2.6). If required, inhibitors and DMSO as solvent control were directly applied before infection. Samples were infected with an MOI 100 and incubated at 37°C on a rotary shaker for the indicated infection time. The survival of neutrophils was measured via Annexin V-APC/7AAD staining for apoptosis and necrosis. The samples were analyzed via flow cytometry.

2.2.8 Flow Cytometry

2.2.8.1 Neutrophil survival assay

Neutrophils were pre-treated and infected as described in section 2.2.7.3. At the desired infection time samples were centrifuged for 5 minutes at 800xg and carefully resuspended in medium. $CaCl_2$, annexin V-APC and 7AAD were added and incubated for 10 minutes protected from light at room temperature. After this incubation, the samples were put on ice and analyzed by flow cytometry. The cell population was identified by adjustment of forward and sideward scatter (FSC-A and SSC-A). Doublet discrimination was performed via FSC-H vs. FSC-W and SSC-H vs. SSC-W gating strategy and fluorescence was measured using a 633 nm or 561nm laser for APC and 7AAD, respectively. The detection was performed with 660/20 nm or 610/20 nm band pass filters. 10,000 events were recorded for each sample. Uninfected cells served as negative control and unstained cells were used to determine autofluorescence. Gates were set accordingly.

2.2.8.2 Apoptosis analysis

Chang cells ($1x10^5$) were seeded and grown to 80 – 90% confluence in 12-well plates. Before the different treatments, either with inhibitors or clickable analogues, the medium was changed to phosphate-free Hepes. The inhibitor experiments were carried out by treating the cells with the indicated concentrations of inhibitors or DMSO as solvent control for 2 hours. For the click chemistry experiments cells were fed with the indicated concentrations of the sphingosine analogues and DMSO for 30 minutes, followed by exchanging the medium for fresh Hepes medium

for 1, 2 or 4 hours according to infection times. After the indicated incubation times, the cells were trypsinized, collected and centrifuged (800 g, 5 minutes at 4°C). The supernatant was discarded and the cell pellet was resuspended in 500 µl PBS. 1 µl propidium iodide (PI; 250 µg/ml) was added to the cell suspension and incubated for 10 minutes in the dark. The cells were put on ice and one sample was treated with 0.1% Triton-X as a negative control shortly before analyzing the cell viability by using flow cytometry as described in 2.2.8.1.

2.2.9 Click chemistry

The SPAAC reaction was performed to visualize the molecules of interest, which were modified with an unnatural azide group (clickable analogues) to provide the clicking reaction with an alkyne (cyclooctyne) dye. Because one copper-free click chemistry reaction was chosen, SPAAC could be performed for live cell imaging as well.

The synthesis of clickable analogues was performed by Julian Fink and Pauline Pfister of the organic and biological chemistry department (AG Seibel), University Würzburg.

The confocal microscope was operated by Dr. Tobias Kunz. Adjustments of the SP5 for live cell imaging were done by Dr. Kathrin Stelzner and Dr. Tobias Kunz.

2.2.9.1 Super-resolution microscopy

Cells were seeded on 15 mm^2 cover slips in 12-wells on the day before the experiment to reach a confluency of about 70% in the respective medium. Cells were washed and the medium was changed to phosphate-free Hepes medium. Cells were fed with functionalized analogue(s) or respective endogenous sphingolipid for 30 minutes at 37 °C and 5% CO_2. DMSO was used as solvent control. The applied final concentrations are listed in Table 2.9. For the inhibitor studies, cells were pre-treated with the SphK inhibitors (5 µM 5C, 2.5 µM K145 and 2.5 µM SKI-II) 30 minutes before sphingolipid feeding. To remove residual analogue from the media, cells were washed with pre-warmed Hepes medium after the indicated feeding time. Inhibitors were applied again and the cells were infected with an MOI of 30 for 4 hours. After the infection time, cells were washed three times to stop the infection. For the click reaction clicking buffer, containing 5 µM alkyne dye, was added to the cells and incubated 30 minutes in a humidified atmosphere at 37 °C. Alternatively, if the dye was not permeable, i.e. for example all used DBCO-dyes, the click reaction

was performed after fixation and permeabilization. Cells were fixed with 4% PFA for 30 minutes and afterwards permeabilized with 0.1% Triton-X in PBS for 15 minutes, followed by a blocking step with 1% BSA in PBS for 1 hour. All used antibodies for the immunolabeling were dissolved in 1% BSA in PBS. The primary antibody (1:100) for gonococcal detection was applied for 1 hour followed by brief washing with PBS. Together with the secondary antibody (1:300), the actin cytoskeleton was stained with Phalloidin (1:300) for 1 hour. The immunolabeling was completed by post-fixation with 4% PFA for 30 minutes. Samples were washed with PBS and the cover slips were embedded in mowiol mounting medium on object slides.

For imaging Zeiss ELYRA S.1 SR-SIM structured illumination platform (Plan-Apochromat 63x oil-immersion objective with a numerical aperture of 1.4) was used. The acquired super-resolution images were reconstructed with the ZEN image-processing platform with a SIM module. Z-stacks were processed using Fiji.

2.2.9.2 Expansion microscopy (ExM)

Before the actual expansion, Chang cells were treated as described in 2.2.9.1 until the embedding in mounting medium. Here, the click reaction was done with 488 DIBO Alkyne dye prior fixation. The expansion, gel preparation and microscopy were performed in cooperation with Dr. Tobias C. Kunz.

The expansion was performed according to Kunz *et al.* (Kunz et al., 2019). Briefly, cells were treated with 0.25% GA for 10 minutes at room temperature, followed by 3 washing steps. For gelation, the cover slips were put on monomer solution for 1 hour at room temperature followed by proteinase digestion. Afterwards, the samples were put in digestion buffer overnight. For the digestion of the neisserial membrane additionally 1 mg/ml lysozyme according to Lim *et al.* (Lim et al., 2019) had to be added for an efficient expansion. After digestion, the gels were expanded in hourly changed ddH_2O until the expansion saturated. With this method a 4x expansion of *Neisseria* was achieved, which was determined by the gel size of the digested and expanded samples. Gels were stored in ddH_2O at 4°C. For microscopy, gels were cut as precisely as possible to put in PDL-coated glass chambers. The super-resolution images and Z-stacks were obtained as previously described.

2.2.9.3 Live cell imaging

Wildtype (WT) and YFP-expressing Chang cells were seeded to µ-Slide 8 Well ibiTreat and grown to 70% confluency. To provide phosphate-free conditions, cell culture medium was changed to Hepes medium and cells were incubated for 20 minutes. Afterwards, Chang cells were fed with sphingosine analogue(s), endogenous sphingosine or DMSO as solvent control at the indicated concentrations for 30 minutes at 37°C and 5% CO_2. Following a brief washing with Hepes medium, the clicking buffer was applied and the previous incubation was repeated. The clicking buffer was removed and wells were washed with Hepes medium before infecting with fluorescent protein-expressing bacteria at an MOI of 20.

In cases of infecting YFP-expressing Chang cells, WT N927 were used and stained with NHS-ester dye. Concentration was used according to Eriksson *et al.* (Eriksson et al., 2015) but the incubation time was prolonged to 30 minutes at 37°C and shaking at 120 rpm. Bacteria were centrifuged for 1 minute at 14000xg and resuspended in Hepes medium for infection.

µ-slides were transferred to a pre-warmed live-cell incubation chamber at 37°C. Imaging was performed on confocal microscope Leica TCS SP5 (oil immersion objectives 40x Leica HC PL APO, NA=1.3 or 63x Leica HC PL APO, NA=1.3-0.6) at predefined time intervals. Adjustment and image acquisition were done with the LAS AF software (1024x1024 pixels, 8-bit mode). Z-stacks were imaged with a step size of 1 µm. Imaging was processed using Fiji.

2.2.10 Mass Spectrometry

The mass spectrometry experiments were performed and analyzed by Dr. Fabian Schumacher and Prof. Burkhard Kleuser at the Institute of Food Science, University of Potsdam.

2.2.10.1 In vitro metabolization

Both sphingosine analogues, ω-N_3- and 1-N_3-sphingosine, were separately tested for enzyme-driven phosphorylation by incubation of 10 µM analogue with 4 mM ATP and 10 U recombinant, human SphK1 in 40 mM HEPES-NaOH buffer (pH 7.4) for 1 h at 37 °C under gentle shaking. Lipids were extracted and analyzed with LC-HRMS as described in (Wigger et al., 2019). The chromatographic separations were performed with an Agilent 1260 Infinity HPLC coupled to an Agilent 6530 quadrupole-time-of-flight mass spectrometer (QTOF MS) via electrospray ion

sources operating in the positive ion mode (ESI+). The QTOF MS was operated in full scan mode, acquiring data in the mass-to-charge ratio (*m/z*) range of 100 - 750 with a scan rate of 2 spectra/s.

2.2.10.2 SphK inhibition assay and phosphorylation capability for ω-N_3-sphingosine

Chang cells were cultured in RPMI-1640 medium with 10% FBS and supplemented with 1% penicillin-streptomycin at 37 °C and 5% CO_2 in a humidified atmosphere. 2 x 10^6 cells were seeded in 10 cm cell culture dishes and grown to confluency of 70-80%. Cells were incubated for 1 h with the SphK inhibitors 5C, K145 or SKI-II in the two concentrations of 2.5 and 5 µM. DMSO solvent control was included. The treatments were performed in technical triplicates. Additionally, subsets of triplicates were treated with the clickable azido-sphingosine analogues 1-N_3-Sph and ω-N_3-Sph at a final concentration of 10 µM. Afterwards, the pre-stimulated cells were incubated with 100 µM palmitic acid (16,16,16-d_3) applied as a BSA complex. The addition of labeled palmitate was omitted for the cells treated with azido-sphingosine analogues. After incubation of 16 h at 37 °C, cells were washed with 5 ml PBS and subsequently harvested in 500 µl MeOH. Sphingolipids were extracted using 1.5 ml methanol/chloroform (2:1, v:v) as described in Gulbins *et al.* (Gulbins et al., 2018) with the extraction solvent contained sphingosine-d_7 (Sph-d_7) and C16-d_{31}-sphingomyelin (C16-d_{31} SM) as internal standards. The samples were analyzed via LC-ESI(+)-MS/MS by using 1260 Infinity HPLC coupled to a 6490 triple-quadrupole mass spectrometer as recently described (Naser et al., 2020). The following mass transitions were recorded (collision energies in parentheses, parent mass → fragment mass): *m/z* 303.3 → 285.3 for Sph-d_3 (8 eV), *m/z* 305.3 → 287.3 for dhSph-d_3 (12 eV), *m/z* 307.3 → 289.3 for Sph-d_7 (8 eV), *m/z* 325.3 → 307.3 for 1-N_3-Sph (8 eV), *m/z* 341.3 → 323.3 for ω-N_3-Sph (8 eV), *m/z* 405.3 → 264.3 for 1-N_3-S3P (16 eV), *m/z* 421.3 → 305.3 for ω-N_3-S1P (16 eV), *m/z* 731.6 → 184.1 for C18 SM (25 eV) and *m/z* 734.8 → 184.1 for C16-d_{31} SM (25 eV). The detected *de novo* formed deuterated long-chain sphingolipid levels were normalized to the C18 SM content of the lipid extract.

2.2.11 Statistical analysis

Statistical significance was calculated with unpaired Student *t* test with ****p<0.0001, ***p<0.001, **p<0.01, *p<0.05 using GraphPad Prism9.

For mass spectrometry data the statistically significant differences to the solvent control (DMSO) were determined using one-way ANOVA with Dunnett's multiple comparisons test with ****p<0,0001, ***p<0,001, **p<0,01, *p<0,05.

If not indicated otherwise, all experiments were performed for three biological replicates. All data show error bars with the mean ± standard deviation (SD).

3 Results

3.1 Inhibition of sphingolipid signalling and its effect on neisserial infection

3.1.1 Prolonged lifespan of neutrophils

Since neutrophils are professional phagocytes, pathogenic *Neisseria* spp. developed different mechanisms to avoid phagocytosis and to facilitate neutrophils for their own progression of infection. It appears that a sub-population of *N. gonorrhoeae* is able to survive inside neutrophils and inhibit apoptosis of these short-lived PMNs for potential transmission and replication (Chen and Seifert, 2011). The efficiency of neisserial uptake and survival inside neutrophils seems to be depending on the expression pattern of surface proteins, i.e. opa proteins, LOS and pili (Johnson et al., 2015; Palmer and Criss, 2018).

Therefore, freshly isolated neutrophils were infected with neisserial strains at MOI 100, expressing different combinations of the above-mentioned surface proteins/virulence factors (see Table 2.1, Fig. 3.1 A). The viability of neutrophils was measured in intervals of 24 hours. With the performed isolation method neutrophils are viable for approximately 8 hours, for the uninfected control a strong decrease of viable neutrophils is measured after 24 hours. All infected samples show a decrease as well, but not to the extent as the uninfected control. Even after 72 hours, about 50% of infected neutrophils are viable whereas all neutrophils of the uninfected control are degraded. Between the four different strains only small differences are detectable for the timepoints 24 and 48 hours. The piliated strain F3 showed, compared to the others, less viable neutrophils, in contrast N924 less decrease for 48 hours. The last time point at 72 hours did not show differences between the used strains. To see if sphingolipid metabolism is involved in neisserial infection and survival in neutrophils, PMNs were treated with inhibitors against SMases and SphKs before infection with N927. After 24 hours of infection the prolonged lifespan of neutrophils is detected in less apoptotic cells compared to the uninfected sample (Fig. 3.1 B) and in the percentage of viable neutrophils which is comparable to the rate of freshly isolated PMNs (Fig. 3.1 C). It appeared that none of the inhibitors seemed to affect the invasion and survival of gonococci since neither the rate of apoptosis nor viability changes compared to the untreated control. Only for the inhibitor K145 a slight but not significant increase for early apoptotic (Fig. 3.1 B) and a decrease of viable neutrophils (Fig. 3.1 C, grey bars) was detectable 24 hours post infection (hpi).

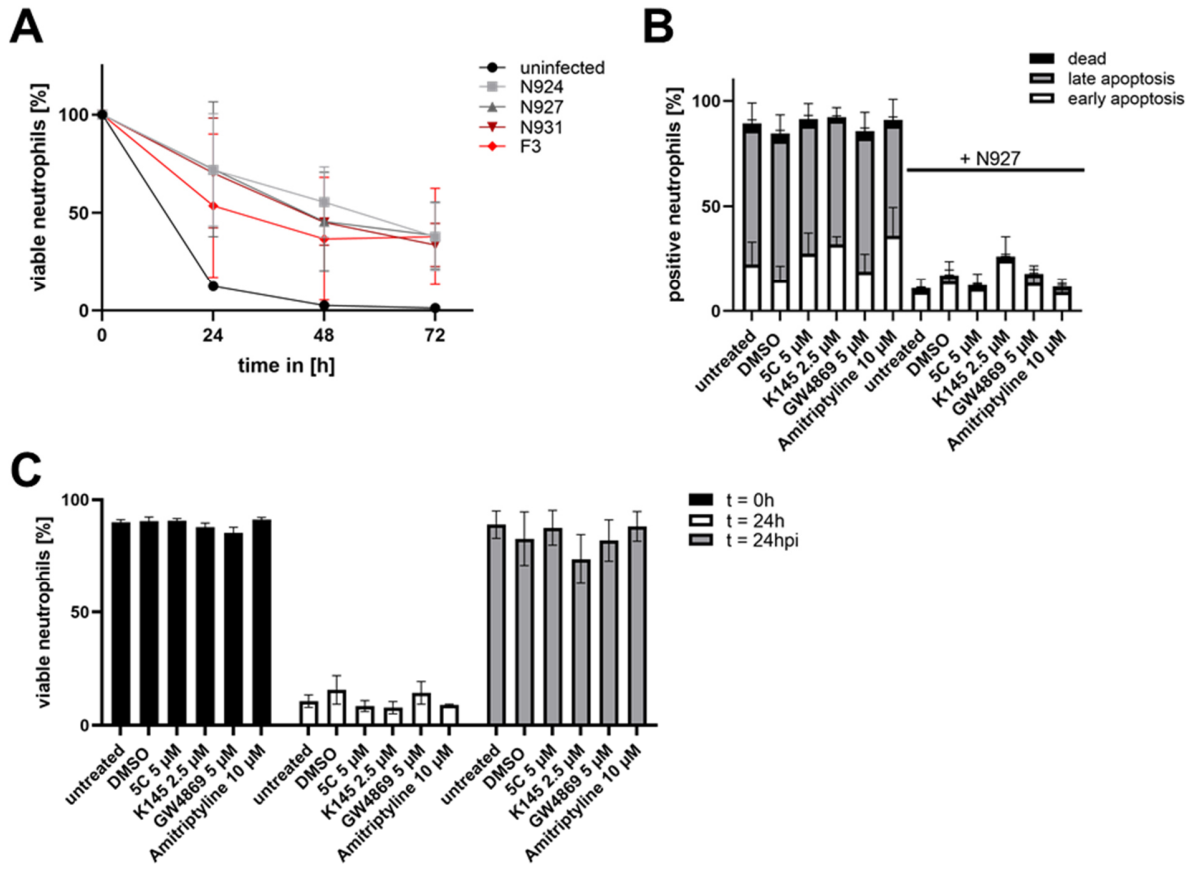

Figure 3.1 Neutrophil survival with *N. gonorrhoeae.*
Freshly isolated neutrophils were infected with *N. gonorrhoeae*. A) Different *Neisseria* strains are able to extend the viability of neutrophils up to 50% compared to the uninfected control for at least 72 hours after infection. B) Treatment with inhibitors and/or infection with N927 do not alter rates of apoptotic and necrotic neutrophils after 24 hours. C) Prolonged viability of neutrophils (infected with N927) is not changed due to the inhibition of SMases or SphKs 24hpi.

3.1.2 Knockout approaches for SphK1 and SphK2 using CRISPR/Cas9-system

As a versatile and precise method CRISPR/Cas9 was chosen to remove gene sequences of the enzymes SphK1 and SphK2 to investigate their role in neisserial infection and avoiding the usage of inhibitors which might have not-known off-target effects. After single-cell clones for ΔSphK1 and ΔSphK2 were cultivated, different clones were sequenced and checked for out-of-frame deletions in the respective gene. For further experiments, clone 5 ΔSphK1 and clone 9 ΔSphK2 were selected. The efficiency for the single-knockouts was determined by measuring the mRNA-levels of the respective gene compared to WT Chang cells by qRT-PCR (Fig. 3.2 A). For each knockout approach a significant decrease in expression level of the target gene is detected. For ΔSphK1 a reduction of about 50% compared to WT levels of SphK1-mRNA was measured, ΔSphK2 showed a less strong decrease of about 30%. Contrary, the quantification of the mRNA-levels showed approximately 1.5x increase of the alternative kinase, speaking for redundancy of SphKs. However, Gentamicin protection assay was performed with these CRISPR-Cas9-generated cell lines infected with the neisserial strain N927 under phosphate-free conditions (Fig. 3.2 B). The number of invasive and adherent *Neisseria* were normalized to the values of WT Chang cells. Reduced SphK1 did not change the adherence, but a reduction of about 50% invasive gonococci was revealed. For the SphK2-knockdown contrary effects were detected, meaning a significant reduction of adherent bacteria and a strong increase in invasion with an average of 150% compared to WT Chang cells.

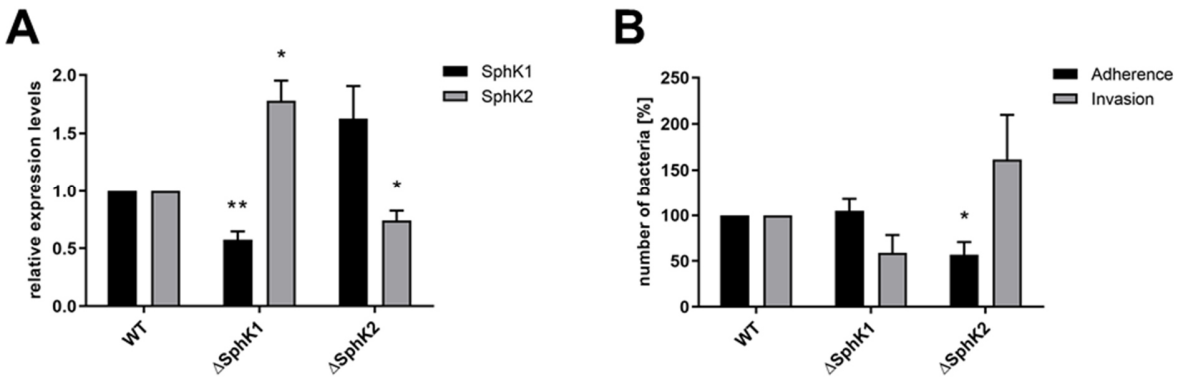

Figure 3.2 Knockout approaches for SphK1 and SphK2 in Chang cells
CRISPR/Cas9 was used to knockout the genes for SphK1 (ΔSphK1) and SphK2 (ΔSphK2). Clone 5 (ΔSphK1) and clone 9 (ΔSphK2) were chosen for further experiments. A) The success of these approaches was firstly determined by the mRNA-expression levels of the target genes compared to WT Chang cells. B) Adherence and invasion of N927 was measured in the new generated cell lines.
**p<0.01, *p<0.05

Taken together, the generated cell lines showed altered features compared to WT Chang cells, including much slower growth and altered morphology. Combined with the upregulation of the alternative kinase, it was decided to continue further experiments with chemical inhibition of SphKs in WT Chang cells.

3.1.3 Inhibition of SphKs and the implications on gonococcal infection

3.1.3.1 Survival defect of *Neisseria* in epithelial cells

It is known that the $PorB_{IA}$-dependent invasion of *N. gonorrhoeae* requires sphingolipid-rich membrane rafts of the host cell (Faulstich et al., 2015). This invasion mechanism is mediated by the interaction of $PorB_{IA}$ with SREC-I receptors, leading to an activation of nSMase. Through the activation of this enzyme, SM is broken down into phosphocholine and ceramide, causing major changes in the composition of these membrane rafts, i.e. accumulation of ceramide (Faulstich et al., 2015). Here, downstream signaling events on the neisserial infection process were investigated by the inhibition of SphKs. Therefore, to block the enzymatic activity of one or both sphingosine kinases, three specific inhibitors were chosen: 5C for SphK1 (Wong et al., 2009), K145 for SphK2

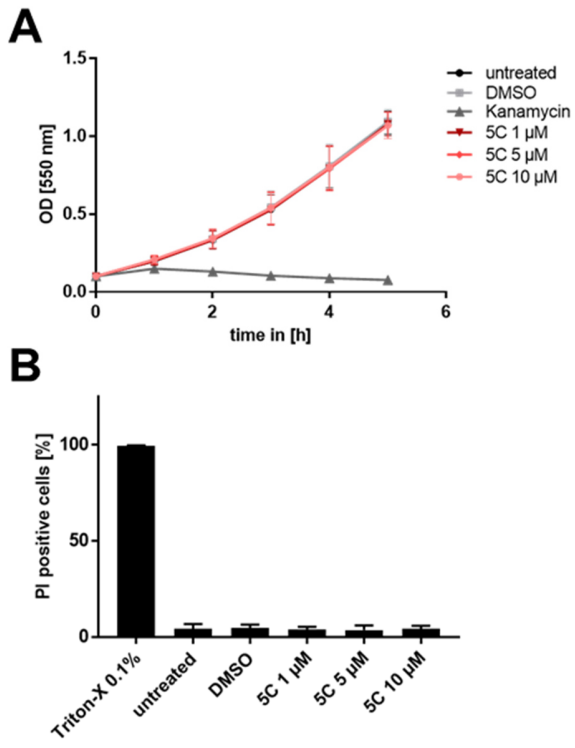

Figure 3.3 Effect of the SphK1-inhibitor 5C on N927 *in vitro* (A) and Chang cells (B).
A) Different concentrations of 5C were tested on the growth of N927 by measuring OD every hour. B) Chang cells were treated with different concentrations of 5C for 2 h. PI staining was used as marker for cytotoxic effects. The detergent Triton-X was used as positive and DMSO as solvent control. Further experiments were performed with the concentration of 5 µM.
With permission from Solger et al., 2020.

(Liu et al., 2013) and SKI-II for both SphKs (French et al., 2003). Two cell culture models were used for this study, Chang and End1 cells, infected with one of the $PorB_{IA}$-expressing strains N927 or the clinical isolate 24871 (see Table 2.1). To avoid cytotoxic effects of the inhibitors (Liu et al., 2013), different concentrations were tested on the cell culture models by apoptosis analysis and on the neisserial growth of the used strains as well to choose sub-toxic concentration for each chemical (Fig. 3.3-3.6). Liquid cultures of *Neisseria* were supplemented with the indicated concentrations of the different inhibitors or DMSO as solvent control and their growth was measured hourly (Fig. 3.3 A). Chang cells were treated with the indicated concentrations and incubated for 2 hours. Cytotoxicity was assessed by PI staining and apoptosis analysis to distinguish between dead and viable cells (Fig. 3.3 B). Triton-X was used as positive control. For 5C no toxic effects for bacteria and cells were observed, all further experiments were performed with 5 µM of this inhibitor. The SphK2-inhibitor K145 showed diverse effects on bacteria and epithelial cells, no toxicity of the used concentrations on the neisserial growth (Fig. 3.4 A) but slight dose-dependent cytotoxicity (Fig. 3.4 B). Therefore, the used concentrations for further experiments were 2.5 µM or 5 µM of K145. The tested concentrations of the SphK1/2-inhibitor SKI-II did not display any cytotoxicity in Chang cells (Fig. 3.5 B). In contrast, the growth of N927 was inhibited (Fig. 3.5 A).

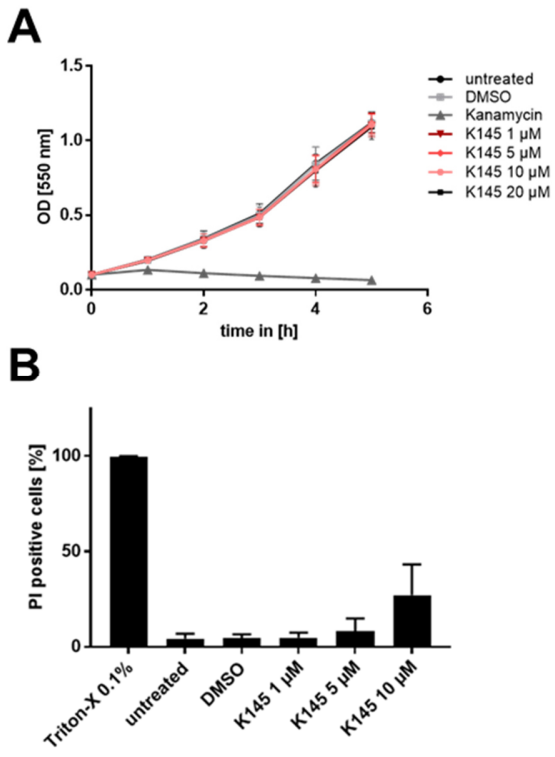

Figure 3.4 Effect of the SphK2-inhibitor K145 on N927 in vitro (A) and Chang cells (B).
A) Different concentrations of K145 were tested on the growth of N927 by measuring OD every hour. B) Chang cells were treated with different concentrations of K145 for 2 h. PI staining was used as marker for cytotoxic effects. The detergent Triton-X was used as positive and DMSO as solvent control. Further experiments were performed either with 2.5 µM or 5 µM.
With permission from Solger et al., 2020.

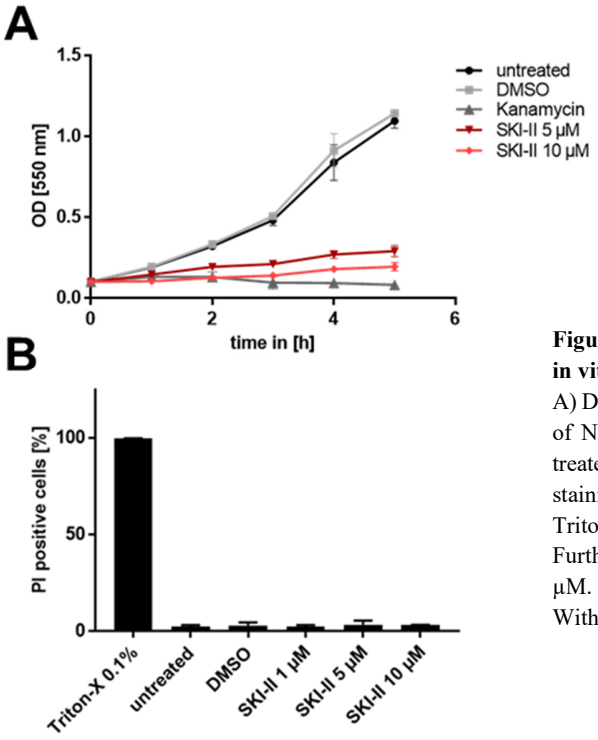

Figure 3.6 Effect of the SphK1/2-inhibitor SKI-II on N927 in vitro (A) and Chang cells (B).
A) Different concentrations of SKI-II were tested on the growth of N927 by measuring OD every hour. B) Chang cells were treated with different concentrations of SKI-II for 2 h. PI staining was used as marker for cytotoxic effects. The detergent Triton-X was used as positive and DMSO as solvent control. Further experiments were performed either with 2.5 µM or 5 µM.
With permission from Solger et al., 2020.

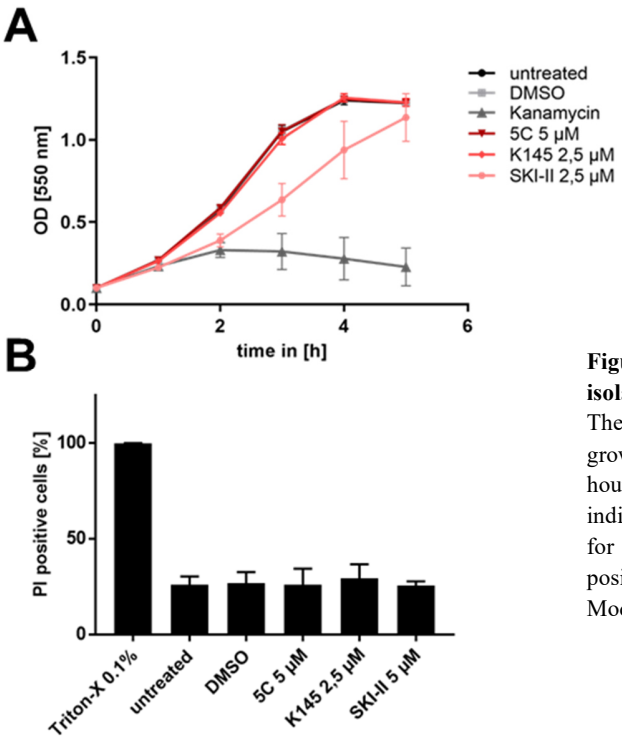

Figure 3.5 Effects of the SphK-inhibitors on the clinical isolate 24871 in vitro (A) and End1 cells (B).
The chosen concentrations of the inhibitors were tested on the growth of the clinical isolate 24871 by measuring OD every hour (A) and on End1 cells (B), which were treated with the indicated concentrations for 2 h. PI staining was used as marker for cytotoxic effects. The detergent Triton-X was used as positive and DMSO as solvent control.
Modified according to Solger et al., 2020.

Following experiments were performed with 5 µM of SKI-II, but were down scaled to 2.5 µM during progression of this study. These results were confirmed on the clinical isolate 24871 and End1 cells (Fig. 3.6).

To investigate the influence of SphKs on gonococcal infection, Chang and End1 cells were pretreated with the inhibitors or the solvent DMSO and infected with the respective strain (Fig. 3.7). These two cell lines are well-established infection models for *N. gonorrhoeae* and were chosen to mimic two infections sites, eye epithelium and endocervix, to gather a more global view. For both cell lines infected with N927 comparable numbers of adherent and invasive bacteria were detected (Fig. 3.7 A and B). The inhibition of SphKs did not affect the adherence, only the highest concentration of SKI-II (10 µM, Fig. 3.7 A) did significantly decrease the number of adherent *Neisseria*. This effect was most likely due to the toxicity of this inhibitor (Fig. 3.5 A). To avoid this, all further experiments were performed with 5 µM or 2.5 µM of SKI-II, which did not alter the ability to adhere compared to the untreated samples (Fig. 3.7 A and B).

In contrast, the number of invasive N927 was drastically reduced by all three inhibitors (Fig. 3.7 A and B). The SphK1-inhibitor 5C showed the weakest effect with a reduction of about 50% and 25% in Chang and End1 cells, respectively. In case of blocking SphK2-activity, either exclusively or in

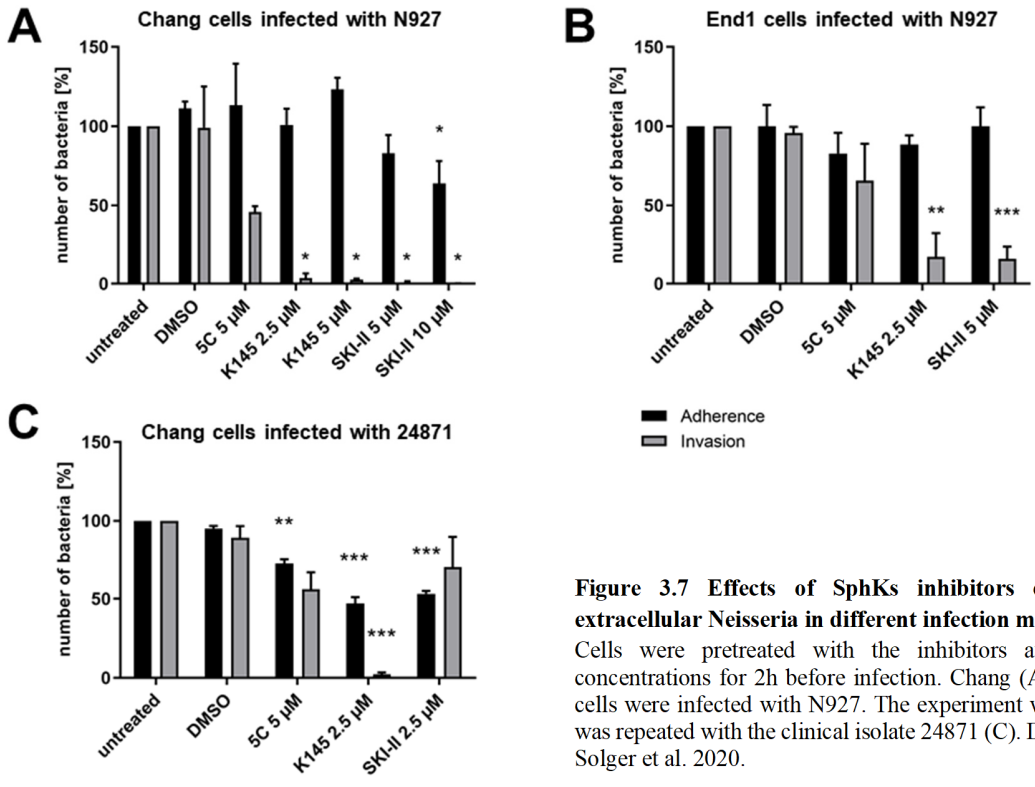

Figure 3.7 Effects of SphKs inhibitors on intra- and extracellular Neisseria in different infection models.
Cells were pretreated with the inhibitors at the indicated concentrations for 2h before infection. Chang (A) and End1 (B) cells were infected with N927. The experiment with Chang cells was repeated with the clinical isolate 24871 (C). Data published in Solger et al. 2020.

combination with kinase 1, significant reduction of invasive bacteria was detected in both infection models.

This assay was repeated with Chang cells infected with the clinical isolate 24871 (Fig. 3.7 C). In contrast to N927, all three inhibitors decreased adherence of 24871, but not to the same extent as for invasion. Similar patterns on invasive bacteria for the treatments with 5C and K145 were detected. Treatment with 2.5 µM SKI-II did not affect the number of intracellular gonococci. This result was confirmed by mass spectrometry, showing reduced effect of this concentration on sphingosine levels (Fig. 3.9). These results of different infection models with one laboratory strain and a clinical isolate strongly suggest a more prominent role of SphK2 for intracellular *N. gonorrhoeae* than SphK1.

This observation led to the question if the reduced number of invasive gonococci was mediated by an impairment of the invasion mechanism or of the intracellular survival. To address this, differential immunofluorescence staining of the Chang infection model with the laboratory strain N927 or the clinical isolate 24871 was performed to distinguish between extra- (adherent) and intracellular (invasive) bacteria (Fig. 3.8). The results for N927 infection were quantified by

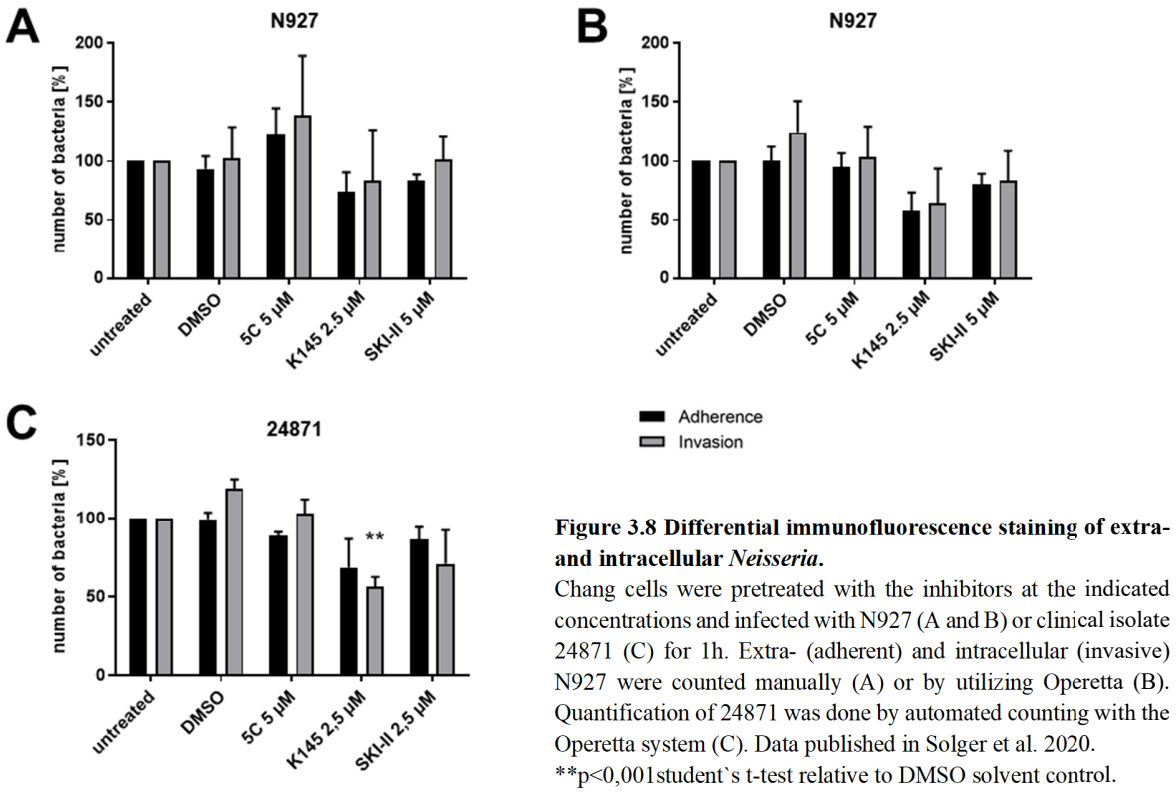

Figure 3.8 Differential immunofluorescence staining of extra- and intracellular *Neisseria*.
Chang cells were pretreated with the inhibitors at the indicated concentrations and infected with N927 (A and B) or clinical isolate 24871 (C) for 1h. Extra- (adherent) and intracellular (invasive) N927 were counted manually (A) or by utilizing Operetta (B). Quantification of 24871 was done by automated counting with the Operetta system (C). Data published in Solger et al. 2020.
**p<0,001student`s t-test relative to DMSO solvent control.

manual counting (Fig. 3.8 A) and using an automated fluorescence microscope (Operetta, Fig. 3.8 B). Since both quantification methods provided comparable results, further differential immunofluorescence staining of 24871 was automatically counted with the Operetta system (Fig. 3.8 C). Like the gentamicin protection assay (Fig. 3.7), number of adherent bacteria were not altered significantly. Contrary to the previous invasion results, numbers of intracellular gonococci were not reduced upon SphK inhibition (Fig. 3.8).

Taken together, inhibition of SphKs influences the survival of intracellular *Neisseria* and not the process of invasion itself, which could be due to increased intracellular sphingosine concentration.

3.1.3.2 Verification of inhibitory efficiencies by mass spectrometry

The biological function of SphKs is the phosphorylation of sphingosine to S1P. By applying inhibitors to block the kinase activity, levels of S1P should decrease and consequently levels of sphingosine increase, which might be the source for the observed survival defect on intracellular gonococci (Fig. 3.6 and 3.7). Therefore, we tested if the treatment with the inhibitors 5C, K145 and SKI-II alters the intracellular sphingolipids levels in Chang cells. The quantification was done by LC-MS/MS to monitor the *de novo* synthesis of isotope-labeled sphingolipids (Wigger et al., 2019). Briefly, Chang cells were pretreated with the inhibitors at 2.5 µM or 5 µM and fed with 100 µM stable isotope-labeled palmitate-d_3, one initial substrate of the *de novo* synthesis of sphingolipids which is further activated to d_3-palmitoyl-coenzyme A (d_3-palmitoyl-CoA) and metabolized. After lipid extraction (Gulbins et al., 2018), the sphingolipids-of-interest were tracked by their deuterated form. These experiments were conducted and analyzed by Dr. Fabian Schumacher at University of Potsdam.

The quantification of *de novo* formed dihydrosphingosine (dhSph-d_3) and sphingosine (Sph-d_3) confirms the consideration of increased intracellular sphingosine levels in a dose-dependent manner for K145 and SKI-II (Fig. 3.9 A). Inhibition of SphK1 with 5C did not alter the amount of sphingosine in comparison to the solvent control. These results were in line with the drastic reduction of invasive gonococci in the gentamicin protection assays (Fig. 3.6). Not only different sphingosine species were quantified, also the levels of dihydroS1P (dhS1P-d_3, Fig. 3.9 B) and S1P (S1P-d_3, Fig. 3.9 C) were measured. Compared to the DMSO control, samples pretreated with one of the single SphK inhibitors (5C or K145) showed higher concentration of labeled (dihydro-) S1P.

For dhS1P-d_3 a dose-dependency was detected (Fig. 3.9 B). Inhibition of both SphKs by SKI-II did not elevate the levels of dihydroS1P (dhS1P-d_3, Fig. 3.9 B) and S1P (S1P-d_3, Fig. 3.9 C). The lower concentration of 2.5 µM SKI-II kept the S1P levels constant as the solvent control and for 5 µM a decrease was detected. This clearly indicated that the survival defect must be due to increased sphingosine levels and is independent of S1P. Furthermore, these results together with mRNA-levels of the CRISPR/Cas9-generated Chang cells ΔSphK1 and ΔSphK2 (Fig. 3.2 A) could be evidence for compensatory roles of both SphKs.

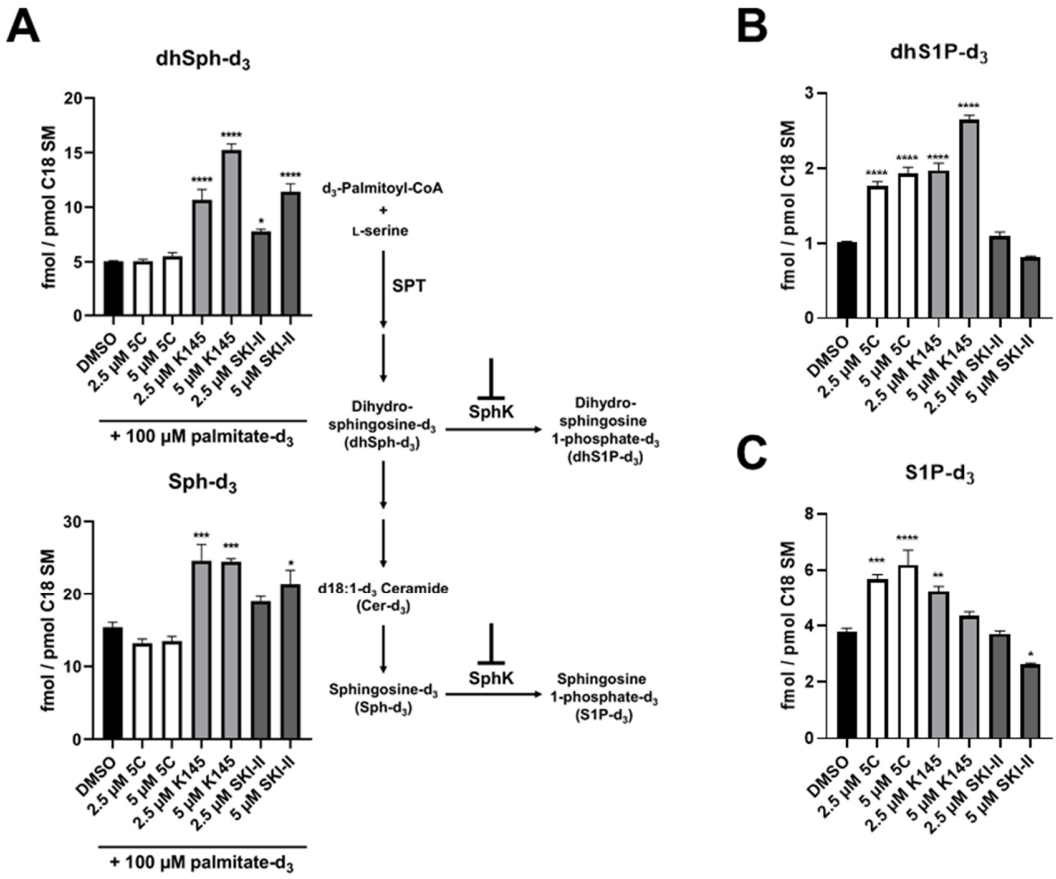

Figure 3.9 Quantification of *de novo* formed (dihydro-)sphingosine and (dihydro-)S1P in response to SphK inhibition in Chang cells.

Chang cells were pre-treated with the SphK inhibitors 5C, K145 and SKI-II (2.5 and 5 µM) for 1 h and then incubated with the deuterated sphingolipid *de novo* synthesis precursor palmitate-d_3 (100 µM) for 16 h. Quantification of the sphingolipid levels were done by LC-MS/MS and normalized to the C18 sphingomyelin (SM) content of the lipid extract. A) Levels of *de novo* formed, deuterated dihydrosphingosine (dhSph-d_3, upper graph) and sphingosine (Sph-d_3, lower graph) are shown with a simplified scheme of the relevant sphingolipid metabolism pathway. B) Levels of *de novo* formed, deuterated dihydrosphingosine-1-phosphate (dhS1P-d_3). C) Levels of *de novo* formed, deuterated sphingosine-1-phosphate (S1P-d_3). The mass spectrometry experiments and data analysis were performed by Dr. Fabian Schumacher and Prof. Burkhard Kleuser. Modified according to Solger et al. 2020.

Data are means + SEM of three independent experiments. Statistically significant differences to the solvent control (DMSO) were determined using one-way ANOVA with Dunnett's multiple comparisons test. *p<0,05, **p<0,01, ***p<0,001, ****p<0,0001.

It is not only interesting to see, how inhibitors change the balances of their substrate(s) and product(s) but also down- or upstream molecules. Therefore, the *de novo* synthesis of (dihydro-) ceramide C16 (d_6-C16 dhCer, d_6-C16 Cer) and SM C16 (d_6-C16 SM) in response to SphK inhibition was quantified (Fig. 3.10). As seen for labeled sphingosine species, 5C had no effect on ceramide C16 levels (Fig. 3.10 A and B). In contrast, K145 and SKI-II elevated the ceramide levels in a dose-dependent manner with a stronger effect for K145 (Fig. 3.10 A and B). For d_6-C16 SM contrary effects were detected with increasing effect of 5C and decreasing for the other two inhibitors (Fig. 3.10 C). SKI-II showed a stronger reduction compared to K145. The alterations of C16 SM levels were dose-dependent for all inhibitors.

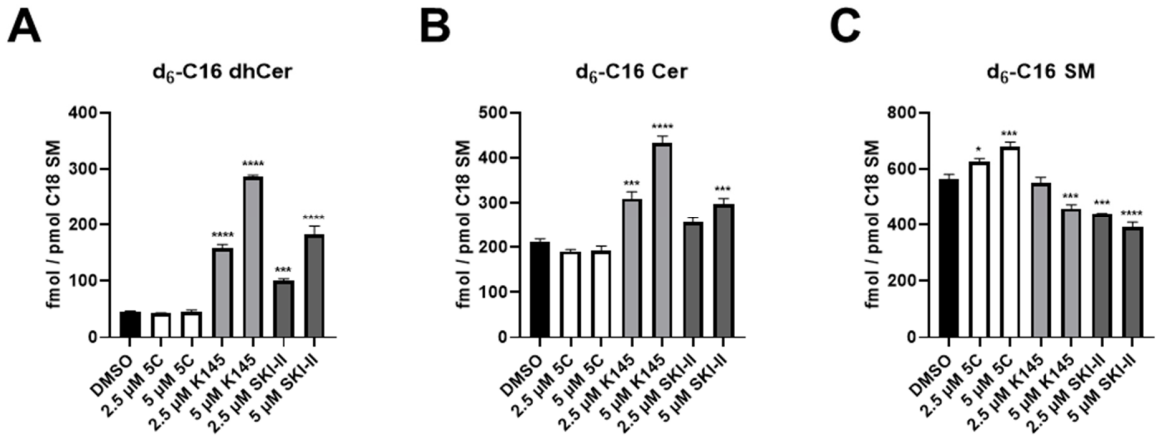

Figure 3.10 Quantification of *de novo* formed (dihydro-)ceramide C16 and SM C16 in response to SphK inhibition in Chang cells.

Chang cells were pre-treated with the SphK inhibitors 5C, K145 and SKI-II (2.5 and 5 µM) for 1 h and then incubated with the deuterated sphingolipid *de novo* synthesis precursor palmitate-d_3 (100 µM) for 16 h. Quantification of the sphingolipid levels were done by LC-MS/MS and normalized to the C18 sphingomyelin (SM) content of the lipid extract. Graphs show the levels of *de novo* formed, deuterated (A) dihydroceramide C16 (d_6-C16 dhCer), (B) ceramide C16 (d_6-C16 Cer) and (C) sphingomyelin C16 (d_6-C16 SM). Mass spectrometry experiments and data analysis were performed by Dr. Fabian Schumacher and Prof. Burkhard Kleuser.

Data are means + SEM of three independent experiments. Statistically significant differences to the solvent control (DMSO) were determined using one-way ANOVA with Dunnett's multiple comparisons test. *p<0,05, ***p<0,001, ****p<0,0001.

3.1.3.3 Toxicity of sphingosine on gonococci

The infection assays and SphK inhibitory assays indicate that intracellular sphingosine mediates the observed effects on the survival of *Neisseria*. To prove this hypothesis, neisserial growth was tested in the presence of sphingosine in liquid culture. Additionally, to the already used strains N927 (Fig. 3.11) and 24871 (Fig. 3.12 A and B), the clinical isolate VP1 (Fig. 3.12 C) and the laboratory strain FA1090 (Fig. 3.12 D) were included in this study to see their sensitivity for sphingosine *in vitro*. It appeared that the laboratory strain N927 had sometimes difficulties to grow in liquid culture (PPM+) under standard conditions, therefore its growth was additionally tested in the fully-defined Graver-Wade medium (Wade and Graver, 2007) (Fig. 3.11).

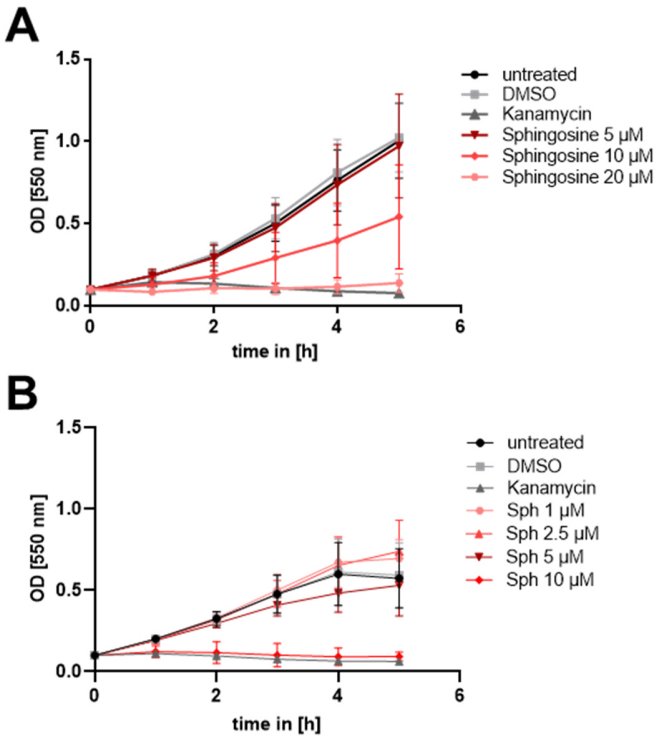

Figure 3.11 Toxic effect of sphingosine on *N. gonorrhoeae* N927.
Gonococci were grown in PPM+ (A) and Graver-Wade medium (B) supplemented with different sphingosine (Sph) concentrations.
Modified according to Solger et al. 2020.

The growth curves of N927 differed in sensitivity towards the used sphingosine concentration between the two used media (Fig. 3.12). In PPM+ the highest concentration of sphingosine (20 µM) killed the gonococci as efficiently as the positive control kanamycin (Fig. 3.12 A). At 10 µM the neisserial growth was reduced by 50%, whereas the lowest concentration (5 µM) did not affect the replication of the bacteria. The growth curves performed with Graver-Wade medium showed reduced replication even in the untreated and DMSO control compared to PPM+ (Fig. 3.11 B). Also, the progression of the curves was more flattened and the logarithmic phase was entered

earlier. Since N927 was not able to grow better in the Graver-Wade medium, the toxicity of sphingosine was even stronger. Already the concentration of 10 µM had a similar effect as kanamycin, which was detected in PPM+ at the double concentration of 20 µM. A minimal reduction in growth was seen for 5 µM and the lowest concentration (1 µM and 2.5 µM) had no effect or even a slight increase in replication for the later time points (4 hours and 5 hours).

Strain FA1090 and the clinical isolates were not as sensitive to sphingosine as N927, but all showed at a distinct concentration growth deficiency (Fig. 3.12). The clinical isolate 24871 was able to survive a treatment with 80 µM sphingosine and only showed a slight reduction in growth (Fig. 3.12 A and B). VP1 (Fig. 3.12 C) and FA1090 (Fig. 3.12 D) had reduced growth for 40 µM and 60 µM, respectively.

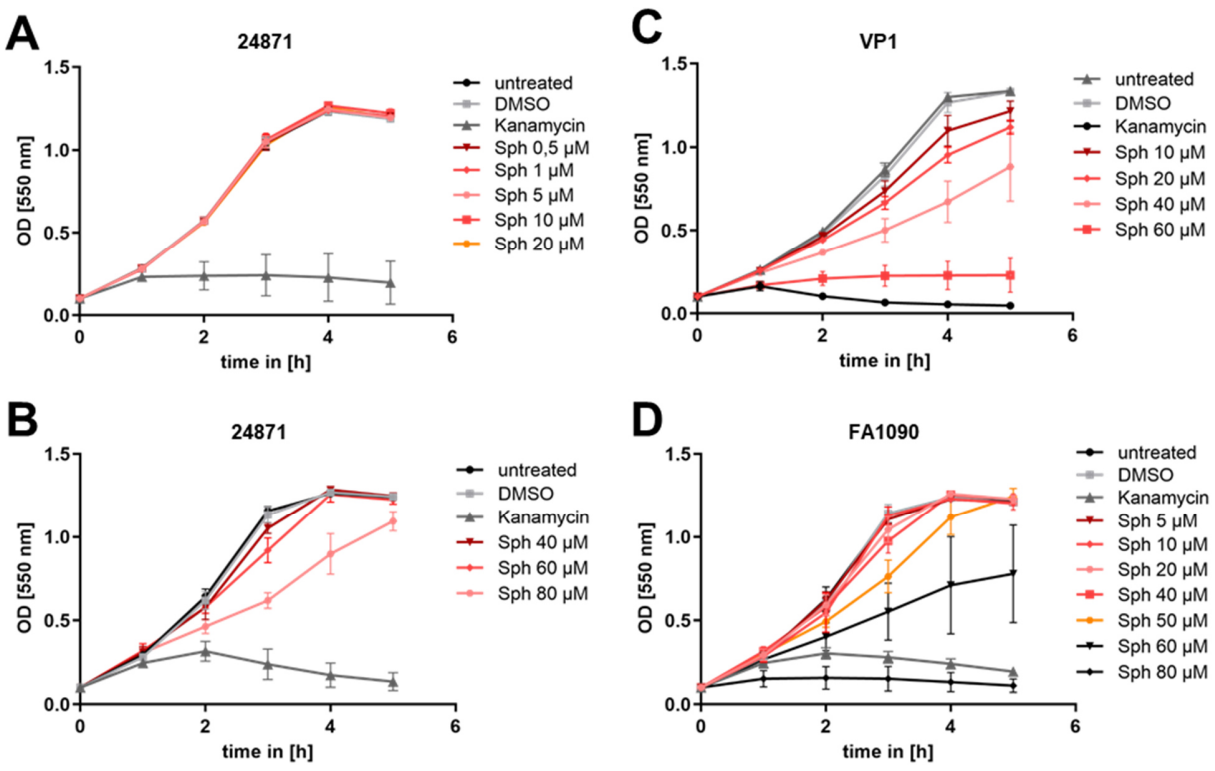

Figure 3.12 Effect of sphingosine on different *Neisseria* strains *in vitro*.
Neisserial strains were grown in PPM+ and treated with different sphingosine (Sph) concentrations. A) Growth of the clinical isolate 24871 is shown for concentrations up to 20 µM sphingosine. B) Effect of higher concentrations on 24871. C) Effect of different sphingosine concentration on VP1 *in vitro*. D) Growth of FA1090 with different sphingosine concentrations. Modified according to Solger et al. 2020.

3.2 Toxicity and visualization of clickable sphingolipid analogues in *Neisseria*

Not only for sphingosine, but also for other classes of sphingolipids toxicity against pathogens is described (Becam et al., 2017; Wertz, 2018). Since now, the exact mode of action is not known. Therefore, the method click chemistry (Kolb et al., 2001) was chosen to visualize different classes of sphingolipids and their interplay with *N. gonorrhoeae* in our cellular infection models to get new insights how these lipids might act on gonococci.

To perform a click reaction, an azido group was added to the sphingolipid of interest which reacts with the alkyne group of the dye. For each class of sphingolipid, different analogues (see Table 2.9) were tested and compared to the native form of the lipid.

3.2.1 Sphingosine

Sphingosine is one of the most investigated sphingolipids and therefore its toxicity against a variety of pathogens, including gram-positive/-negative bacteria (Fischer et al., 2012), enveloped viruses (Sakamoto et al., 2005) and fungi (Rollin-Pinheiro et al., 2016) is well described (Wu et al., 2021). The mechanism of action is not discovered until now, suggestions include for example the formation of micro lesions (Fischer et al., 2013). In the case of *N. gonorrhoeae*, a clear survival defect after invasion upon SphK-inhibition was observed with the hypothesis that increased sphingosine levels intracellularly causes this defect. Until now, a direct link between sphingosine and intracellular bacteria was missing. To elucidate the effect of intracellular sphingosine on *Neisseria* click chemistry was applied by using clickable sphingosine-analogues (ω-N_3-sphingosine and 1-N_3-sphingosine).

3.2.1.1 Verification of the phosphorylation and toxicity of clickable sphingosine analogues

The sphingosine analogues were tested for their enzymatic phosphorylation in cell-free and *in vitro* conditions, for (cyto-)toxicity and specificity of the click reaction. The phosphorylation experiments were performed at the University of Potsdam by Dr. Fabian Schumacher and Prof. Burkhard Kleuser.

The difference of the sphingosine analogues is the position of the azido modification (Fig. 3.13 A). 1-N_3-sphingosine has this modification at the C-1 position of the head group instead of the hydroxy group compared to the native form. Normally, this hydroxy group gets phosphorylated by SphKs. In case of ω-N_3-sphingosine an azido group was added to the carboxyl chain. To test if the position of the azido group has implication on the phosphorylation capability of the analogues, an enzymatic cell-free assay with SphK1 and ATP was performed separately for both analogues. Lipids were extracted and examined by liquid chromatography high-resolution mass spectrometry (LC-HRMS). The sphingosine analogues were identified by means of their accurate mass-to-charge ratios (*m/z*) (Fig. 3.13 B, left and middle panel). Next, the phosphorylated products for both analogue mixtures were analyzed. For ω-N_3-sphingosine a phosphorylated product (ω-N_3-S1P) by SphK1 was detected (Fig. 3.13 B, right panel), which was clearly identified by the protonated molecular ion $[M+H]^+$ (accompanied by sodium and potassium adduct ions) in the mass spectrum with high mass accuracy ($\Delta m/z$ = 1.2 ppm). For 1-N_3-sphingosine no phosphorylated product was obtained (not shown) as expected due to the replacement of the hydroxyl group at C-1. To prove the different metabolism of the sphingosine analogues also occurs *in vitro*, Chang cells were fed either with 1-N_3-sphingosine or ω-N_3-sphingosine (10 µM each) for 17 hours. Lipids were extracted and only for the derivate ω-N_3-sphingosine a phosphorylation product was detected by LC-MS/MS (Fig. 3.13 C). In the lipid extracts both ω-N_3-sphingosine (Fig. 3.13 C, upper chromatogram) and ω-N_3-S1P (Fig. 3.13 C, lower chromatogram) were present, assuming similar MS/MS responses for analogue and phosphorylated product. A conversion rate of about 20% occurred.

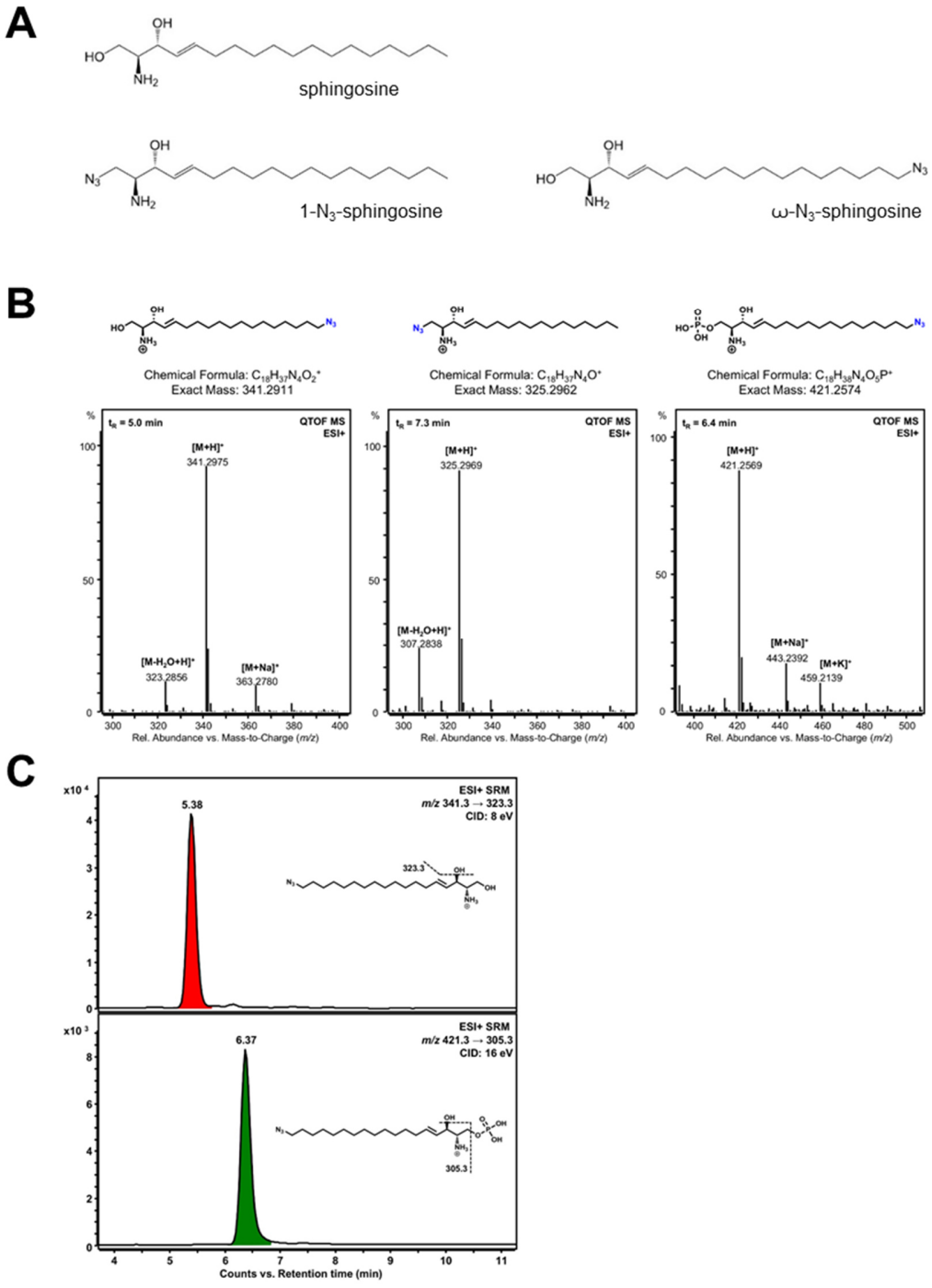
A
sphingosine
1-N3-sphingosine
ω-N3-sphingosine
B
Chemical Formula: C18H37N4O2+
Exact Mass: 341.2911
Chemical Formula: C18H37N4O+
Exact Mass: 325.2962
Chemical Formula: C18H38N4O5P+
Exact Mass: 421.2574
tR = 5.0 min
QTOF MS
ESI+
[M+H]+
341.2975
[M-H2O+H]+
323.2856
[M+Na]+
363.2780
tR = 7.3 min
QTOF MS
ESI+
[M+H]+
325.2969
[M-H2O+H]+
307.2838
tR = 6.4 min
QTOF MS
ESI+
[M+H]+
421.2569
[M+Na]+
443.2392
[M+K]+
459.2139
Rel. Abundance vs. Mass-to-Charge (m/z)
C
ESI+ SRM
m/z 341.3 → 323.3
CID: 8 eV
5.38
323.3
ESI+ SRM
m/z 421.3 → 305.3
CID: 16 eV
6.37
305.3
Counts vs. Retention time (min)

Figure 3.13 Clickable sphingosine analogues and their phosphorylation ability.
A) Chemical structures of native sphingosine and its clickable analogues (1-N_3- and ω-N_3-sphingosine). B) Identification of the clickable sphingosine analogues and detection of their phosphorylated products by LC-HRMS. After lipid extraction of the analogue, SphK1 and ATP mixture, chromatographically separation was performed by HPLC and analyzed with a quadrupole-time-of-flight mass spectrometer (QTOF MS) operating in the positive electrospray ionization mode (ESI+). Panels from left to right show the chemical structures and mass spectra of ionized ω-N_3-sphingosine, 1-N_3-sphingosine and phosphorylation product ω-N_3-S1P, respectively. No phosphorylation product could be detected for 1-N_3-sphingosine. The retention time (tR) is given as inset (top left) in the respective mass spectrum of each analyzed substance. C) Detection of analogue phosphorylation in Chang cells by LC-MS/MS. After 17 hours of incubation with 10 µM derivate, lipids were extracted and analyzed by selected reaction monitoring (SRM) after positive electrospray ionization (ESI+). Only for ω-N_3-sphingosine a phosphorylation product was detected. Lipids extracts contained both ω-N_3-sphingosine (upper chromatogram) and ω-N_3-S1P (lower chromatogram). Peaks are labeled with tR. Insets show the structural formulas and monitored MS/MS fragmentations (CID = collision-induced dissociation). Mass spectrometry experiments were performed by Dr. Fabian Schumacher and Prof. Burkhard Kleuser.
Modified according to Solger et al., 2020

Since the enzymatic metabolism of the analogues was verified, they were tested for their toxicity on the neisserial strain N927 and cytotoxicity on Chang cells *in vitro* (Fig. 3.14 and 3.15). Additionally to the derivates, the chosen clickable dye Click-iT™ Alexa Fluor™ 488 DIBO Alkyne (abbreviated DIBO) was tested on *Neisseria* and Chang cells (Fig. 3.14). Neither the tested concentrations of ω-N_3-sphingosine (5 µM and 10 µM, ω-Sph) nor the dye had a negative effect on the growth of N927 (Fig. 3.14 A). The cytotoxicity of the derivate and DIBO dye in Chang cells were determined via PI staining. Therefore, cells were fed with ω-N_3-sphingosine (5 µM and 10 µM, ω-Sph) and DIBO for 1 hour, which correlated to the feeding time and clicking time combined (Fig. 3.14 B). DMSO was used as solvent control and Triton-X as positive control for the staining. None of the substances did show any cytotoxicity. This staining was repeated with the controls and the analogue ω-N_3-sphingosine with an incubation time of 4 hours, which corresponded to the infection time (Fig. 3.14 C). Compared to the untreated Chang cells, only for 10 µM of sphingosine-analogue a minor increase was detectable. Both concentrations were used for further experiments and are indicated in the respective figure(s). These experiments were repeated with the second derivate 1-N_3-sphingosine (1-N_3-Sph; Fig. 3.15). This derivate showed a drastic effect on the growth of N927 at a concentration of 10 µM *in vitro* (Fig. 3.15 A). It appeared that 10 µM 1-N_3-sphingosine killed *Neisseria* even more efficiently as the kanamycin control. The lower concentration of 5 µM reduced the growth to a minimal extent at later time points. A real cytotoxic effect of this sphingosine analogue was not detected, only for 10 µM a slight increase in PI positive cells over time was seen.

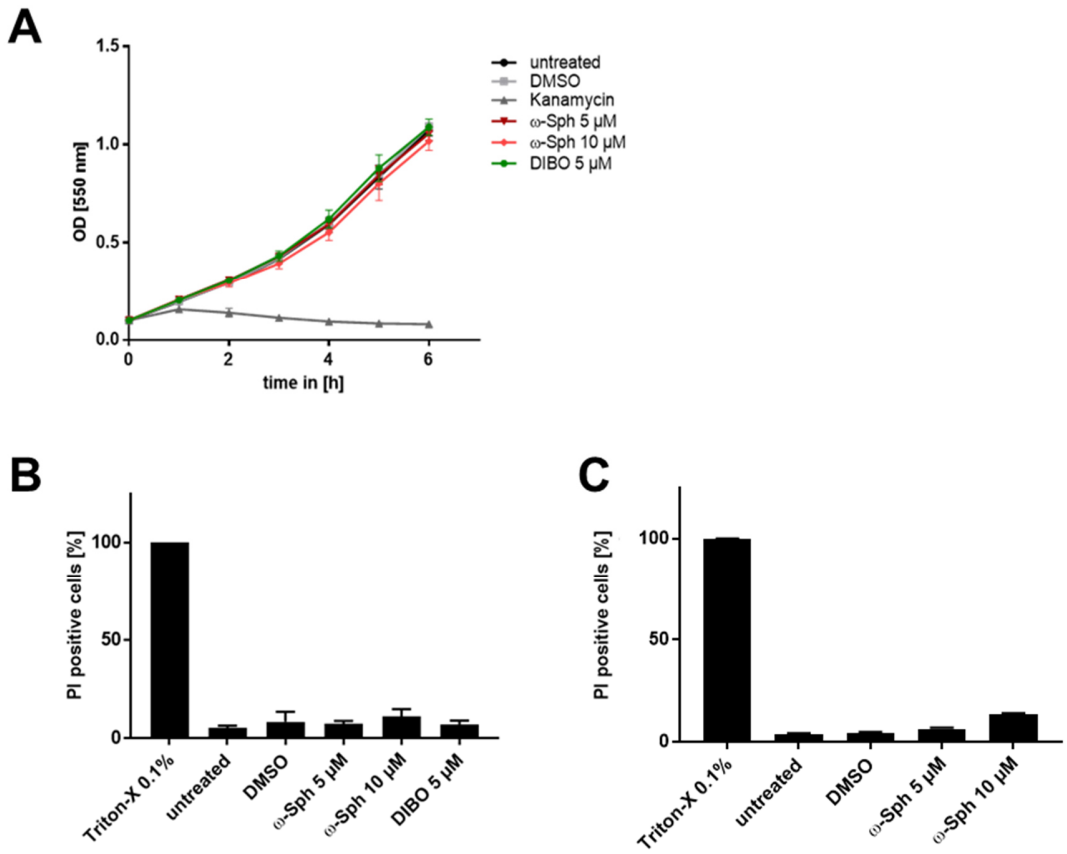

Figure 3.14 Effect of ω-N_3-sphingosine and Click-iT™ Alexa Fluor™ 488 DIBO Alkyne dye on N927 in vitro and the cytotoxicity on Chang cells.
A) Liquid cultures of N927 were supplemented with ω-N3-sphingosine (ω-Sph, 5 µM or 10 µM) and Click-iT™ Alexa Fluor™ 488 DIBO Alkyne dye (DIBO) and the growth was determined hourly. DMSO served as solvent control. Chang cells were incubated with the substances for 1 hour, which corresponds to the feeding time plus the clicking time (B), or further 4 hours, which correlates to the infection time (C). Cells were stained with PI and analyzed via flow cytometry. The detergent Triton-X was added right before the measurement to an untreated sample and was used as positive control.
Modified according to Solger et al., 2020

As already seen for the native sphingosine, the growth of *N. gonorrhoeae* strains differs in the sensitivity towards this sphingolipid (Fig. 3.11 and 3.12). To examine, if this is also the case for the sphingosine analogues, growth curves were performed with the laboratory strain RFP-N927 (Fig. 3.16 A) and the clinical isolate 24871 (Fig. 3.16 B). Interestingly, RFP-N927 did not show any deficiencies in growth, whereas the clinical isolate treated with 10 µM 1-N_3-sphingosine displayed a decrease of about 50% in replication rate. It was also surprising to see the recovery of the isolate 24871 after 1 hour, even though the OD was below the kanamycin value. All other chemicals had no effect. Therefore, the concentration of 5 µM 1-N_3-sphingosine was chosen for all further experiments. Besides the different sensitivities towards sphingosine (analogue) treatments,

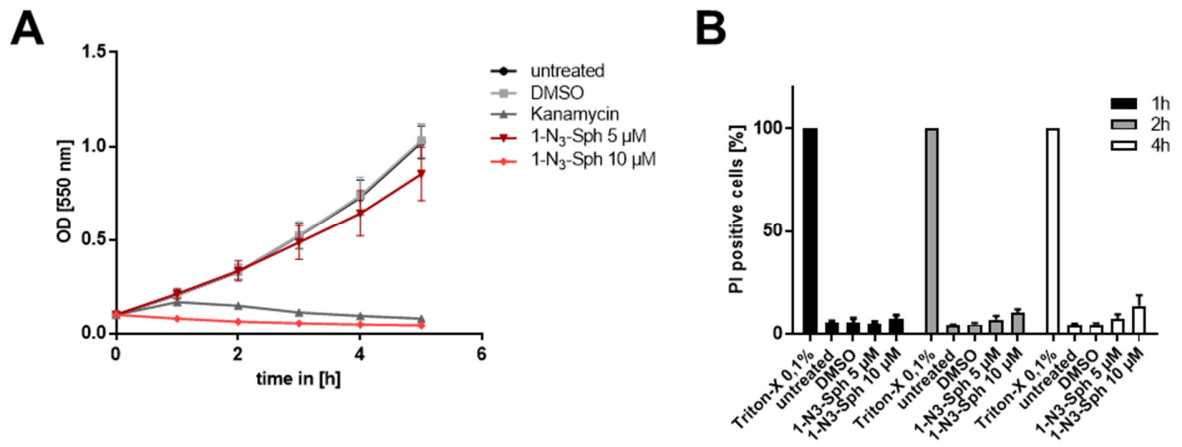

Figure 3.15 Effect of 1-N_3-sphingosine on N927 *in vitro* and its cytotoxicity on Chang cells.
A) Liquid cultures of N927 were supplemented with 1-N_3-sphingosine (1-N_3-Sph, 5 µM or 10 µM). The OD the was measured hourly to determine the bacterial growth. DMSO served as solvent control. B) Chang cells were incubated with the derivate or DMSO for different incubation times. Afterwards, cells were stained with PI and analyzed via flow cytometry. The detergent Triton-X was used as positive control.
Modified according to Solger et al., 2020

the growth behaviour between the laboratory strains and the clinical isolate displayed great differences. The isolate 24871 grew much faster by reaching the logarithmic phase after 3 hours of incubation (Fig. 3.16 B). In contrast, both used laboratory strains were even after 5 hours still exponential growing (Fig. 3.14 A, 3.15 A and 3.16 A).

Additionally to the quantification of the toxic and cytotoxic concentrations of the used derivates, the specificity of the click reaction was checked for *N. gonorrhoeae* (Fig. 3.16 C). Therefore, liquid cultures of N927 in PPM+ were prepared and supplemented with 10 µM of ω-N_3-sphingosine. As control, untreated N927 were grown in parallel. After 2 hours of incubation, the clicking buffer (containing 5 µM 488-DIBO) was added to an aliquot of the liquid culture supplemented with ω-N_3-sphingosine and incubated for another 30 minutes at 37°C. After this clicking time, *Neisseria* samples were washed once and analyzed via flow cytometry. The distribution of *Neisseria* population was similar for all samples in the scatter plots, i.e. higher rate of fragmentation of bacteria due to the feeding and clicking was not observed. The histogram of the untreated control (top right) showed a defined peak for the autofluorescence of the gonococci. This peak was used for gating "clicked" fluorescence. A similar peak was detected for the sample fed with ω-N_3-sphingosine (middle panel). The measured bacteria, which were fed and treated with the clicking buffer, displayed a strong shift in the FITC signal (bottom right). This result proved the specificity of the clicking reaction between ω-N_3-sphingosine and the AF 488-DIBO dye. Additionally, it

showed that *Neisseria* can take up sphingosine from liquid culture. Furthermore, this analysis can be considered as indirect confirmation of the non-toxic impact of sphingosine analogue and dye.

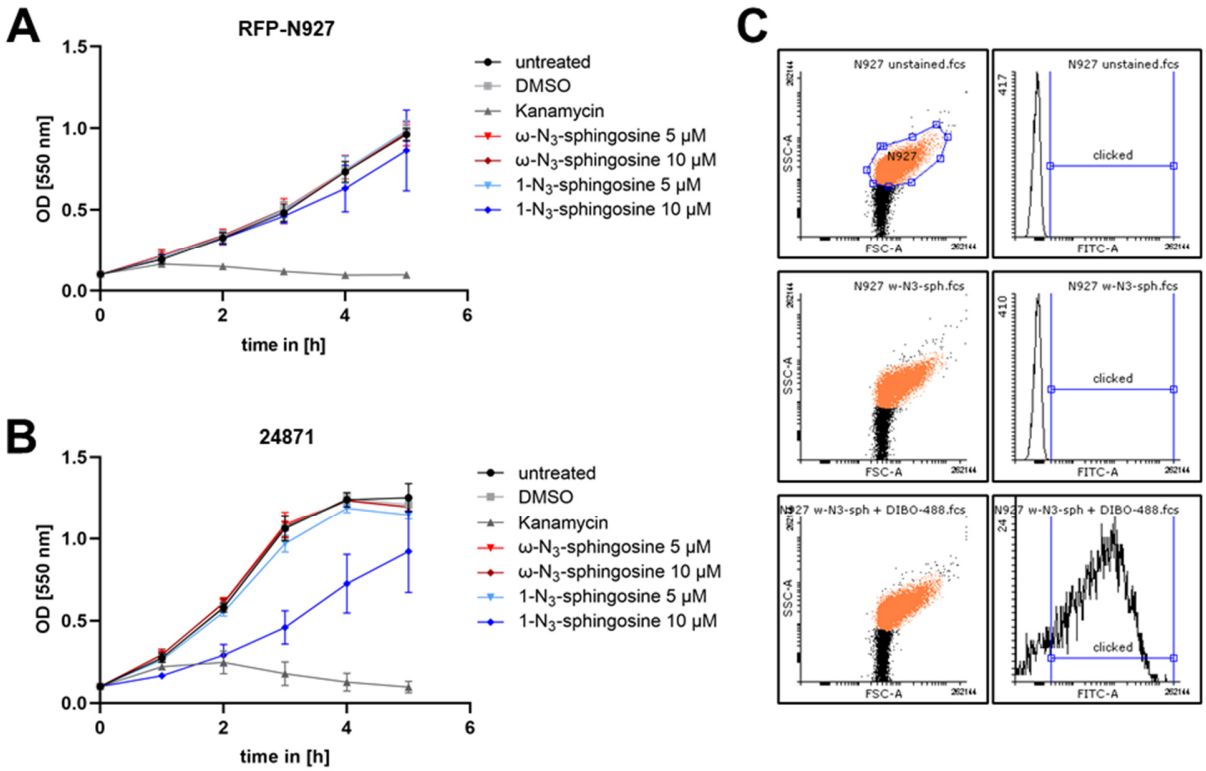

Figure 3.16 Verification of the growth deficiency with sphingosine analogues and specificity of the click reaction in *Neisseria*.

The effects of both sphingosine derivates on neisserial growth were checked for the strain RFP-N927 (A) and the clinical isolate 24871 (B). C) Furthermore, the specificity of the click reaction was confirmed in *Neisseria* (N927). PPM+ liquid cultures were supplemented with 10 µM of ω-N_3-sphingosine. After 2 hours, clicking buffer containing DIBO was added to one sample and incubated for 30 minutes. The specificity was determined via flow cytometry detecting the fluorescent signal of the dye (FITC). The scatter plots (SSC-A vs. FSC-A, left column) and respective histograms for the FITC signal (right column) are displayed for the untreated control, gonococci fed with ω-N_3-sphingosine and combination of ω-N_3-sphingosine feeding followed by adding DIBO from top to bottom. N927 fed with the analogue and no addition of DIBO (middle panel) showed the same distribution in the scatter plot (left column) and fluorescent signal (right column) as the untreated control (top panel). Only the combination of ω-N_3-sphingosine and DIBO (bottom panel) displayed a clear fluorescent shift for FITC (corresponding to AF 488-DIBO). Depicted in the top scatter plot of the untreated control is the gate (blue border), which was the same for all samples (these subpopulations are shown in orange). For each gate, 10,000 events were counted and analyzed for a fluorescence signal in the spectrum of 488 nm (FITC). The panels show representative blots from three independent measurements (n=3).

3.2.1.2 Uptake of sphingosine by *N. gonorrhoeae*

After the verification of the functionality and quantification sub-toxic concentrations of the sphingosine analogues, it was tested if Chang cells were able to take up efficiently ω-N3-sphingosine and the clickable dye AF 488-DIBO. Therefore, cells were fed with 10 µM of this derivate for 30 minutes, following an incubation for 4 hours (correlates to the infection time) and adding clicking buffer with a final concentration of 5 µM dye for another 30 minutes at 37 °C. After fixation and permeabilization the actin cytoskeleton was stained with Phalloidin. The microscopy picture (Fig. 3. 17) clearly showed an intense fluorescence for 488-DIBO, i.e. for clickable ω-N_3-sphingosine, within the cytoskeleton. This result demonstrated that both ω-N_3-sphingosine and AF 488-DIBO were cell permeable and could be used in living cells. Besides that, the localization of the sphingosine signal suggested due to its shape the endoplasmic reticulum as storage compartment.

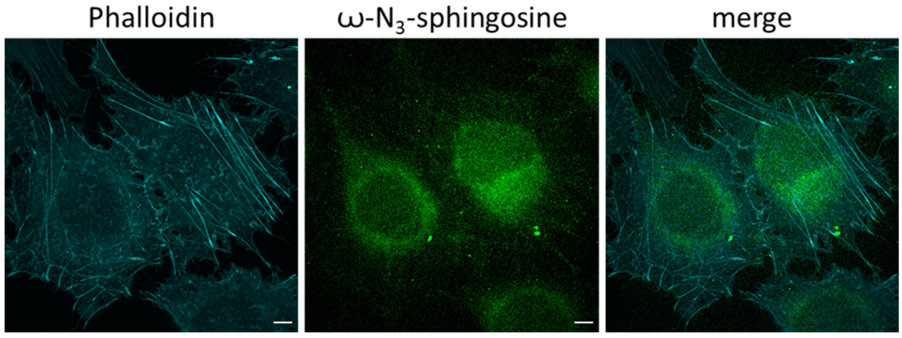

Figure 3.17 Uptake of ω-N_3-sphingosine in Chang cells.
Cells were fed with 10 µM ω-N_3-sphingosine and click reaction was performed with 5 µM AF 488-DIBO. Additionally, cells were stained with Phalloidin after fixation and permeabilization. The microscopy shows the efficient uptake of the sphingosine derivate which is probably transported and accumulated in the endoplasmic reticulum (cyan: actin cytoskeleton, green: ω-N_3-sphingosine, scale bar: 5 µm). The microscopy was performed in cooperation with Dr. Tobias C. Kunz.
Figure published in Solger et al. 2020.

Next, the uptake of ω-N_3-sphingosine (ω-Sph) by intracellular *Neisseria* was monitored (Fig. 3.18) to see if an incorporation into the neisserial membrane could be a cause for its toxicity (Fischer et al., 2013). The super resolution images showed an efficient uptake of sphingosine by gonococci (top panel), indicated by a strong fluorescence of the used dye DIBO-488. Furthermore, the incorporation of ω-N_3-sphingosine into the neisserial membrane was detected, since the DIBO-488 signal colocalized completely with the specific *Neisseria*-antibody labelling (top panel zoom). Cells fed with the native sphingosine (Sph) or without the supplementation of any sphingosine form (w/o Sph) did not show any signal at 488 nm. This was a confirmation of the specificity of the bioorthogonal click reaction even in infection models.

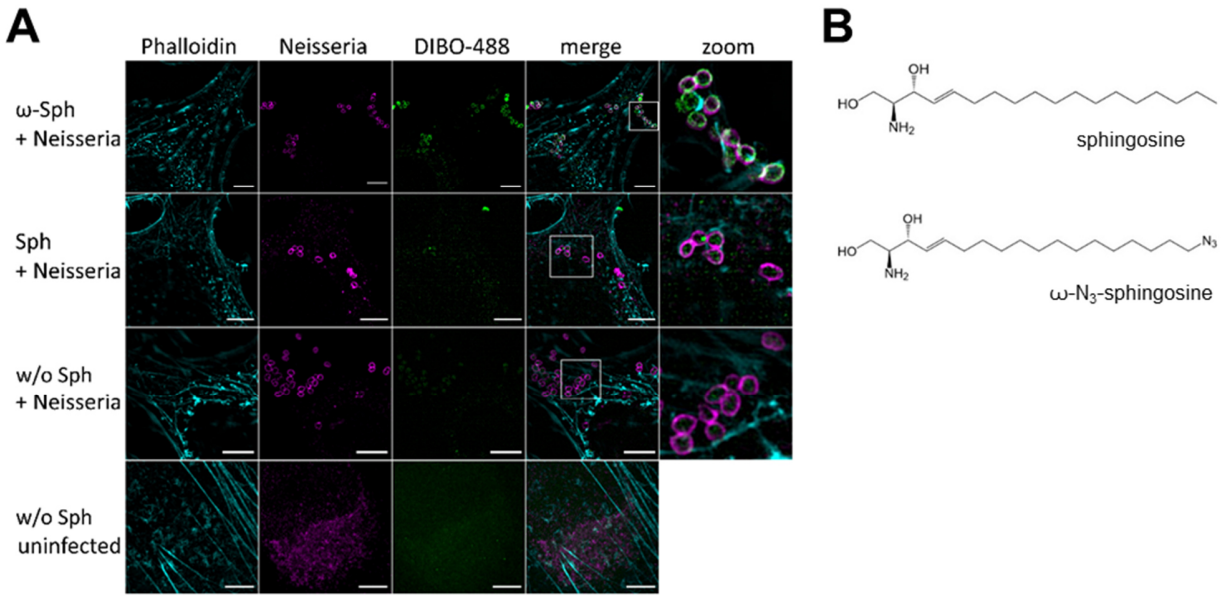

Figure 3.18 Incorporation of ω-N_3-sphingosine into neisserial membrane of N927.
A) Chang cells were fed either with clickable derivate ω-N_3-sphingosine (10 µM, ω-Sph) or native sphingosine (10 µM, Sph) before infection with N927 for 4 hours followed by clicking reaction with dye DIBO-488. Additionally, cells were stained for actin cytoskeleton (MFP™DY-555-Phalloidin) and immunolabeled for *Neisseria*. B) Chemical structures of native sphingosine and the analogue ω-N_3-sphingosine. Images represent a minimum of eight fields viewed per replicate of three independent experiments (cyan: actin cytoskeleton, magenta: *N. gonorrhoeae*, green: ω-N_3-sphingosine, scale bar: 5 µm). The microscopy was performed in cooperation with Dr. Tobias C. Kunz.
Modified according to Solger et al., 2020

To exclude that the observed incorporation of ω-N_3-sphingosine was strain- or cell type-specific, the experiment was repeated with N927 in End1 cells (Fig. 3.19 A) and with VP1 in Chang cells (Fig. 3.19 B).

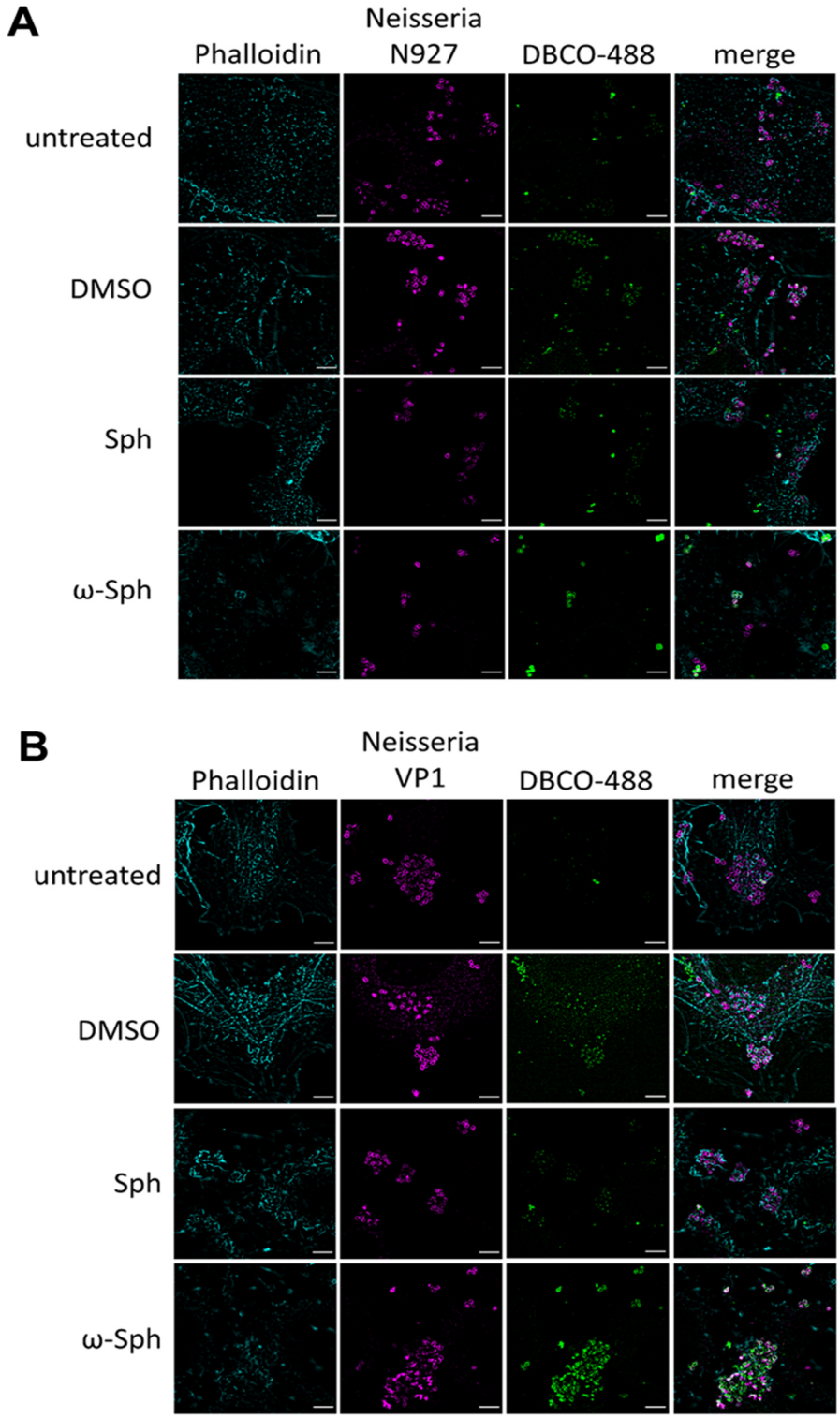

Figure 3.19 Incorporation of ω-N_3-sphingosine into neisserial membranes of different infection models.
Chang (A) and End1 cells (B) were fed either with ω-azido-sphingosine (10 µM, ω-Sph), native sphingosine (10 µM, Sph) or DMSO as solvent control before infection for 4 hours. Click reaction was done with dye DBCO-488. Cells were stained with Phalloidin and *Neisseria* were immunolabeled. A) Infection of End1 cells with the laboratory strain N927. B) Infection of Chang cells with the clinical strain VP1 (cyan: actin cytoskeleton, magenta: *N. gonorrhoeae*, green: ω-N_3-sphingosine, scale bar: 5 µm). The microscopy images were taken by Dr. Tobias C. Kunz.
Modified according to Solger et al., 2020

For these two infection models the same results were obtained as already seen for N927 in Chang cells, an incorporation of the clickable sphingosine (DBCO-488) into neisserial membrane (Fig. 3.19 A and B bottom panel, ω-Sph). These experiments were carried out with the clickable dye DBCO-488. In contrast to the previously used dye 488-DIBO (Fig. 3.17 and 3.18), 488-DBCO was not cell permeable. Therefore, the click reaction was performed after permeabilization of the fixed samples, resulting in a higher background staining of the control samples (untreated, DMSO and Sph) which was weak and diffuse. Nevertheless, a clear discrimination of background and specific clicking signal was clear. Taken together, the uptake was neither restricted to the infection model nor was it strain specific, meaning it might be a more general mechanism.
After knowing of the sphingosine incorporation, we investigated if this sphingolipid clusters in the neisserial membrane or if it is equally distributed as it looked in the SIM microscopy pictures (Fig. 3.18). To further investigate the distribution of ω-N_3-sphingosine, together with Dr. Tobias C. Kunz, a protocol for 4x expansion microscopy (ExM) was established for intracellular gonococci (Fig. 3.20). At this point it has to be noted that the expansion of ω-N_3-sphingosine was possible as it already possesses one primary amine, which is necessary for the linkage to the hydrogel. The comparison of SIM images before (upper panel, see also Fig. 3.18 and 3.19) and after expansion (lower panel, 4x ExM) showed that it was isotropic for both the clicked sphingosine and the antibody labelling. The expansion factor of 4 was achieved by adding lysozyme to the digestion step according to Lim et al. (Lim et al., 2019). The ExM clearly confirmed the incorporation into the bacterial membrane and led to the assumption that ω-N_3-sphingosine was equally distributed.

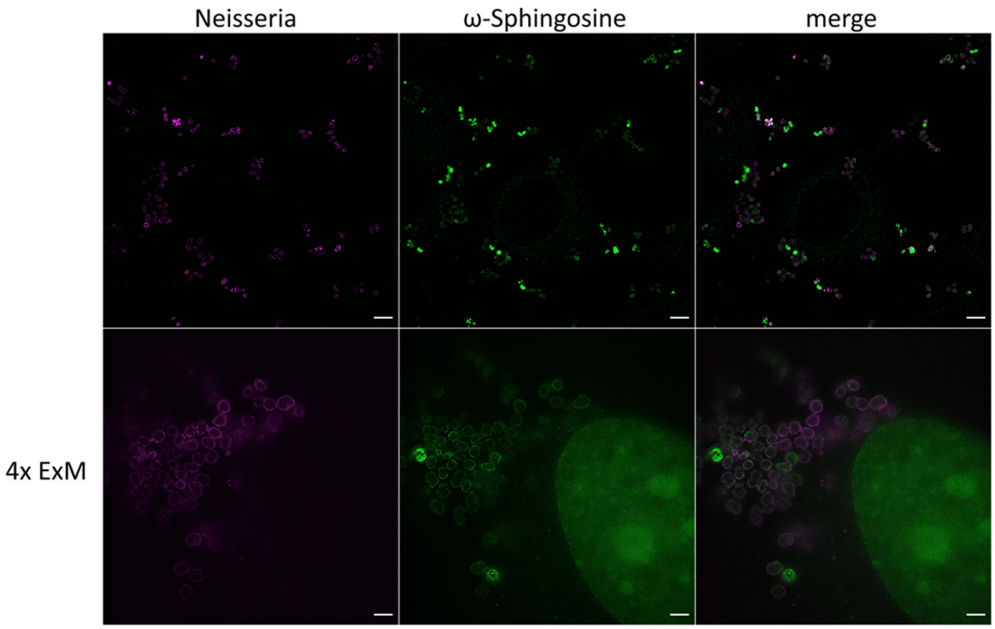

Figure 3.20 Expansion microscopy (ExM) of intracellular *N. gonorrhoeae*.
Chang cells were fed with ω-N_3-sphingosine (ω-Sphingosine) and infected with N927 for 4 hours. Cells were fixed, permeabilized, stained with 488-DIBO and anti-*Neisseria* immunolabelled. Comparison of confocal (upper row) and ExM-SIM images (lower row) shows a 4x magnification. The data were obtained from two independent experiments (n=2) (magenta: *N. gonorrhoeae*, green: ω-N_3-sphingosine, scale bars: 5 µm unexpanded confocal, 4 µm expanded SIM). The expansion, gel preparation and microscopy were performed in cooperation with Dr. Tobias C. Kunz.
With permission from Götz et al., 2020.

This system of click chemistry and infection model was adjusted for live cell imaging to visualize the dynamics of the intracellular sphingosine uptake. It appeared that the uptake of ω-N_3-sphingosine can occur rapidly with complete membrane labelling of the gonococci in at least 15 minutes (Fig. 3.21 upper panel, Video 1). Interestingly, with the time frame of 15 minutes, the uptake of sphingosine was not depicted to one specific area and was not distributed gradually throughout the membrane of the bacteria. After the incorporation of sphingosine, the loss of the RFP fluorescence of the *Neisseria* was detected (time point 165 min). The identical experimental set-up was repeated with the second derivate 1-N_3-sphingosine to exclude an analogue-specific phenotype (Fig. 3.21 lower panel, Video 2). In fact, the uptake of 1-N_3-sphingosine appeared in a similar way as ω-N_3-sphingosine by *Neisseria*.

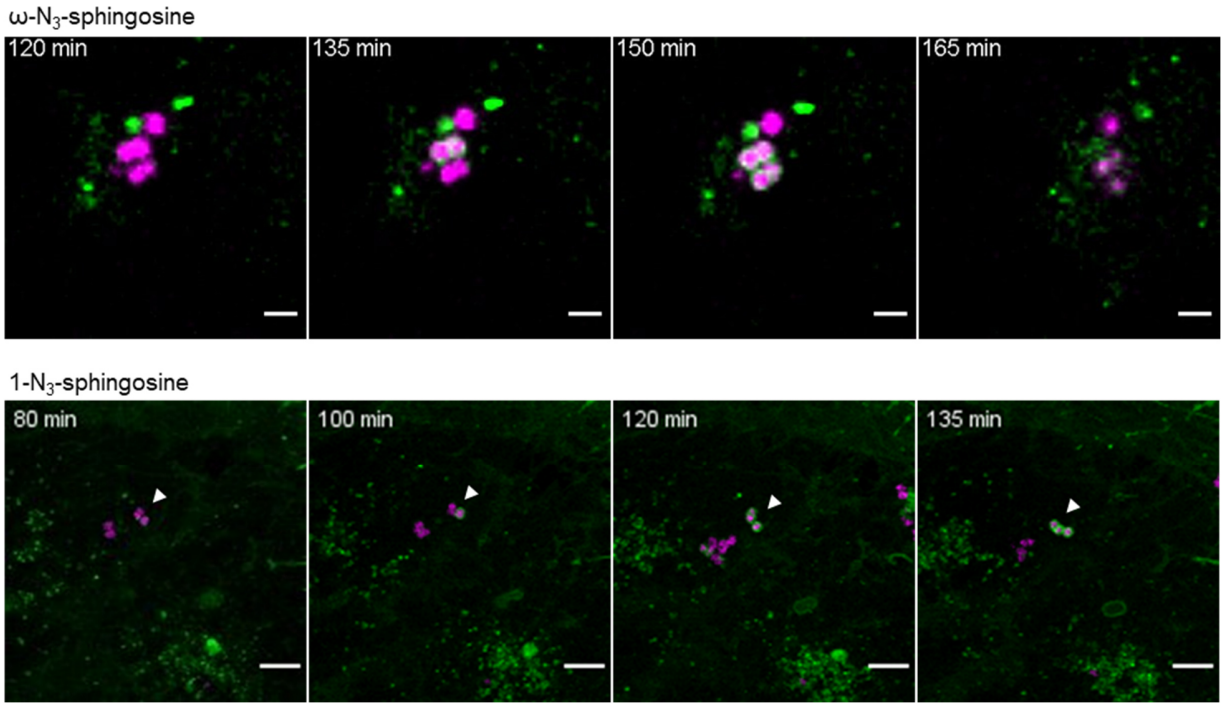

Figure 3.21 Rapid uptake of intracellular clickable sphingosine derivate.
Still pictures of the infection model of Chang cells fed either with ω-N_3-sphingosine (10 µM) or 1-N_3-sphingosine (5 µM) and infected with RFP-N927. Click reaction was performed with DIBO-488 before infection. The time-lapse imaging demonstrates the rapid uptake of ω-N_3-sphingosine and 1-N_3-sphingosine into the neisserial membrane (white arrowhead indicates up taking *Neisseria*; magenta: RFP-N927, green: ω-N_3-sphingosine, scale bars: 2 µm ω-N_3-sphingosine, 5 µm 1-N_3-sphingosine). The microscope was adjusted by Dr. Tobias C. Kunz.

Because the inhibition of SphKs had a greater effect on neisserial survival (Fig. 3.7), the same set of inhibitors was taken to repeat it with the clickable analogue ω-N_3-sphingosine. Since the phosphorylation by SphK of the derivate was confirmed (Fig. 3.13 C), a more drastic effect on the intracellular gonococci was expected in combination with SphK inhibition (Fig. 3.22 A). In fact, the inhibitors K145 and SKI-II reduced the number of gonococci drastically in comparison to the DMSO solvent control (Fig. 3.22 A). Moreover, these samples showed a lower intensity of neisserial antibody-labelling. For the SphK1-specific inhibitor 5C, no obvious differences were observed in the microscopy images. To exclude that the observed effect was due to any side effects and not through the impact of sphingosine, the second clickable analogue 1-N_3-sphingosine (1-N_3-Sph) was used (Fig. 3.22 B and 3.13). As already mentioned, this derivate was specifically acidified on the head group of the sphingosine backbone by replacing the hydroxyl group. This exchange leads to an indirect inhibition of the conversion of sphingosine to S1P (Fig. 3.13 B and C). Therefore, an even stronger toxic effect with this analogue was expected on invasive *Neisseria*.

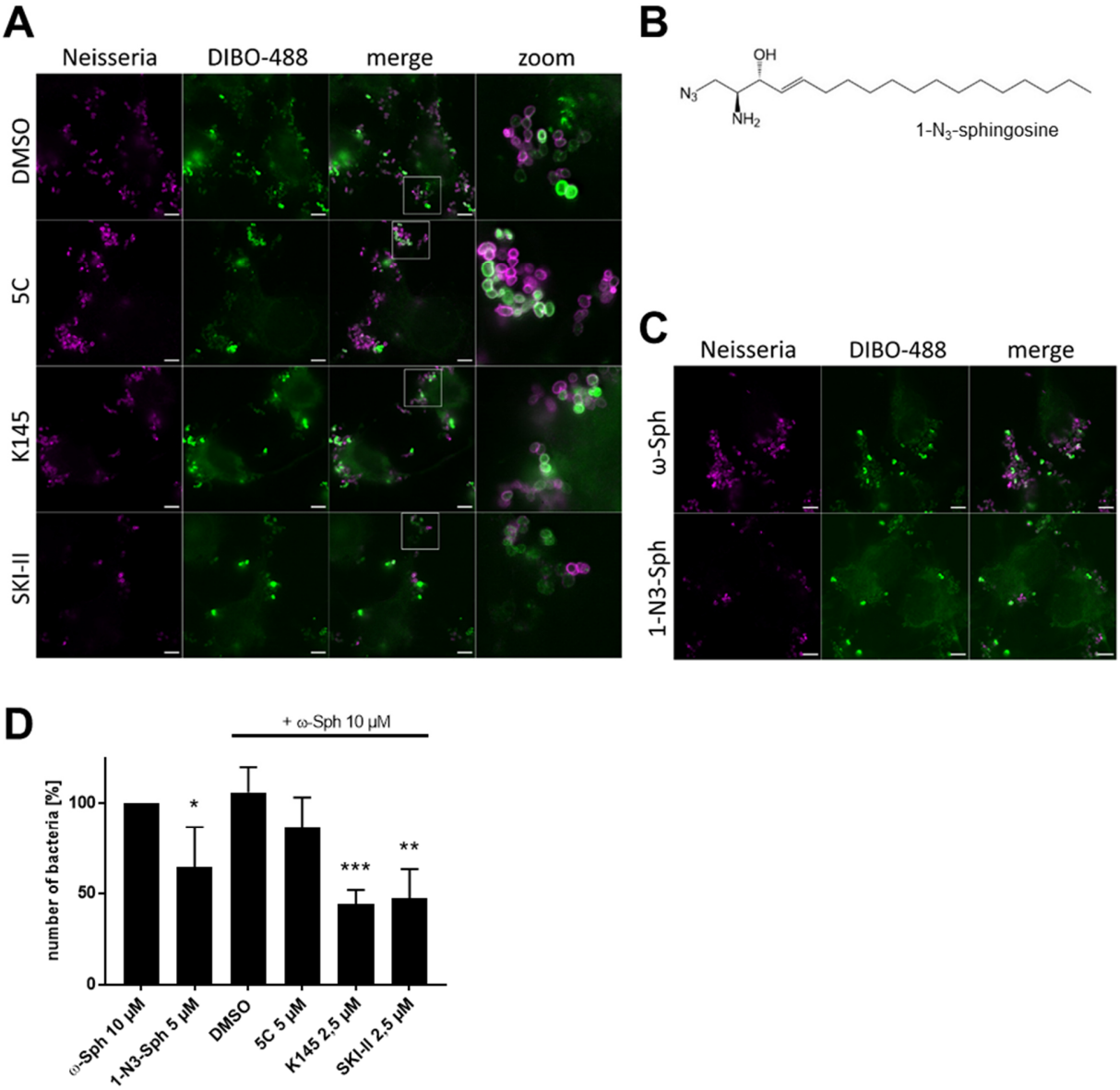

Figure 3.22 Reduction in survival of invasive N927 due to the inhibition of sphingosine phosphorylation.
The conversion of sphingosine to S1P was blocked either by SphK inhibition (A) or by using the clickable analogue 1-N_3-sphingosine (C). A) Chang cells were pre-treated with SphK inhibitors and fed with ω-N_3-sphingosine (ω-Sph) before infection with N927 for 4 hours. The click reaction was performed with DIBO-488 and gonococci were immunolabeled with anti-*Neisseria* antibody. B) Chemical structure of the analogue 1-N_3-sphingosine (1-N_3-Sph). C) Comparison of cells fed with ω-N_3-sphingosine (ω-Sph) or 1-N_3-sphingosine (1-N_3-Sph) after 4 h of infection. D) Quantification of gonococcal survival upon inhibition of sphingosine phosphorylation by inhibitor treatment or feeding 1-N_3-sphingosine (1-N_3-Sph) after 4 hours of infection. A minimum of eight fields viewed per biological replicate of three independent experiments were counted. The microscopy was performed in cooperation with Dr. Tobias C. Kunz.
***p<0,0001, **p<0,001, *p<0,05 student`s t-test relative to ω-Sph. Images represent a minimum of eight fields viewed per replicate of three independent experiments (magenta: *N. gonorrhoeae*, green: clickable sphingosine analogue, scale bars: 5 µm). Modified according to Solger et al., 2020

Since 1-N_3-sphingosine was more toxic on N927 *in vitro* (Fig. 3.15 A), Chang cells were fed with the sub-toxic concentration of 5 µM. After 4 hours of infection with N927, samples fed with 1-N_3-sphingosine showed decreased numbers of gonococci compared to cells fed with ω-N_3-sphingosine (Fig. 3.22 C). Additionally, the reduced intensity of the antibody-labelling reoccurred. The effect of 1-N_3-sphingosine and the combination of SphK-inhibitors with ω-N_3-sphingosine on the gonococcal survival was quantified by super resolution microscopy. Images were taken of three independent experiments (n=3). To assess the number of bacteria per cell, the signal of the anti-*Neisseria* antibody was counted blinded. The cytoskeleton staining and the clicked sphingosine signal was used to determine the cell number of each image. The observed inhibitory effects in this double-blinded assay confirmed the microscopy data (Fig. 3.22 D). Taken together, these data demonstrate that invasive *N. gonorrhoeae* take-up host-cell sphingosine and incorporate it into their membrane, which leads to reduced survival.

3.2.1.3 Sphingosine vesicles

The time-lapse imaging did not only show the fast uptake and incorporation of intracellular sphingosine (Fig. 3.21, Videos 1 and 2), but also the formation of vesicles was observed (Fig. 3.23 A, Video 3 with time stamp indicating hpi). It demonstrates the accumulation of an intense fluorescence signal for ω-N_3-sphingosine to form cellular vesicles, which seem to be transported further in the direction of invasive bacteria, suggesting an involvement of the cytoskeleton in this action as a defence mechanism. Furthermore, this time-lapse imaging confirmed the uptake of sphingosine (timepoints 02:00 and 02:15) in the live cell infection model with Chang cells and the loss of the gonococcal RFP fluorescence, indicating the bacterial death (timepoint 02:30 and on). Interestingly, these vesicles appeared to attach to *Neisseria* and to induce the sphingosine uptake (Fig. 3.23 B, Video 4). In this observation, the gonococcus started to take up sphingosine, leading to its probable death (see timepoints 03:15 and 03:30).

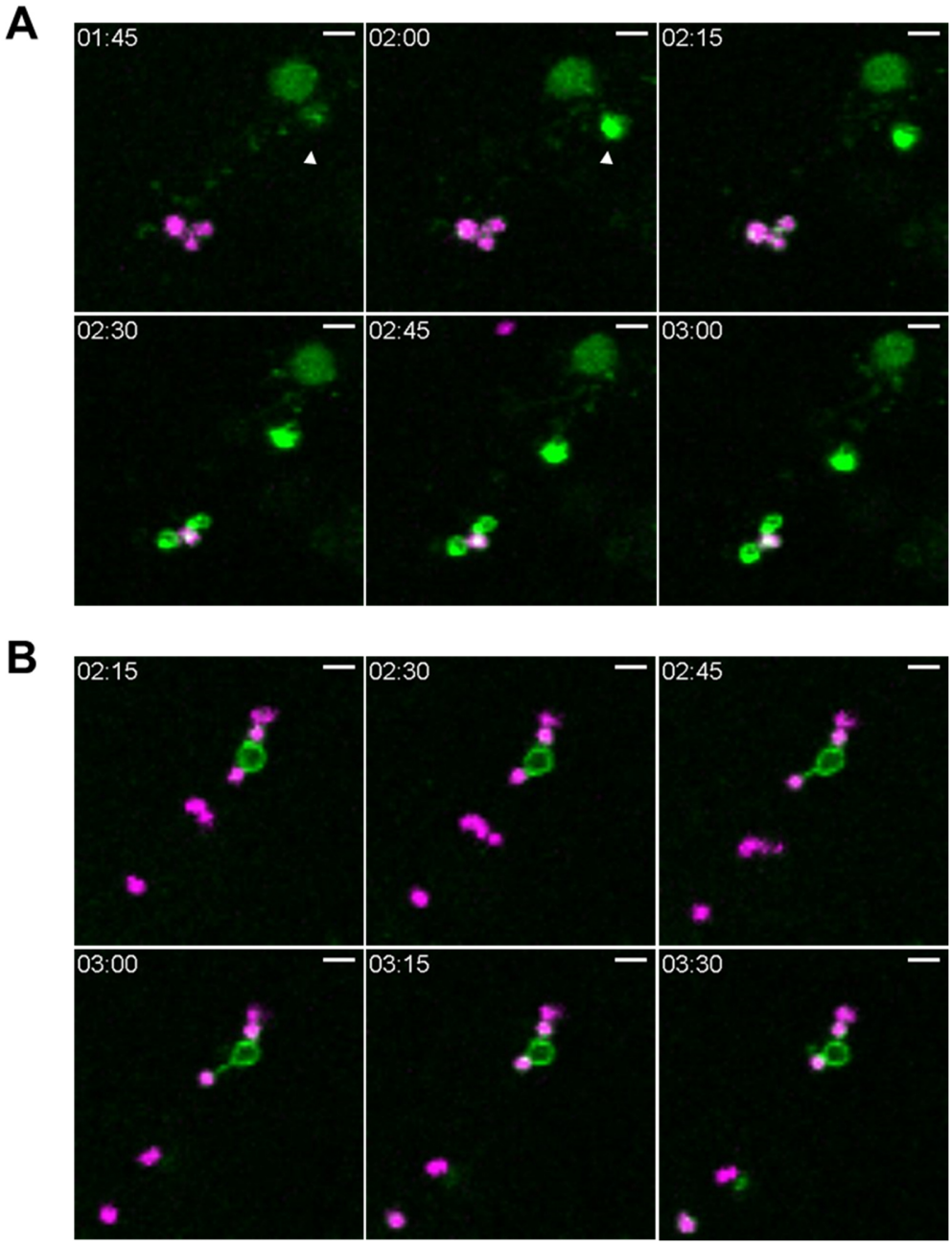

Figure 3.23 Formation of ω-N_3-sphingosine vesicles intracellularly.
Chang cells were fed with ω-N_3-sphingosine, clicked with DIBO-488 and infected with RFP-N927. A) Still pictures show the formation of a sphingosine vesicle (white arrowhead) over time (Video 3). B) Sphingosine vesicle attaches to gonococci and appears to retract the bacteria. Still pictures are taken from Video 4 (time stamp indicates hpi; magenta: RFP-N927, green: ω-N_3-sphingosine, scale bars: 2 µm). The microscopy was performed in cooperation with Dr. Tobias C. Kunz.

In long-time infection experiments for both derivates, it appeared that sphingosine vesicles were also present extracellularly, suggesting the formation of exosomes by Chang cells (Fig. 3.25, Video 5 for 1-N_3-sphingosine and video 6 for ω-N_3-sphingosine). The exemplary still pictures document the replication of *Neisseria* until certain time points (335 minutes post infection), even though they were attached to sphingosine vesicles (Videos 5 and 6). Interestingly, once these vesicles were bound to gonococci, bacteria were not able to detach anymore, concomitant with the loss of RFP-expression and accumulation of sphingosine at later time points. Until the latest time point at 890 minutes or 895 minutes for the respective analogues only few gonococci were left, showing the efficient "catch and kill"-mechanism by sphingosine vesicles. Furthermore, cells, which had taken up sphingosine analogue very efficiently, showed distinct intracellular vesicles. A side effect for the samples fed with 1-N_3-sphingosine was the strong accumulation of sphingosine signal in rounded up cells.

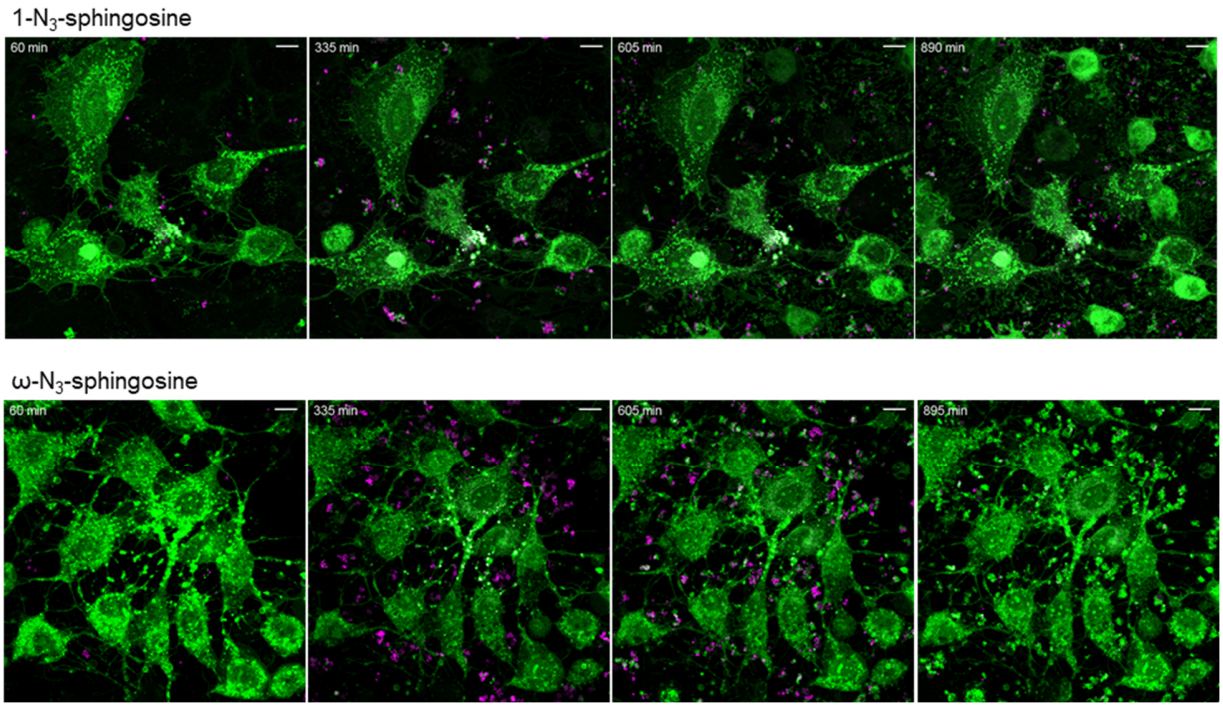

Figure 3.24 Long-term infections of Chang cells fed with sphingosine analogue.
Still pictures of long-time infection with RFP-N927 of Chang cells fed either with 1-N_3-sphingosine (5 µM; video 5) or ω-N_3-sphingosine (10 µM; video 6). Click reaction was performed with DIBO-488 before infection. The time-lapse imaging demonstrates for both analogues the formation of extracellular vesicles, which attach to *Neisseria* resulting in the loss of RFP-expression and the accumulation of sphingosine (magenta: RFP-N927, green: sphingosine, scale bars: 10 µm). Microscopy was performed by Dr. Kathrin Stelzner.

After the observation of vesicles, the question was if these might be part of the cellular defence mechanism phagocytosis since the involvement of sphingosine in endocytosis was already shown (Lima et al., 2017). Chang cells expressing YFP-tagged endosomal (Rab5 or Rab7) or lysosomal (LAMP1) marker protein were used for the characterization of sphingosine vesicles observed in the previous time-lapse imaging (Fig. 3.23 and 3.24, Videos 3-6). It must be admitted that not all cells did express the respective YFP-tagged protein and not all of them were positive for sphingosine uptake (exemplary indicated by a start in Fig. 3.25 A middle panel).

Super resolution microscopy of uninfected YFP-expressing Chang cells was performed to characterize vesicles formed by 1-N_3- and ω-N_3-sphingosine. The click reaction with the sphingosine derivate was performed with the dye Click-iT™ Alexa Fluor™ 594 DIBO Alkyne (DIBO-594). Respective microscopy pictures of two independent experiments (n=2) are shown (Fig. 3.25). The expression level for Rab5 was very low compared to Rab7 and especially LAMP1. In the case of LAMP1, big patches of accumulated proteins were observed intracellularly. These LAMP1-clumps did not allow to detect any kind of colocalization of the YFP- and sphingosine-signal, rather these accumulations hinder the incorporation of sphingosine (upper panel, Fig. 3.25 A). Only for Rab7 intense and distinct expression was observed, but no overlap with any sphingosine signal could be detected (lower panel, Fig. 3.25). Even though the overall expression of Rab5 was quite low, in some cells, which did show an intense YFP-signal, some ω-N_3-sphingosine vesicles were surrounded by Rab5 proteins (Fig. 3.25 B).

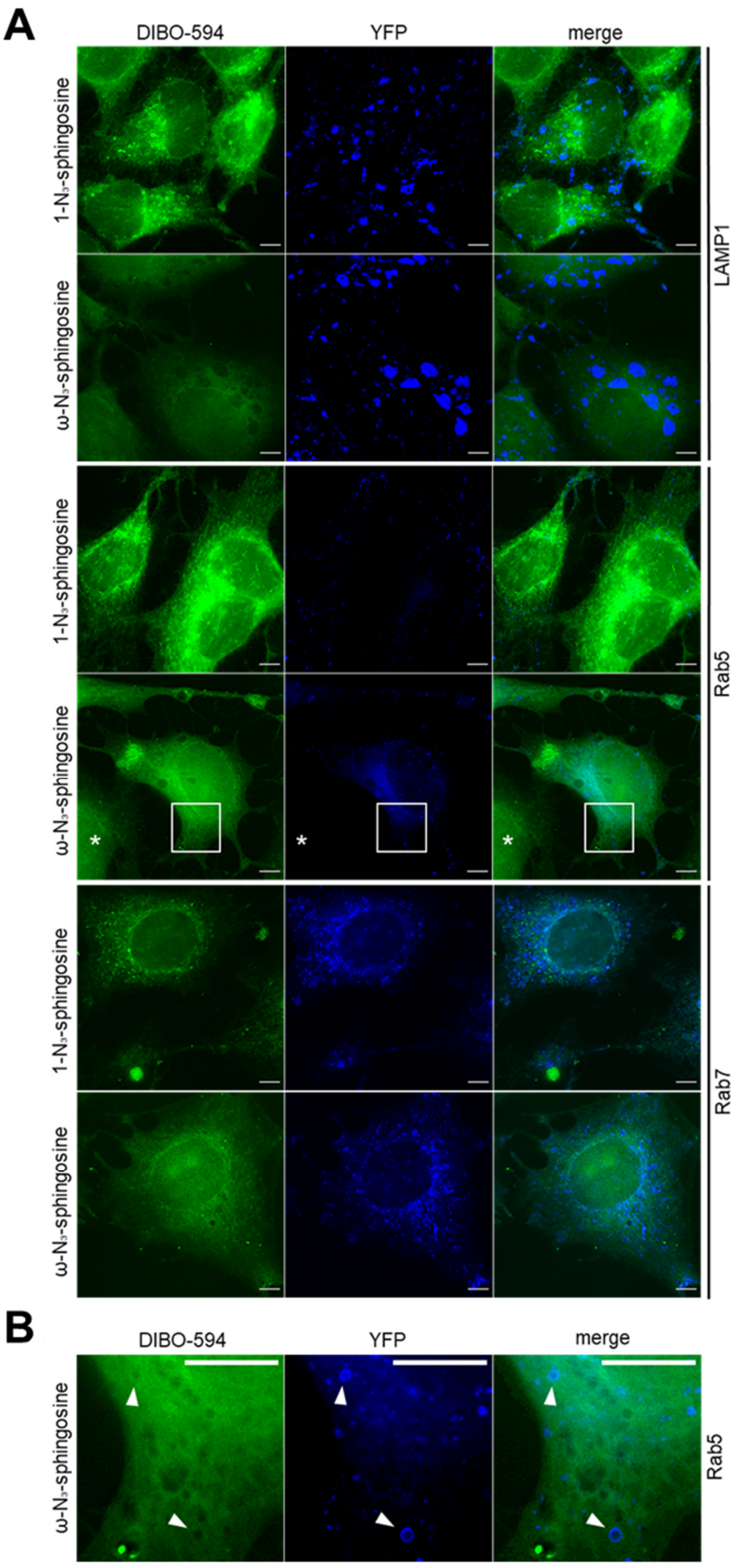
A
DIBO-594
YFP
merge
1-N₃-sphingosine
ω-N₃-sphingosine
LAMP1
Rab5
Rab7
B

Figure 3.25 Characterization of sphingosine vesicles in Chang cells expressing YFP-tagged endo-/lysosomal proteins.
A) Super resolution images of Chang cells expressing YFP-tagged LAMP1, Rab5 or Rab7, which were fed either with 1-N_3-sphingosine or ω-N_3-sphingosine. Each analogue was applied at 5 µM for 1 hour and clicked with 5 µM DIBO-594 for 30 minutes, followed by fixation and direct embedding without permeabilization. The star marks a YFP-negative cell but positive for the sphingosine uptake (middle panel for ω-N_3-sphingosine in Rab5-YFP cells). The boxes of the same panel are magnified in (B). B). ω-N_3-sphingosine vesicles encircled by Rab5 proteins (indicated by white arrow heads) (green: sphingosine, blue: YFP-tagged protein, scale bar: 5 µm). The microscopy images were taken by Dr. Tobias C. Kunz.
.

To detect possible dynamics between (especially extracellular) sphingosine vesicles and endo-/ lysosomal protein, YFP-expressing Chang cells were fed with one of the sphingosine analogues and infected with the laboratory strain N927 for time lapse-imaging. To avoid any fluorescence overlap or -spill, N927 were stained with DyLight™ 650-4xPEG NHS Ester before infecting clicked YFP-expressing Chang cells. Here, the same problem as for super resolution microscopy occurred to find cells which were positive for both sphingosine uptake and expressing YFP-tagged proteins. All used Chang cell lines did show the formation of sphingosine vesicles, which attached to gonococci. But no vesicles with a clear YFP-signal could be detected for the different cell lines (Videos 7-12). Additionally, no changes in the localization of the YFP-signals inside the cells could be detected throughout the time-lapse imaging. Unfortunately, the imaging with 1-N_3-sphingosine could have only been done once (n=1, Videos 7-10). Furthermore, it must be admitted that during some live cell imaging the microscope was not stable, i.e. shifting out of the selected area or z-stack (Videos 7, 8, 9 and 11).

Because the lysosomal marker LAMP1 did not allow any detection of colocalization with the sphingosine signal, a different approach was followed (n=1). Therefore, WT Chang cells were fed with ω-N_3-sphingosine (5 µM), clicked and stained with the cell probe SiR-lysosome. This dye is cell permeable and highly specific for lysosomes in live cell samples. To avoid a fluorescence overlap between the spectra of the fluorochromes SiR and AF594 (coupled to DIBO), two different lasers and the most distant possible excitations of both fluorochromes were chosen. Despite these adjustments, an overlap could not have been avoided and therefore, the combination of SiR and AF594 was not suitable (data not shown).

3.2.2 Ceramides

Ceramides are a heterogenous group of sphingolipids which can differ very much in their chemical structure, but they all have in common to be *N*-acylated sphingosines, i.e. sphingosine backbone has an amide link to a fatty acid. This fatty acid can vary for example in chain length, hydroxylation and saturation. One possibility to group ceramides is based on the chain length which displays different chemical and biological properties. Here, we investigated the role of the short-chain ceramide C6 (d18:1/6:0) and the long-chain ceramide C16 (d14:1/16:0) on gonococci by using clickable analogues of these ceramides. At this point it must be noted that the further clicking experiments had to be done with another dye (488-DBCO). This DBCO-dye is not cell permeable as DIBO-dyes and therefore, cells had to be treated with Triton-X in advance for clicking. This is also the reason why a higher background signal is detected for samples clicked with DBCO instead of DIBO.

3.2.2.1 Short-chain ceramide C6

It was demonstrated that the chain length of ceramides correlates with their antibacterial activity, including pathogenic *Neisseria* (Becam et al., 2017). In this study, the endogenous form of C6 ceramide and clickable analogues (1-N_3-C6 ceramide, 18-N_3-C6 ceramide and ω-N_3-C6 ceramide) were tested. The chemical structures of the C6 ceramide compounds with their respective names are shown in Fig. 3.26 A. To determine the subtoxic concentration of endogenous C6 ceramide and each analogue *in vitro* growth curves with the *N. gonorrhoeae* strain N927 were performed (Fig. 3.26 B and C). For C6 ceramide a concentration dependency was detected, where the lowest concentration of 0.5 µM reduced the replication capability already (Fig. 3.26 B). Treatment with 5 µM and 10 µM killed the gonococci efficiently as the Kanamycin control. To observe drastic differences of the analogues compared to the endogenous form, liquid cultures of N927 were supplemented with 5 µM or 10 µM of each analogue (Fig. 3.26 C, upper graph). 18-N_3-C6 ceramide and ω-N_3-C6 ceramide were as toxic as C6 ceramide, whereas 1-N_3-C6 ceramide had no effect on the growth for both used concentrations. The experiments were repeated with lower concentrations of 18-N_3-C6 ceramide and ω-N_3-C6 ceramide (Fig. 3.26 C, lower graph) to determine the subtoxic

concentrations. Here, a similar pattern as for C6 ceramide was observed with comparable reduced growth for each concentration.

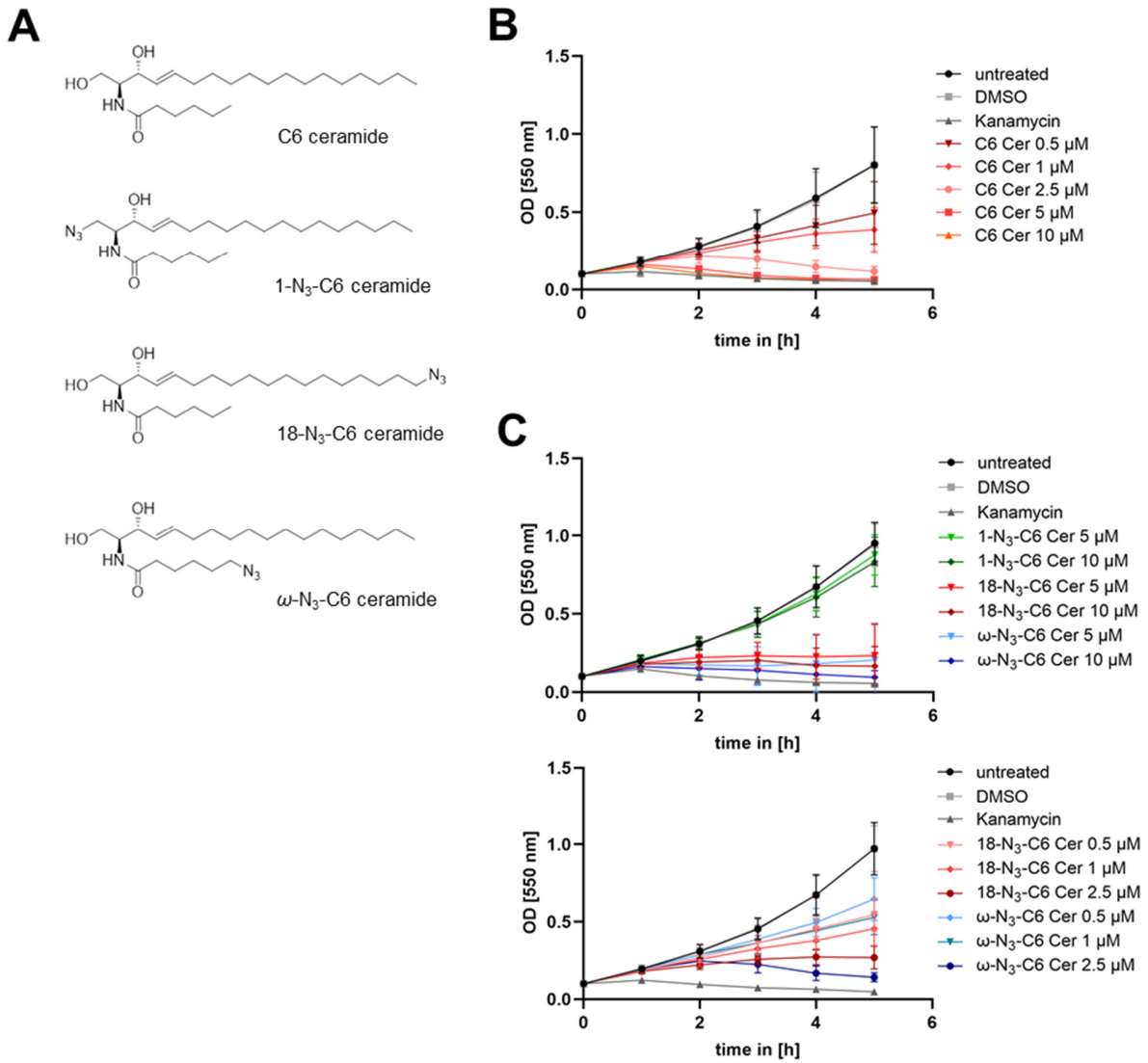

Figure 3.26 Effect of the short-chain ceramide C6 and its clickable analogues on N927.
The effect of ceramide C6 (C6 Cer) and its clickable analogues (A) were tested on strain N927 *in vitro* (B and C) and in the Chang infection model. A) The chemical structure of the endogenous ceramide C6 compared to the clickable azido compounds (1-N_3-C6 ceramide, 18-N_3-C6 ceramide and ω-N_3-C6 ceramide). B) Endogenous C6 Cer showed a concentration-depended toxicity on gonococci. C) The upper graph display differences of the three analogues on the growth of N927. 18-N_3-C6 cer and ω-N_3-C6 cer have comparable effects as C6 cer. 1-N_3-C6 ceramide doesn't show any toxic effect at 5 µM and 10 µM. Lower concentrations (0.5 µM, 1 µM and 2.5 µM) of 18-N_3-C6 cer and ω-N_3-C6 cer were tested (seen in the lower graph).).

These analogues were used as well to visualize the possible incorporation of these clickable sphingolipids into the neisserial membrane by using super-resolution microscopy (Fig. 3.27). Therefore, Chang cells were fed in advance with the sub-toxic concentrations of endogenous C6 ceramide (0.5 µM) and the clickable analogues (5 µM 1-N_3-C6 ceramide, 0.5 µM 18-N_3-C6 ceramide and ω-N_3-C6 ceramide each). Cells were infected with N927 for 2 hours, 4 hours or 6 hours. The different timepoints did not show any significant differences in localization and intensity of the stainings. Therefore, the time point of 4 hours was chosen to display representative pictures of this experiment. Additionally to the C6 ceramide samples, controls were included (upper panels of Fig. 3.27), i.e. control (unfed) and DMSO as solvent control. The unclickable samples (Fig. 3.27 left column control, DMSO and C6 cer) show a green signal in the cells for the dye 488-DBCO. This is most likely due to the application of the dye after the permeabilization step since DBCO dyes are not membrane permeable as mentioned above. Nevertheless, the dye did not intercalate to the same extent into gonococci of control and DMSO samples. The intensity of the 488-DBCO signal in C6 cer-fed cells was at least comparable to the sample of the one fed with the clickable analogue 1-N_3-C6 cer. For 18-N_3-C6 cer a slight increase of the signal was detected, in contrary a decrease of intensity for the samples fed with ω-N_3-C6 cer. For this treatment also a decrease in the *Neisseria* signal was detected. The intensities of the antibody labelling for *Neisseria* was for the other controls and treatments comparable and much stronger. The merged pictures (right column Fig. 3.27) clearly showed that the taken-up analogues did not colocalize with the gonococcal membrane. It also appeared that the replication of *Neisseria* was not impaired at that time point of infection.

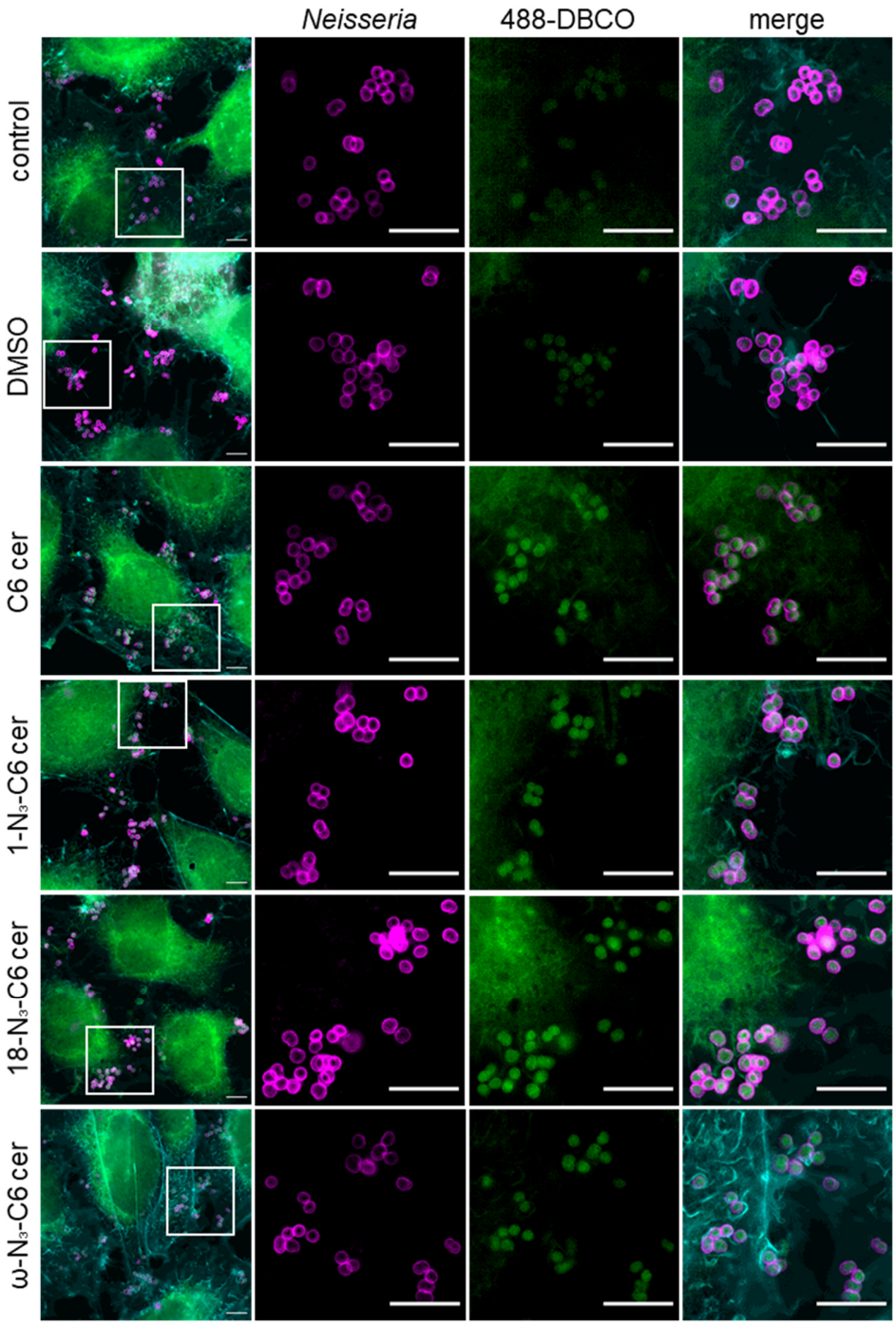

Figure 3.27 SIM pictures of C6 ceramide analogues in Chang cells infected with N927.
The panels show the substances with which the Chang cells were fed in advance of infection with N927 for 4 hours. The highest panel serves as negative control (no feeding). Additionally, a solvent control (DMSO) and a control for the specificity of the click reaction (C6 cer) were included. The click reaction with 488-DBCO was performed after permeabilization with Triton-X. The pictures show the *Neisseria* antibody labelled in magenta and the clickable analogues in green (488-DBCO). The merged microscopy pictures (outer left and right of each panel) show the actin cytoskeleton in cyan as well. Representative pictures were chosen from two independent experiments (n=2). The control and DMSO images are identical for Fig. 3.27, 3.29 and 3.32 because all chosen images are from the same set of samples. The white boxes mark the zoomed areas (magenta: N927, green: click reaction, cyan: actin cytoskeleton, scale bar: 5 µm). The microscopy images were taken by Dr. Tobias C. Kunz.

3.2.2.2 Long-chain ceramide C16

The experiments carried out with C6 ceramides were repeated with endogenous C16 ceramide and four different clickable analogues. The chemical structures with the different azido-modifications are listed in Fig. 3.28 A. For further infection experiments, the sub-toxic concentrations for these chemicals had to be determined on the strain N927. The *in vitro* growth curves for endogenous C16 ceramide (Fig. 3.28 B) and the analogues (Fig. 3.28 C) did not differ to the untreated and DMSO controls for both used concentrations of 5 µM and 10 µM. To make the experiments with the C6 ceramide more comparable, all C16 ceramides were used at the concentration of 5 µM for the infection experiment with N927 in Chang cells (Fig. 3.29). It must be noticed that the SIM images could have only been taken from one single experiment. Therefore, the presented microscopy pictures are observations which need to be verified. As already seen in Fig. 3.27, both controls

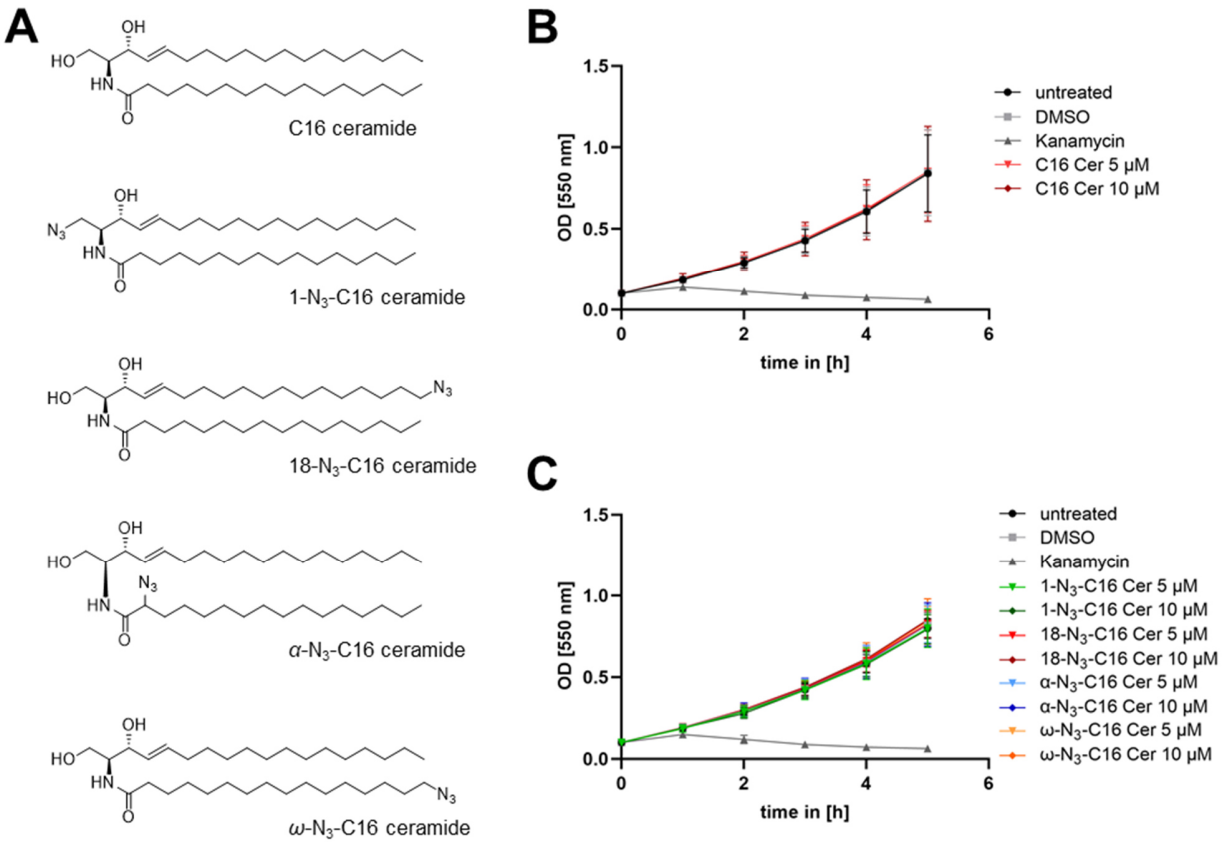

Figure 3.28 Effects of C16 ceramide and its clickable analogues on the *in vitro* growth of N927.
The effect of ceramide C16 (C16 Cer) and its clickable analogues (A) were tested on strain N927 *in vitro* (B and C). A) The chemical structure of the endogenous ceramide C16 compared to the clickable azido analogues (1-N_3-C16 ceramide, 18-N_3-C16 ceramide, α-N_3-C16 ceramide and ω-N_3-C6 ceramide). B) The used concentration of endogenous C16 Cer had no influence on the gonococcal replication. C) Neither the azido-modifications nor the used concentrations influenced the growth of N927.

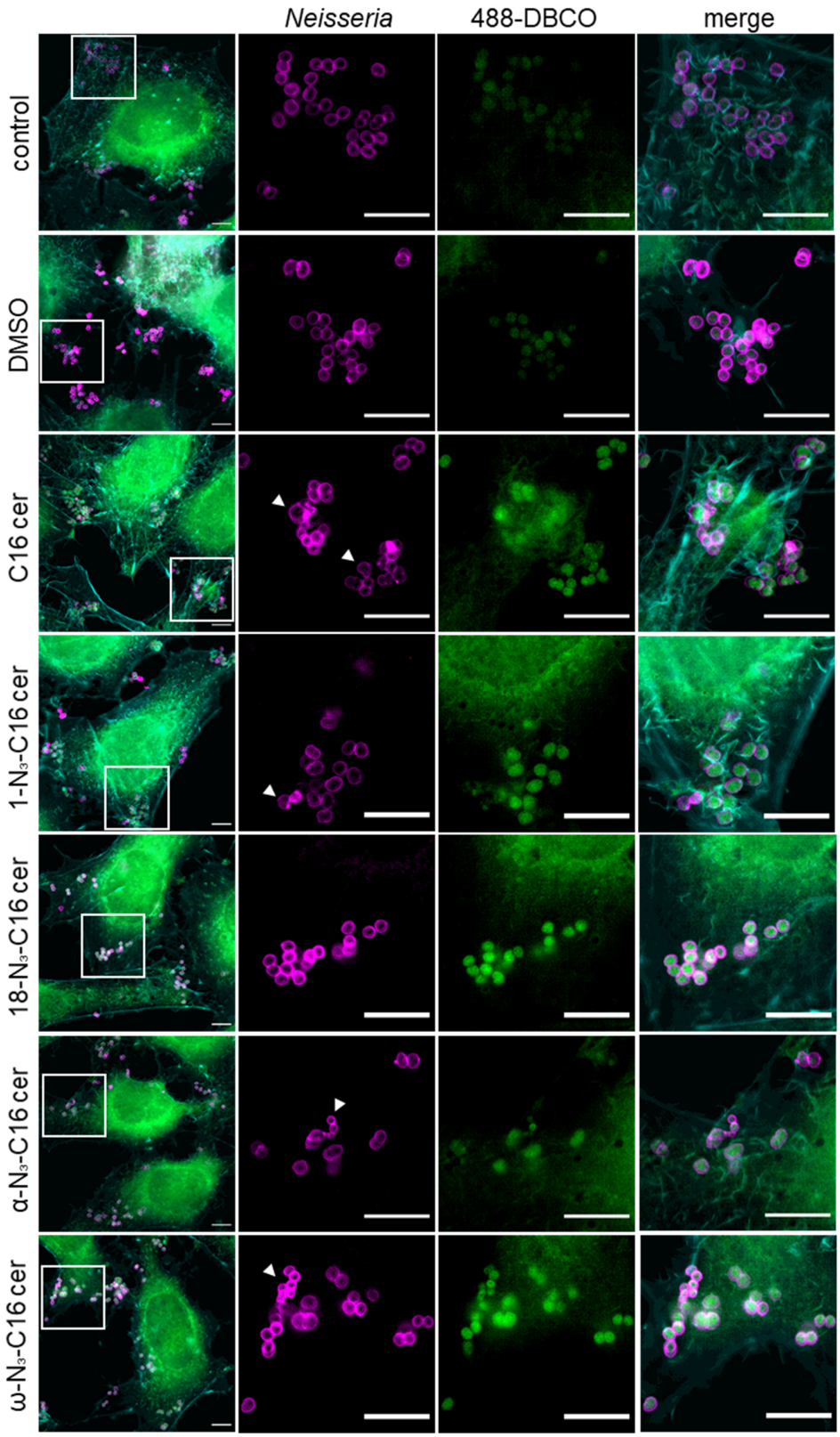
Neisseria
488-DBCO
merge
control
DMSO
C16 cer
1-N3-C16 cer
18-N3-C16 cer
α-N3-C16 cer
ω-N3-C16 cer

Figure 3.29 SIM pictures of C16 ceramide analogues in Chang cells infected with N927 for 4 hours.
The panels show Chang cells fed with different substances in advance before the infection with N927 for 4 hours. The highest panel serves as negative control (no feeding). Additionally, a solvent control (DMSO) and a control for the specificity of the click reaction (C6 cer) were included. The click reaction with 488-DBCO was performed after permeabilization with Triton-X. The pictures show the *Neisseria* antibody labelled in magenta and the clickable C16 analogues in green (488-DBCO). The merged microscopy pictures (outer left and right of each panel) show the actin cytoskeleton in cyan as well. White arrow heads indicate uncommon phenotypes of the gonococcal shape. The microscopy pictures were taken from one single experiment (n=1). The control and DMSO images are identical for Fig. 3.27, 3.29 and 3.32 because all chosen images are from the same set of samples. The white boxes mark the zoomed areas (magenta: N927, green: click reaction, cyan: actin cytoskeleton, scale bar: 5 µm). The microscopy images were taken by Dr. Tobias C. Kunz.

displayed a clicking signal inside of the cells but not in the gonococci after 4 hours of infection. This strongly indicated that the used dye was incorporated into cellular compartments due to the permeabilization but not into the bacteria. For the endogenous C16 ceramide a 488-DBCO signal was detected, even though there should be no click reaction be possible. This could be evidence that C16 ceramide disrupted the neisserial membrane to allow an incorporation of the dye as well as for C6 ceramide (Fig. 3.27). The intensity of the gonococcal DBCO-signals for the samples fed with 1-N_3-C16 ceramide and α-N_3-C16 ceramide were comparable to those of the C16 cer control. These samples displayed also a decreased antibody labelling against *Neisseria* compared to DMSO and C16 cer controls. An increase of the 488-DBCO intensity was detected for the 18-N_3-C16 ceramide and ω-N_3-C16 ceramide samples. Here, no changes in the immunolabelling of the gonococci were observed. All samples fed with C16 cer or one of its analogues displayed an abnormal gonococcal phenotype, meaning a loss of the typical gonococcal shape and reduction in size (indicated by the white arrowheads in Fig. 3.29). Accumulations of all analogues were detected inside the *Neisseria* but did not colocalize with the bacterial membrane. The same set of samples was also infected with N927 for 6 hours. All used analogues so far formed cellular vesicles, but in the case of 18-N_3-C16 ceramide a different phenotype could be detected (Fig. 3.30). These vesicles appeared to accumulate a strong *Neisseria* signal. Due to its intensity and constant microscopy parameters, an unspecific binding of the antibody was unlikely also since the control with C16 ceramide did not show such accumulations. The origin of these accumulations could not be determined because, as already mentioned, it was the observation of a single experiment. A possible explanation could be the degradation of gonococci during later infection times which would suggest an intracellular survival defect.

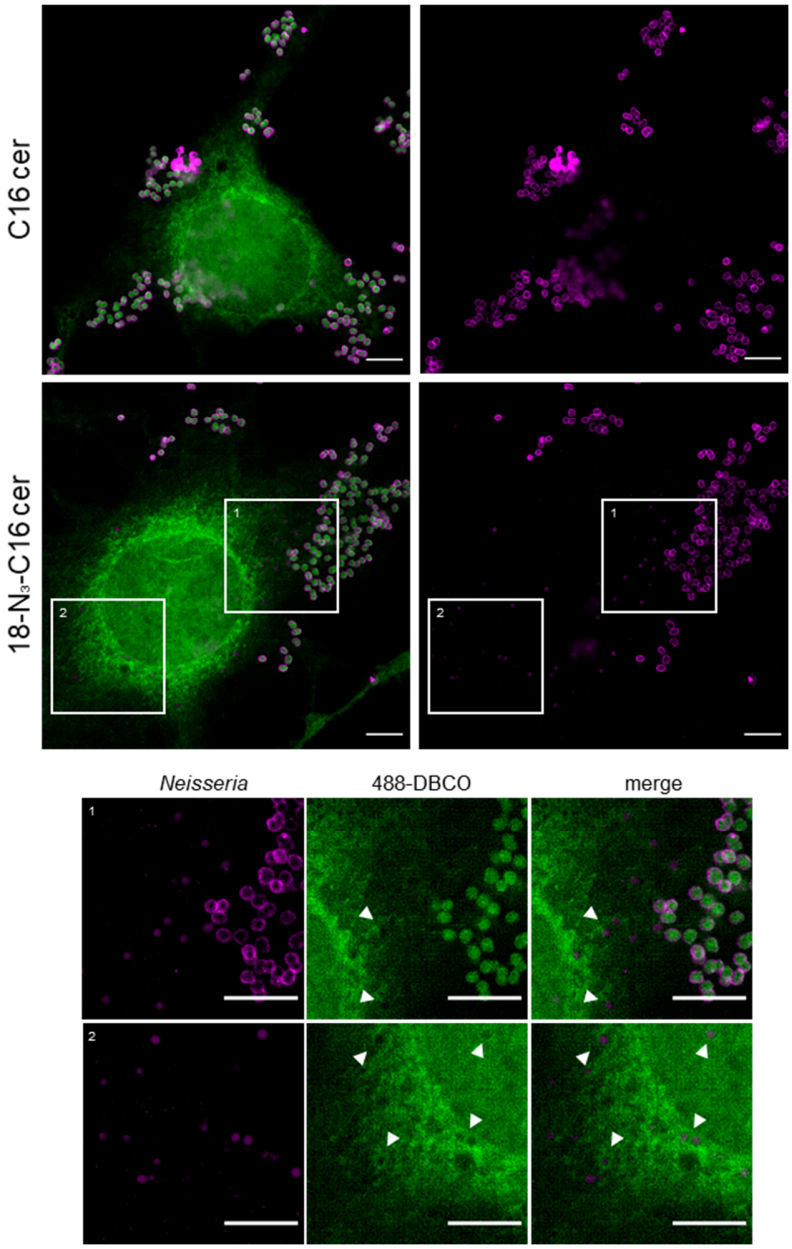

Figure 3.30 18-N_3-C16 ceramide vesicles accumulate neisserial particles after 6 hours of infection. Intracellular vesicles formed by 18-N_3-C16 ceramide accumulate strong neisserial signal only after 6 hours of infection. This phenotype was specific for this analogue but must be repeated to determine the origin of these specific vesicles. The pictures show the *Neisseria* antibody labelled in magenta. The C16 ceramide and 18-N_3-C16 ceramide analogue are shown in green (488-DBCO). White arrow heads indicate vesicles with fluorescence signal for *Neisseria* inside. The microscopy pictures were taken from one single experiment (n=1). The white boxes mark the zoomed areas (magenta: N927, green: click reaction, scale bar: 5 µm). The microscopy images were taken by Dr. Tobias C. Kunz.

3.2.3 Sphinganine

A lot of the sphingolipid research focuses on the implications of sphingosine. Since the exact mechanism is not elucidated yet, the usage of sphinganine and its clickable analogues (Fig. 3.31 A) might be a good starting point to shed some light since the only difference of both sphingolipids is the grade of saturation, i.e. sphinganine (dihydrosphingosine) is the fully saturated form of sphingosine. Firstly, the toxicity of sphinganine and its analogues (1-N_3-sphinganine and ω-N_3-sphinganine) were tested on the laboratory strain N927 *in vitro* (Fig. 3.31 B and C) to determine sub-toxic concentrations for further infection experiments in Chang cells (Fig. 3.31 D and Fig. 3.32). The growth curves of N927 either supplemented with the endogenous sphinganine (Fig. 3.31

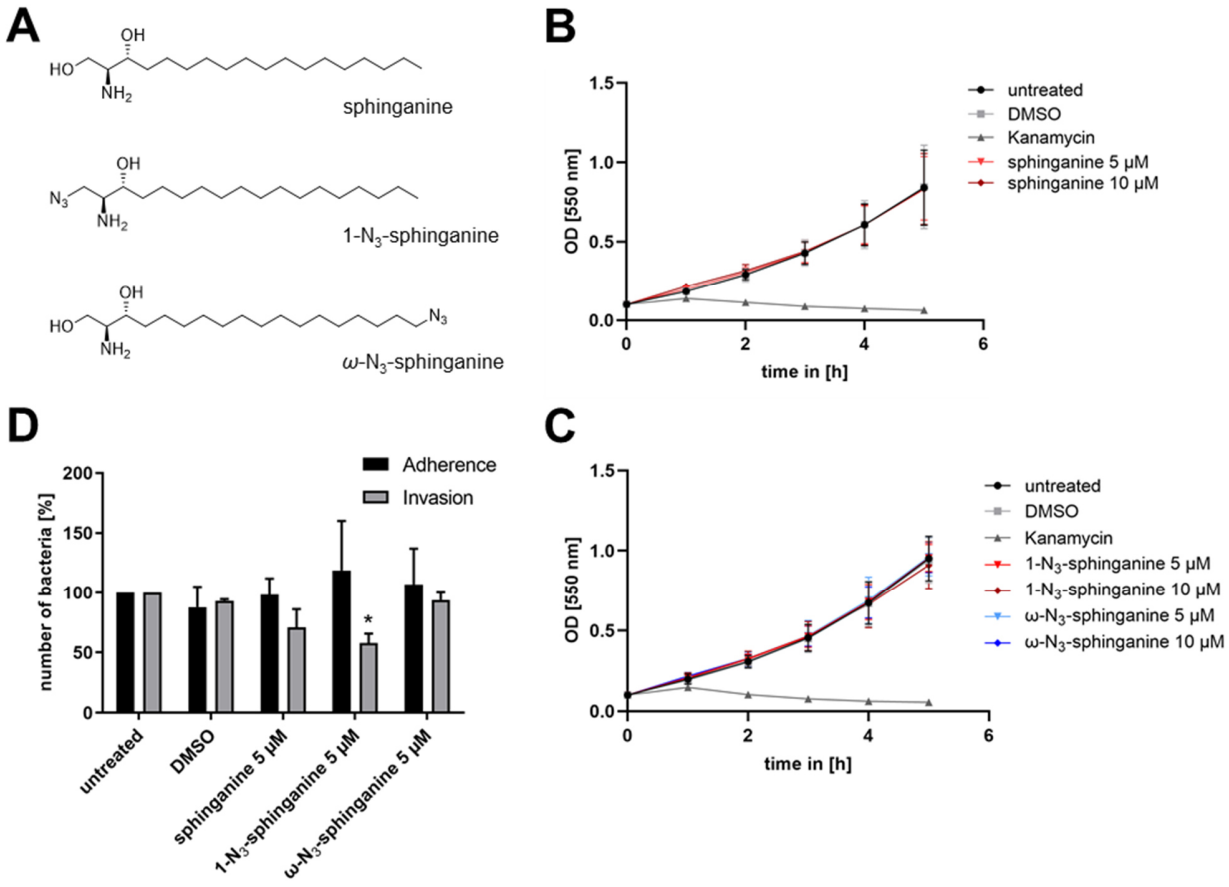

Figure 3.31 Effect of sphinganine and its clickable analogues on the in vitro growth and extra-/intracellular N927.
The structures of sphinganine and the clickable analogues (1-N_3-sphinganine and ω-N_3-sphinganine) are shown in (A). B) The toxicity of 5 µM and 10 µM endogenous sphinganine was tested on the *in vitro* growth of the neisserial strain N927. C) Growth curves were also performed with adding 5 µM or 10 µM of the clickable analogue to the liquid culture of N927. D) The effect of sphinganine analogues on the adherence and invasion efficiency of N927 was determined by performing gentamicin protection assays in Chang cells. Cells were pre-treated with 5 µM of each sphinganine analogue 30 minutes prior infection.
*p<0,05 student`s t-test relative to DMSO solvent control.

B) nor both analogues (Fig. 3.31 C) had impact on the replication of the bacteria at 5 µM and 10 µM. Because the highest concentration for fed ceramide was 5 µM, this concentration was resumed for further infection experiments with sphinganines. To do so, Chang cells were fed with DMSO as solvent control or the different sphinganine analogues at 5 µM prior to the infection with N927. The number of adherent and invasive gonococci was determined by performing gentamicin protection assays (Fig. 3.31 D). For both measured parameters DMSO had no effect on them compared to the untreated control. The sphinganine sample showed no alteration for the number of adherent *Neisseria* but a slight decrease in invasion. The results for both clickable analogues differ from these insofar as adherence was increased. Contrary, ω-N_3-sphinganine had no effect on the number of invasive bacteria whereas 1-N_3-sphinganine induced a significant reduction of about 50%. This brought up the question, if these observed effects were linked to differing uptake potentials of the sphinganine analogues on cellular and/or gonococcal level. To examine this question, super resolution microscopy (SIM) was performed to detect the uptake of the clickable analogues in the infection model of Chang cell with N927 (Fig. 3.32). The figure shows representative pictures of each treatment at 4 hours post infection of two independent experiments (n=2). As already seen for C6 and C16 ceramides, the controls for unfed, DMSO and the endogenous sphinganine showed cellular incorporation of the 488-DBCO dye but not to the same extent in gonococci. The intensity of the 488-DBCO signal of the 1-N_3-sphinganine samples did not differ from the endogenous sphingolipid control. In contrast, for ω-N_3-sphinganine an intense and distinct DBCO signal was detected which colocalized with the labelling of the anti-*Neisseria* antibody. This strongly suggested that only ω-N_3-sphinganine was taken up by the gonococci and got integrated in the bacterial membrane. The intensity of the *Neisseria*-signal was throughout all treatments comparable and no significant changes of the gonococcal shape were discovered. Besides the incorporation of ω-N_3-sphinganine, timepoints 2 hours post infection and 6 hours post infection did show distinctive features (Fig. 3.33). First, the colocalization of ω-N_3-sphinganine and neisserial membrane occurred already at 2 hours post infection and could be detected at 6 hours post infection as well. The incorporation of the sphinganine analogue did not hinder the replication of gonococci, since an increase in the number of bacteria was clearly visible during the infection time. Interestingly, at the timepoint 2 hours post infection ω-N_3-sphinganine formed distinct vesicles with a higher intensity of the 488-DBCO signal (white arrowheads in the middle panel pinpoint cellular vesicles, Fig. 3.33).

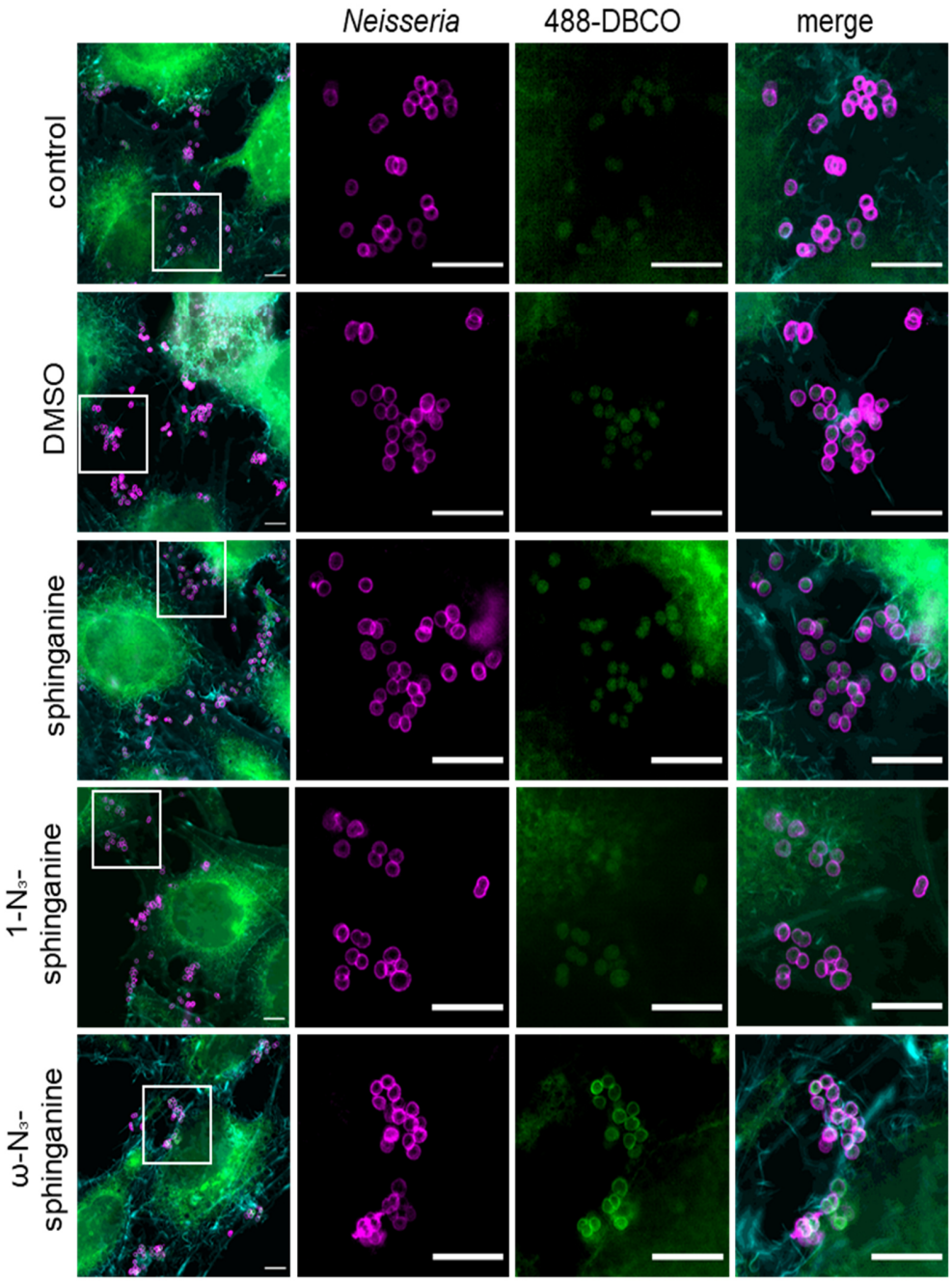

Figure 3.32 SIM pictures of sphinganine analogues in Chang cells infected with N927 for 4 hours.
Chang cells were fed with DMSO as solvent control or 5 µM of sphinganine analogue before infection with N927 for 4 hours. The highest panel shows the unfed control. The sphinganine sample serves as control for the click reaction. Clicking was performed with 488-DBCO after permeabilization. The pictures show the *Neisseria* antibody labelled in magenta and the clickable analogues in green (488-DBCO). The merged microscopy pictures (left and right column) show the actin cytoskeleton in cyan as well. Representative microscopy pictures of two independent experiments are shown (n=2). The control and DMSO images are identical for Fig. 3.27, 3.29 and 3.32 because all chosen images are from the same set of samples. The white boxes mark the zoomed areas (magenta: N927, green: click reaction, cyan: actin cytoskeleton, scale bar: 5 µm). The microscopy images were taken by Dr. Tobias C. Kunz.

These vesicles were not detected at 4 hours post infection (Fig. 3.32) and 6 hours post infection (Fig. 3.33), this might be due to technical reasons and unlikely to a vesicle formation at this specific time point. The time course also showed that ω-N_3-sphinganine accumulated stronger to the nucleus with longer incubation time. Due to the shape of the accumulated 488-DBCO-signal, sphinganine appeared to get stored in the endoplasmic reticulum.

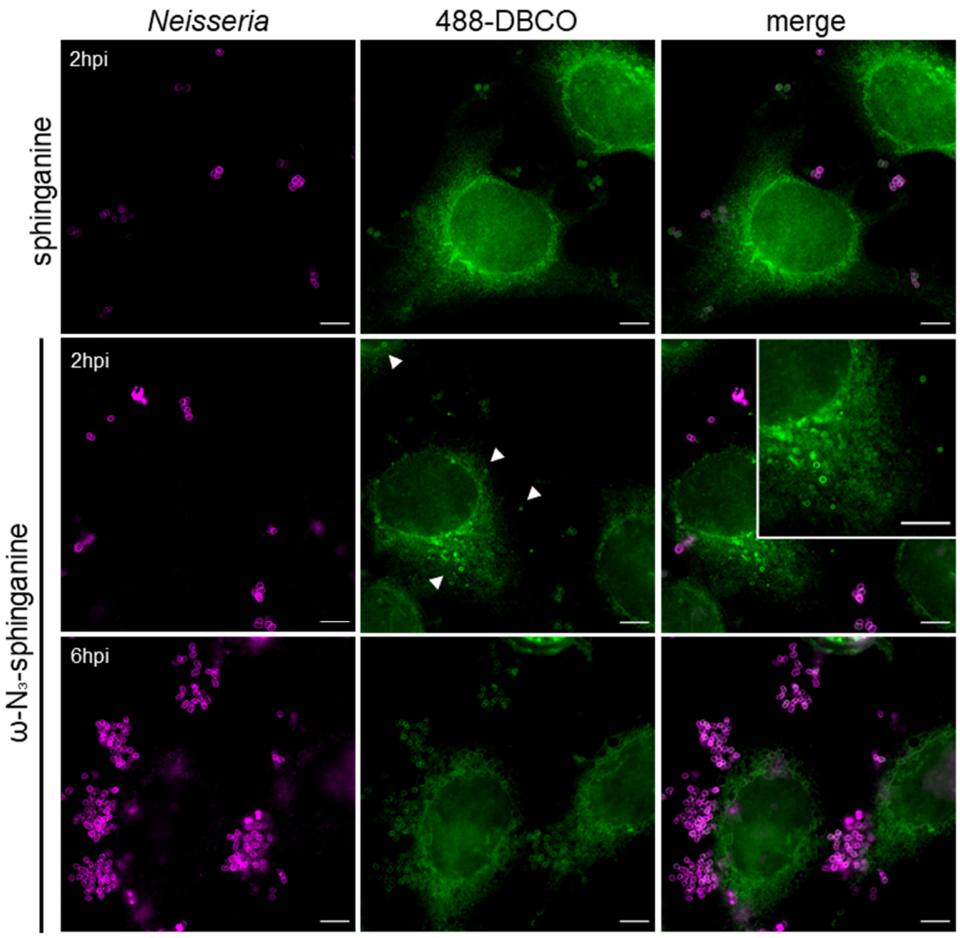

Figure 3.33 Accumulation and vesicle formation of ω-N_3-sphinganine throughout the course of infection.
After 2 hpi Chang cells fed with ω-N_3-sphinganine formed clearly visible, distinct vesicles (indicated by the white arrow heads). This phenotype could not be observed for the endogenous sphinganine samples. The timepoint 6 hpi showed a stronger accumulation of the clickable analogue, due to the shape probably in the endoplasmic reticulum. During the time course of infection *Neisseria* were able to replicate upon ω-N_3-sphinganine uptake (magenta: N927, green: click reaction, scale bar: 5 µm). The microscopy images were taken by Dr. Tobias C. Kunz.

4 Discussion

The importance of sphingolipids for different pathogenic bacteria in all stages of infection becomes clearer and clearer. In this study, a drastic reduction of intracellular *N. gonorrhoeae* was observed upon the inhibition of SphKs in epithelial cells. The host-cell derived sphingosine was identified as origin of this survival defect. Furthermore, intra- and extracellular sphingosine vesicles and their dynamic interplay with this pathogen were visualized. Additionally, this work tried to elucidate the roles of cellular sphingolipid classes and their different structural features. It appeared that different enzymes of the sphingolipid signaling pathway are more important to gonococci than others. This work focuses on SphKs, of which SphK2 might be more essential for the survival of invasive *Neisseria* in epithelial cells. It cannot be excluded that this specific enzyme might also play a role during neutrophil infection.

4.1 Neutrophil viability upon neisserial infection and inhibition of sphingolipid enzymes

PMNs are the first innate immune responders to phagocytose bacterial and fungal microorganisms (Borregaard, 2010; Kobayashi et al., 2018). All infections with gonococci result in a neutrophil influx independent of the anatomic site (Criss and Seifert, 2012). Gonorrhoeal exudates consist mainly of neutrophils, some of which have gonococci attached and internalized (Ovcinnikov and Delektorskij, 1971; Veale et al., 1979; Shafer and Rest, 1989; Cohen and Cannon, 1999). Viable gonococci can be cultured from the exudates, proofing the neisserial survival inside professional phagocytes (Hook and Holmes, 1985). It is suggested that this recruitment of neutrophils is used by *Neisseria* as a shuttle to secondary infection sites of their host (Criss and Seifert, 2012). Additionally, there is evidence of intracellular replication in neutrophils (Casey et al., 1979; Simons et al., 2005). To survive and replicate inside of PMNs, different mechanisms against the antimicrobial activities have been developed by this bacterium. One mechanism is to delay apoptosis in these short-living cells (Simons et al., 2006; Cho et al., 2020). Until now, it is not solved how gonococci exactly mediate this anti-apoptotic signalling. Since *N. gonorrhoeae* undergoes phase- and antigenic variation during infection, effects of virulence factors on the modulation of professional phagocytes were subjects of several studies (Lorenzen et al., 2000;

Johnson and Criss, 2011; Ball and Criss, 2013). Here, we compared four MS11 derivates (strains N924, N927, N931 and F3) expressing different combinations of porin, pili and opa (see Table 2.1) in their ability to delay apoptosis in freshly isolated human neutrophils (Fig. 3.1 A). All tested strains showed apoptotic delay and similar percentage of viable neutrophils at the measured timepoints of 24, 48 and 72 hpi which is surprising since a study by Simons et al. described a viability timeframe of the latest examined infection time at 24 hours (Simons et al., 2006). Reasons for this discrepancy are variable, for example incubation in a multiwell-plate or on a tumbler, infection medium, used MOI and strain. This experimental set-up on a rotary should be seen as preliminary for distinct questions concerning the interplay of gonococci and neutrophils, since this cell type is very sensitive in handling. Furthermore, differences at later time points and in the number of surviving internalized gonococci cannot be excluded. In future, parallel to flow cytometry analysis neutrophils infected with *Neisseria* should be plated to monitor the survival.

Because SMases are important components of neisserial invasion processes in non-professional phagocytes (Grassmé et al., 1997; Faulstich et al., 2015), we were wondering if this was also true for neutrophils. Different processes of neutrophil regulation are mediated by bioactive sphingolipids (Espaillat et al., 2017). During phagocytosis increased nSMase levels of the plasma membrane have been detected (Hinkovska-Galcheva et al., 1998). A role of aSMase activation in neutrophils has been observed during bacterial invasion (Managò et al., 2015), making both SMase isoforms interesting targets in gonococcal infection (Fig. 3.1 B and C). Since ceramide and S1P signalling plays a prominent role (Espaillat et al., 2017), together with the naturally high activity of SphKs in peripheral blood cells (Yang et al., 1999), the downstream salvage pathway was blocked as well. These inhibitory studies (Fig. 3.1 B and C) did not lead to clear and significant results but the treatment with the SphK2-inhibitor K145 could indicate for a pro-survival effect of SphK2 for *Neisseria* compared to the other inhibited enzymes aSMase, nSMase and SphK1. Because this effect is only observed in infected samples, the possibility of induced apoptosis by elevated sphingosine levels (Ohta et al., 1994) is most likely excluded. To make sure this is the case, mass spectrometry would need to be conducted. These infection experiments were performed only with the strain N927 in RPMI and is one limitation regarding the $PorB_{IA}$-dependent phosphate-sensitive invasion. To overcome this problem, this experiment should be repeated under low phosphate conditions by using Hepes medium and reducing the infection time.

4.2 Knock-down and redundancy of isozymes SphK1 and SphK2

To avoid possible off-target effects of the used inhibitors, the gene-editing technique of CRISPR/Cas9 was chosen to knockout the isozymes SphK1 and 2. The efficiency of the CRISPR/Cas9 deletions for SphK1 and 2 were checked by Sanger sequencing of different clones. All tested clones possessed an out-of-frame deletion, which led to the assumption of misfolded, unfunctional kinases. Furthermore, visible changes of the morphology and in growth behaviour of the chosen clones compared to WT Chang cells did strengthen this conclusion. The quantification of mRNA levels in the generated Chang cells did show a significant reduction of the respective kinase, but bulk of mRNA was still detectable, meaning a clean knockout failed (Fig. 3.2 A). Nevertheless, an interesting observation of the qPCR results is the redundancy of the SphKs. Even though these two isozymes catalyse the phosphorylation of sphingosine to S1P (Liu et al., 2000), they have opposing functions on cell growth and apoptosis with SphK1 promoting proliferation and SphK2 being pro-apoptotic (Maceyka et al., 2005). These opposite functions can be explained by the localization of both SphKs, meaning the compartment of S1P production determines the functionality (Maceyka et al., 2005). While SphK1 is mainly found in the cytoplasm (Wattenberg, 2010) or at the plasma membrane after activation (Pitson et al., 2003), SphK2 is predominantly found in the endoplasmic reticulum (Maceyka et al., 2005). Studies in knockout mice showed that a single SphK knockout did not cause abnormalities in these animals (Alemany et al., 2007; Zemann et al., 2007), whereas a double knockout for both SphKs is embryologically lethal (Mizugishi et al., 2005). Therefore, a shuttle of SphKs between subcellular compartments might be an explanation for this compensatory upregulation (Venkataraman et al., 2006; Hatoum et al., 2017). Nevertheless, infection experiments with N927 under low phosphate conditions were conducted with the CRISPR/Cas9-generated cell lines ΔSphK1 and ΔSphK2 (Fig. 3.2 B). Due to the compensatory role of the SphKs to each other, it is hard to tell if the genome-editing or overexpression causes the observed effects on invasion and adherence. To further examine the interplay of SphKs and *Neisseria*, haploid HAP1 cells were selected as candidate to generate knockouts with the assumption of being easier to apply compared to other cell lines with multiple chromosomal alterations. Before starting with genome-editing, infection experiments were performed with these cells (data not shown) and compared to previous results with the common infection model of Chang cells, displaying major differences in the invasion process of gonococci. Therefore, it was decided that all further infection experiments were conducted with the specific

inhibitors against SphKs or with the modified sphingosine analogue (1-N_3-sphingosine), which cannot be converted to S1P by SphK due to the position of the azido group (Fig. 3.13).

4.3 Sphingosine and *N. gonorrhoeae*

4.3.1 Intracellular survival defect of *Neisseria* and importance of SphKs

The involvement of SMases during neisserial infection has been established for different invasion mechanisms and cell types (Grassmé et al., 1997; Hauck et al., 2000; Faulstich et al., 2015). Here, the focus was on the downstream signalling pathway of ceramide, i.e. the sphingolipid salvage pathway (Fig. 1.4 B). Especially the role of sphingosine in infection was investigated by inhibiting the metabolization of sphingosine to S1P through the activity of SphKs. The inhibition of either one (5C and K145) or both SphKs (SKI-II) affected the intracellular survival of *Neisseria* in different infection models (Fig. 3.7 and 3.8). Together with CFU quantifications of the laboratory strain N927 treated with a subtoxic concentration of sphingosine, which showed a decrease in CFU formation (Hagen, 2017; Solger et al., 2020), suggesting sphingosine itself to be the cause for the decreased survival. Another interesting result of the inhibitor studies (Fig. 3.7 and 3.8) was the dependency of the intracellular survival on one particular SphK even though catalysing the same reaction. Both used strains, N927 and the clinical isolate, showed less survival in cells pre-treated with SphK2-inhibitor K145. Since both SphK isozymes have different physiological functions and localization in subcellular compartments as already mentioned (Spiegel and Milstien, 2007), it provides the possibility that *N. gonorrhoeae* developed a survival strategy by facilitating the activity of SphK2 for protection against cellular sphingosine. Recruitment of sphingolipids and corresponding enzymes are a powerful tool applied by different bacteria for invasion or intracellular survival (Kunz and Kozjak-Pavlovic, 2019; Rolando and Buchrieser, 2019).

For validation of sphingosine as cause for the survival defect, efficiency of the SphK inhibitors were checked by mass spectrometry (Fig. 3.9). This analysis was in line with the results of the inhibitor studies, that 5C did not alter intracellular sphingosine levels. Further mass spectrometric analysis provided changes of sphingolipids upstream of sphingosine (Fig. 3.10). The increase of C16 ceramide could be the result of upregulated ceramide synthase expressions to maintain the balance between sphingosine and ceramide. This balance is known as “sphingolipid rheostat”

(Cuvillier et al., 1996). If this regulatory process involves more classes of sphingolipids and ceramide species was not further determined. However, focusing on sphingosine, its toxicity was tested on different neisserial strains *in vitro*, including the laboratory strain N927 (Fig. 3.11) and clinical isolates from DGI (Fig. 3.12). The clinical isolates showed some heterogeneity in their susceptibility towards sphingosine but were more resistant compared to N927. An explanation for this observation could be that a certain resistance towards sphingosine is needed for invading the bloodstream and being challenged by neutrophils, which are able to take sphingosine up and metabolize it (Yang et al., 1999). Taken together, these results pinpoint to host-cell derived sphingosine as source for the observed survival defect. This hypothesis was strengthened by the differences in toxicity observed for the two sphingosine analogues 1-N_3- and ω-N_3-sphingosine (Fig. 3.22). Because 1-N_3-sphingosine cannot be phosphorylated by SphKs (Fig. 3.13), it had a comparable bactericidal effect on the gonococcal survival as the combination of SphK-inhibitor and ω-N_3-sphingosine (Fig. 3.22 D), confirming host cell derived sphingosine as source for this drastic effect. By using click chemistry of these novel sphingosine analogues a direct interaction between intra- and extracellular sphingosine and *N. gonorrhoeae* could have been visualized.

4.3.2 Equal integration of sphingosine into neisserial membrane

So far, sphingosine as source of the survival defect was identified but a direct connection between the pathogen and this sphingolipid was missing. Therefore, click chemistry was chosen to visualize and being able to track sphingosine in our neisserial infection model of Chang cells. The advantages of the chosen SPAAC reaction are the specificity, fast kinetics of labelling the target molecules and the broad range of applications, including SIM, ExM and live cell imaging. The analyses of the super-resolution microscopy images of both sphingosine analogues revealed an equal distribution of sphingosine in the neisserial membrane of different infection models (Fig. 3.18, 3.19 and 3.22). The next question was if sphingosine clusters into microdomains in the membrane (Bramkamp and Lopez, 2015). Therefore, a higher magnification was necessary which was achieved by applying 4x ExM (Fig. 3.20) (Götz et al., 2020). To do so, one essential requirement for expanding lipids is a primary amine. This functional group provides polymer-linkage to glutaraldehyde (GA) of the gel matrix (Chozinski et al., 2016), without that linkage the sphingolipids would be washed out during the following procedure of expansion. Sphingosine carries naturally a primary amine and

the azido modification of ω-N_3-sphingosine was introduced in a different position, making it a suitable candidate for ExM. The expansion of *Neisseria* verified the incorporation of ω-N_3-sphingosine into the bacterial membrane which displayed disruptions in the fluorescence of the immunolabeling and the clicking as well. This fragmentation could indicate the formation of microdomains, but it could also be based on the necessary step of digestion followed by hydrogel swelling during the sample preparation. To rule the second possibility out, the expansion of gonococci should be repeated with increase in sphingosine signal (for example clicking in parallel with the antibody immunolabeling) and in magnification factor of the expansion, since 10x ExM is already established (Truckenbrodt et al., 2018; Truckenbrodt et al., 2019; Götz et al., 2020). Additionally, it would be also interesting to see if the second derivate 1-N_3-sphingosine shows the same phenotype in expanded samples.

The live cell imaging revealed another fascinating aspect of the sphingosine uptake and incorporation, which occurs very fast (Fig. 3.21). The complete membrane staining was observed for both sphingosine analogues during the respective timeframe. For ω-N_3-sphingosine complete membrane staining of diplococci happened within 15 minutes (Video 2). The timeframe between two images could have been reduced to 5 minutes for 1-N_3-sphingosine (Video 1) which also appeared to be sufficient time for complete membrane staining increasing during the next minutes. This time frame should be minimized to investigate if the uptake and incorporation of sphingosine has a specific starting point in the gonococcal membrane. After this incorporation the loss of neisserial RFP-signal was observed, speaking for an efficient and fast killing of *Neisseria*.

The different approaches clearly demonstrate that the incorporation of sphingosine into the neisserial membrane appears to interfere with the intracellular survival. The exact uptake and killing mechanism of sphingosine is unknown, but the postulated theory of "microlesions" (Fischer et al., 2012) and the specific incorporation of azido-modified sphingolipids in the outer membrane of *N. meningitidis* (Peters et al., 2021) are in line with the observation, that *N. gonorrhoeae* integrated efficiently sphingosine into their membrane had reduced antibody labelling (Fig. 3.22). These sphingosine "microlesions" could be induced by formation of channels (Siskind et al., 2005) or permeabilizing bilayers containing phospholipids (Jiménez-Rojo et al., 2014), as it was shown in *Pseudomonas aeruginosa* and *Staphylococcus aureus* through the binding to cardiolipin in the bacterial plasma membrane (Verhaegh et al., 2020).

4.3.3 Formation of sphingosine vesicles as innate immune response

Although subtoxic concentration of sphingosine and its derivates were used for feeding, efficient killing of intracellular gonococci was observed as described in the previous sections. This observation can be explained by the formation of vesicles containing high concentrations of sphingosine (Fig. 3.23 A, Video 3). These vesicles appeared intracellularly (Fig. 3.23, Videos 3 and 4) as well extracellularly for both clickable analogues (Fig. 3.24, Videos 5 and 6). Both types of sphingosine vesicles attach to *N. gonorrhoeae* and stunningly once caught gonococci are not able to escape (Video 4-6). Video 4 impressively demonstrates the intracellular retraction of an escaping gonococcus and its subsequent killing mediated by the incorporation of sphingosine ("catch-and-kill"). As seen in the long-term infection experiments (Videos 5 and 6), the single RFP-neisserial signals get lost and proportionally the number of extracellular sphingosine vesicles increase over time. In general, extracellular vesicles can be categorized in ectosomes and exosomes (Kalluri and LeBleu, 2020), varying in size between 100-500 nm and 50-150 nm respectively (Meldolesi, 2018). These vesicles function as cargo for proteins, lipids, nucleic acids and other bioactive substances (Zhang et al., 2019; Zhang et al., 2020). Ectosomal vesicles are generated by budding of the plasma membrane, whereas exosomes have an endosomal origin (Kalluri and LeBleu, 2020). Since intracellular sphingosine vesicles appeared to be positive for the early endosomal marker Rab5 (Fig. 3.25 B, discussed further in the next section), this could lead to the speculation of an endosomal origin of the observed extracellular sphingosine vesicles and consequently could be categorized as exosomes. But this hypothesis needs to be further validated to fully characterize the origin and the released sphingosine vesicle itself.

Besides the observation of extracellular vesicles, the focus was more on the characterization of the intracellular sphingosine vesicles. Together with the indication of a direct vesicular transport to invasive *Neisseria* (Video 3), it was tried to classify the vesicles into the endosomal-lysosomal system which consists of the dynamically changing compartments of early endosomes, recycling endosomes, late endosomes and lysosome (Hu et al., 2015). The different endocytic compartments are characterized by the localization of Rab proteins (Pfeffer, 2013), which are not associated to lysosomes in contrast to LAMP1 proteins (Shearer and Petersen, 2019). The markers Rab5, Rab7 and LAMP1 were chosen for the characterization into classes of early endosome (Gorvel et al., 1991; Bucci et al., 1992), late endosome (Rink et al., 2005; Poteryaev et al., 2010) and lysosome (Eskelinen, 2006; Wartosch et al., 2015), respectively (Fig. 3.25, Videos 7-12). Other studies

investigating cellular sphingosine vesicles in this regard, defining these vesicles as late endosomes (Young et al., 2016; Lima et al., 2017). Rab7-positive vesicles were not detected in the presented results (Fig. 3.25 A), contrary a small percentage of ω-N_3-sphingosine vesicles were Rab5-positive (Fig. 3.25 B) and consequently classified as early endosomes. Rab5-positive early endosomes and earlier endocytic intermediates have been reported to recruit SphK1 (Shen et al., 2014). Live cell imaging could not confirm this observation, since for none of the markers any dynamics with and without the clicked sphingosine vesicles could have been observed (Videos 7-12). Since these experiments could have been performed only once or twice, the observation for early endosomes needs to be further validated also by other approaches, for example immunolabelling of marker proteins, pH indicator dyes or nanoprobes specific for the grade of acidification in the endo-/lysosomal compartments (Wang et al., 2017). The YFP-expressing cell lines had several drawbacks making it hard to detect colocalizations, either they overexpressed the tagged protein leading to LAMP1-accumulations inside the cell or YFP-expressing cells did not take up fluorescent dye (respective image Fig. 3.25 A). A lot of questions concerning this exciting topic of sphingosine vesicles remain open. The reported involvement of SphK1 in endocytic membrane trafficking (Shen et al., 2014; Young et al., 2016; Lima et al., 2017) could be connected to the decreased intracellular survival of *N. gonorrhoeae* and the role of SphK2 should be examined in this context. Furthermore, the fascinating mechanism of catching the pathogens needs to be investigated. This “catch-and-kill”-mechanism might be part of the innate immune response and could be a new therapeutic tool against intracellular pathogens.

4.4 Effect of ceramide and sphinganine analogues on invasive gonococci

Because the exact killing mechanism of sphingosine is not solved yet, clickable ceramide and sphinganine analogues were chosen to narrow structural features which mediate the uptake and incorporation into the neisserial membrane.

The *in vitro* growth curves of *N. gonorrhoeae* confirmed the higher toxicity of short-chain ceramides compared to long-chain ones except for the 1-N_3-C6 ceramide (Fig. 3.26 and 3.28). These results match with a previous study using partially the same ceramide derivates on the

pathogenic *Neisseria* species (Becam et al., 2017). The combination of click chemistry and SIM could not detect any incorporation of ceramides into neisserial membranes nor the formation of ceramide-rich platforms as described previous for bacteria and eukaryotic cells (Fig. 3.27 and 3.29) (Becam et al., 2017; Burgert et al., 2017). Nevertheless, 18-N_3-C6 ceramide vesicles occurred to have enclosed *Neisseria* particles to later infection time points (Fig. 3.30). Because of the distinct anti-*Neisseria* signal which colocalizes with ceramide vesicles and conventional immunolabeling in the same image, unspecific binding or other technical issues are most unlikely. Contrary to short-chain ceramides, both sphinganine analogues did not alter growth properties (Fig. 3.31) but only ω-N_3-sphinganine was incorporated into the neisserial membrane comparable to sphingosine probes (Fig. 3.32). For this specific derivate the formation of vesicles was observed, giving the possibility to speculate for a similar mechanism as for sphingosine. Unfortunately, the gentamicin protection assay demonstrated the opposite on invasive gonococci with a survival defect induced by 1-N_3-sphinganine (Fig. 3.31 D). Thus, making it hard to interpret and compare the results of the *in vitro* assays and the infection models. As proven for sphingosine analogues, the cellular sphingolipid metabolism can convert clickable analogues if the functional groups are not exchanged to an azide. Therefore, for example different cofactors and the actin cytoskeleton of the host cell do probably play an important role in the outcome. As seen for sphingosine, sphingolipids are involved in highly dynamic cellular processes, for example ceramide is required for exosome formation (Trajkovic et al., 2008). Therefore, it is not enough to observe the status quo in infections, the complex interplay of cellular vesicles containing sphingolipids with the pathogen must be examined under living conditions. However, mass spectrometry analyses might gain even more insights into the composition of sphingolipid-derived vesicles and associated enzymes.

The presented results demonstrate the diversity of sphingolipids and their derivates in relation to invasive *N. gonorrhoeae*. Furthermore, the action of associated enzymes should not be underestimated as seen for SphKs in neisserial infections. By visualizing four different sphingolipid species and their clickable analogues – sphinganine, C6 ceramide, C16 ceramide and sphingosine – structural features were identified to be important for neisserial uptake. These determining features are the size of the molecule, the double bond of the sphingoid backbone and the C1 hydroxyl group at the polar headgroup (Fig. 1.4 A).

4.5 Summary and perspective

Until now a direct link between the toxicity of sphingosine and intracellular pathogens was missing. This study was able to visualize the dynamics of cellular sphingosine vesicles and their ability to efficiently "catch-and-kill" invasive *Neisseria* resulting in decreased intracellular survival of this bacterium. This survival defect and uptake of sphingosine was validated for laboratory and clinical isolated strains of *N. gonorrhoeae* in different infection models, suggesting a universal eukaryotic defence mechanism. Additionally, extracellular vesicles were observed which displayed the same feature of tight attachment to gonococci. The observations made with the other investigated classes of sphingolipids tempt to speculate for similar mechanisms. All presented click chemistry experiments are not performed under physiological conditions due to the external feeding of the specific analogue. But this study provides a short overview of possible click chemistry applications and their advantages, describing it as a useful tool to explore the interaction dynamics of sphingolipids and the human pathogen *N. gonorrhoeae*.

Taken together, the presented data suggest that sphingolipids and especially sphingosine are important components of the host cell defence against bacteria. With regard to the emerging XDR and MDR gonococcal strains, synthesised sphingolipid analogues and the observed vesicles could be functionalized as a new therapeutic agent and versatile tool against bacterial infections as they are already as cancer treatments (Li et al., 2018; Shaw et al., 2018).

5 References

Adeolu, M., and Gupta, R.S. (2013). Phylogenomics and molecular signatures for the order Neisseriales: proposal for division of the order Neisseriales into the emended family Neisseriaceae and Chromobacteriaceae fam. nov. *Antonie Van Leeuwenhoek* 104**,** 1-24.

Agard, N.J., Prescher, J.A., and Bertozzi, C.R. (2004). A Strain-Promoted [3 + 2] Azide−Alkyne Cycloaddition for Covalent Modification of Biomolecules in Living Systems. *Journal of the American Chemical Society* 126**,** 15046-15047.

Alemany, R., Van Koppen, C.J., Danneberg, K., Ter Braak, M., and Meyer Zu Heringdorf, D. (2007). Regulation and functional roles of sphingosine kinases. *Naunyn-Schmiedeberg's Archives of Pharmacology* 374**,** 413-428.

Ball, L.M., and Criss, A.K. (2013). Constitutively Opa-expressing and Opa-deficient neisseria gonorrhoeae strains differentially stimulate and survive exposure to human neutrophils. *Journal of bacteriology* 195**,** 2982-2990.

Banhart, S., Schäfer, E.K., Gensch, J.-M., and Heuer, D. (2019). Sphingolipid Metabolism and Transport in Chlamydia trachomatis and Chlamydia psittaci Infections. *Frontiers in cell and developmental biology* 7**,** 223-223.

Bartke, N., and Hannun, Y.A. (2009). Bioactive sphingolipids: metabolism and function. *Journal of lipid research* 50 Suppl**,** S91-S96.

Bauer, F.J. (1997). Herstellung von PorB-Mutanten und Untersuchungen zur möglichen Rolle von PorB als Virulenzfaktor von *Neisseria gonorrhoeae*. *Dissertation, Eberhard Karls Universität Tübingen*.

Becam, J., Walter, T., Burgert, A., Schlegel, J., Sauer, M., Seibel, J., and Schubert-Unkmeir, A. (2017). Antibacterial activity of ceramide and ceramide analogs against pathogenic Neisseria. *Science Report* 7**,** 17627.

Bennett, J., Bratcher, H.B., Brehony, C., Harrison, O., and Maiden, M. (2013). The Genus Neisseria. *The Prokaryotes: Alphaproteobacteria and Betaproteobacteria***,** 881-900.

Besanceney-Webler, C., Jiang, H., Zheng, T., Feng, L., Soriano Del Amo, D., Wang, W., Klivansky, L.M., Marlow, F.L., Liu, Y., and Wu, P. (2011). Increasing the efficacy of bioorthogonal click reactions for bioconjugation: a comparative study. *Angewandte Chemie (International ed. in English)* 50**,** 8051-8056.

Bibel, D.J., Aly, R., and Shinefield, H.R. (1992). Antimicrobial activity of sphingosines. *Journal of Investigative Dermatology* 98**,** 269-273.

Bieberich, E. (2018). Sphingolipids and lipid rafts: Novel concepts and methods of analysis. *Chemistry and physics of lipids* 216**,** 114-131.

Biswas, G.D., Sox, T., Blackman, E., and Sparling, P.F. (1977). Factors affecting genetic transformation of Neisseria gonorrhoeae. *Journal of Bacteriology* 129**,** 983-992.

Blackman, M.L., Royzen, M., and Fox, J.M. (2008). Tetrazine ligation: fast bioconjugation based on inverse-electron-demand Diels-Alder reactivity. *Journal of the American Chemical Society* 130**,** 13518-13519.

Borregaard, N. (2010). Neutrophils, from marrow to microbes. *Immunity* 33**,** 657-670.

Bramkamp, M., and Lopez, D. (2015). Exploring the existence of lipid rafts in bacteria. *Microbiology and Molecular Biology Reviews* 79**,** 81-100.

Britigan, B.E., Cohen, M.S., and Sparling, P.F. (1985). Gonococcal infection: a model of molecular pathogenesis. *The New England Journal of Medicine* 312**,** 1683-1694.

Bucci, C., Parton, R.G., Mather, I.H., Stunnenberg, H., Simons, K., Hoflack, B., and Zerial, M. (1992). The small GTPase rab5 functions as a regulatory factor in the early endocytic pathway. *Cell* 70**,** 715-728.

Burgert, A., Schlegel, J., Bécam, J., Doose, S., Bieberich, E., Schubert-Unkmeir, A., and Sauer, M. (2017). Characterization of Plasma Membrane Ceramides by Super-Resolution Microscopy. *Angewandte Chemie (International ed. in English)* 56**,** 6131-6135.

Cannon, J.G., Buchanan, T.M., and Sparling, P.F. (1983). Confirmation of association of protein I serotype of Neisseria gonorrhoeae with ability to cause disseminated infection. *Infection and immunity* 40**,** 816-819.

Cartwright, K.A., Stuart, J.M., Jones, D.M., and Noah, N.D. (1987). The Stonehouse survey: nasopharyngeal carriage of meningococci and Neisseria lactamica. *Epidemiology and infection* 99**,** 591-601.

Casey, S.G., Veale, D.R., and Smith, H. (1979). Demonstration of intracellular growth of gonococci in human phagocytes using spectinomycin to kill extracellular organisms. *Journal of General Microbiology* 113**,** 395-398.

Chen, A., and Seifert, H.S. (2011). Neisseria gonorrhoeae-mediated inhibition of apoptotic signalling in polymorphonuclear leukocytes. *Infection and immunity* 79**,** 4447-4458.

Chen, Y., Liu, Y., Sullards, M.C., and Merrill, A.H. (2010). An Introduction to Sphingolipid Metabolism and Analysis by New Technologies. *NeuroMolecular Medicine* 12**,** 306-319.

Cho, C., Teghanemt, A., Apicella, M.A., and Nauseef, W.M. (2020). Modulation of phagocytosis-induced cell death of human neutrophils by Neisseria gonorrhoeae. *Journal of leukocyte biology* 108**,** 1543-1553.

Chozinski, T.J., Halpern, A.R., Okawa, H., Kim, H.-J., Tremel, G.J., Wong, R.O.L., and Vaughan, J.C. (2016). Expansion microscopy with conventional antibodies and fluorescent proteins. *Nature Methods* 13**,** 485-488.

Cohen, M.S., and Cannon, J.G. (1999). Human experimentation with Neisseria gonorrhoeae: progress and goals. *Journal of Infectious Diseases* 179 Suppl 2**,** S375-379.

Connell, T.D., Black, W.J., Kawula, T.H., Barritt, D.S., Dempsey, J.A., Kverneland, K., Jr., Stephenson, A., Schepart, B.S., Murphy, G.L., and Cannon, J.G. (1988). Recombination among protein II genes of Neisseria gonorrhoeae generates new coding sequences and increases structural variability in the protein II family. *Molecular Microbiology* 2**,** 227-236.

Coureuil, M., Join-Lambert, O., Lécuyer, H., Bourdoulous, S., Marullo, S., and Nassif, X. (2013). Pathogenesis of meningococcemia. *Cold Spring Harbor perspectives in medicine* 3**,** a012393.

Criss, A.K., and Seifert, H.S. (2012). A bacterial siren song: intimate interactions between Neisseria and neutrophils. *Nature Reviews Microbiology* 10**,** 178-190.

Cuvillier, O. (2002). Sphingosine in apoptosis signaling. *Biochimica et Biophysica Acta (BBA) - Molecular and Cell Biology of Lipids* 1585**,** 153-162.

Cuvillier, O., Pirianov, G., Kleuser, B., Vanek, P.G., Coso, O.A., Gutkind, S., and Spiegel, S. (1996). Suppression of ceramide-mediated programmed cell death by sphingosine-1-phosphate. *Nature* 381**,** 800-803.

Dehio, C., Gray-Owen, S.D., and Meyer, T.F. (1998). The role of neisserial Opa proteins in interactions with host cells. *Trends in Microbiology* 6**,** 489-495.

Dommerholt, J., Rutjes, F.P.J.T., and Van Delft, F.L. (2016). Strain-Promoted 1,3-Dipolar Cycloaddition of Cycloalkynes and Organic Azides. *Topics in Current Chemistry* 374**,** 16.

Ecdc (2019). Gonorrhoea. *Annual epidemiological report for 2017*.

Edwards, J.L., Shao, J.Q., Ault, K.A., and Apicella, M.A. (2000). Neisseria gonorrhoeae elicits membrane ruffling and cytoskeletal rearrangements upon infection of primary human endocervical and ectocervical cells. *Infection and immunity* 68**,** 5354-5363.

Elwell, C.A., Jiang, S., Kim, J.H., Lee, A., Wittmann, T., Hanada, K., Melancon, P., and Engel, J.N. (2011). Chlamydia trachomatis co-opts GBF1 and CERT to acquire host sphingomyelin for distinct roles during intracellular development. *PLoS pathogens* 7**,** e1002198-e1002198.

Eriksson, J., Eriksson, O.S., Maudsdotter, L., Palm, O., Engman, J., Sarkissian, T., Aro, H., Wallin, M., and Jonsson, A.-B. (2015). Characterization of motility and piliation in pathogenic Neisseria. *BMC microbiology* 15**,** 92-92.

Eskelinen, E.-L. (2006). Roles of LAMP-1 and LAMP-2 in lysosome biogenesis and autophagy. *Molecular Aspects of Medicine* 27**,** 495-502.

Espaillat, M.P., Kew, R.R., and Obeid, L.M. (2017). Sphingolipids in neutrophil function and inflammatory responses: Mechanisms and implications for intestinal immunity and inflammation in ulcerative colitis. *Advances in biological regulation* 63**,** 140-155.

Eyre, D.W., Sanderson, N.D., Lord, E., Regisford-Reimmer, N., Chau, K., Barker, L., Morgan, M., Newnham, R., Golparian, D., Unemo, M., Crook, D.W., Peto, T.E., Hughes, G., Cole, M.J., Fifer, H., Edwards, A., and Andersson, M.I. (2018). Gonorrhoea treatment failure caused by a Neisseria gonorrhoeae strain with combined ceftriaxone and high-level azithromycin resistance, England, February 2018. *Eurosurveillance* 23**,** 1800323.

Eyre, D.W., Town, K., Street, T., Barker, L., Sanderson, N., Cole, M.J., Mohammed, H., Pitt, R., Gobin, M., Irish, C., Gardiner, D., Sedgwick, J., Beck, C., Saunders, J., Turbitt, D., Cook, C., Phin, N., Nathan, B., Horner, P., and Fifer, H. (2019). Detection in the United Kingdom of the Neisseria gonorrhoeae FC428 clone, with ceftriaxone resistance and intermediate resistance to azithromycin, October to December 2018. *Euro surveillance : bulletin Europeen sur les maladies transmissibles = European communicable disease bulletin* 24**,** 1900147.

Faulstich, M., Böttcher, J.-P., Meyer, T.F., Fraunholz, M., and Rudel, T. (2013). Pilus Phase Variation Switches Gonococcal Adherence to Invasion by Caveolin-1-Dependent Host Cell Signaling. *PLOS Pathogens* 9**,** e1003373.

Faulstich, M., Hagen, F., Avota, E., Kozjak-Pavlovic, V., Winkler, A.C., Xian, Y., Schneider-Schaulies, S., and Rudel, T. (2015). Neutral sphingomyelinase 2 is a key factor for PorB-dependent invasion of Neisseria gonorrhoeae. *Cellular Microbiology* 17**,** 241-253.

Fichorova, R.N., Rheinwald, J.G., and Anderson, D.J. (1997). Generation of papillomavirus-immortalized cell lines from normal human ectocervical, endocervical, and vaginal epithelium that maintain expression of tissue-specific differentiation proteins. *Biology of Reproduction* 57**,** 847-855.

Fischer, C.L. (2020). Antimicrobial Activity of Host-Derived Lipids. *Antibiotics (Basel, Switzerland)* 9**,** 75.

Fischer, C.L., Drake, D.R., Dawson, D.V., Blanchette, D.R., Brogden, K.A., and Wertz, P.W. (2012). Antibacterial activity of sphingoid bases and fatty acids against Gram-positive and Gram-negative bacteria. *Antimicrobial Agents and Chemotherapy* 56**,** 1157-1161.

Fischer, C.L., Walters, K.S., Drake, D.R., Blanchette, D.R., Dawson, D.V., Brogden, K.A., and Wertz, P.W. (2013). Sphingoid bases are taken up by Escherichia coli and Staphylococcus aureus and induce ultrastructural damage. *Skin pharmacology and physiology* 26**,** 36-44.

French, K.J., Schrecengost, R.S., Lee, B.D., Zhuang, Y., Smith, S.N., Eberly, J.L., Yun, J.K., and Smith, C.D. (2003). Discovery and evaluation of inhibitors of human sphingosine kinase. *Cancer Research* 63**,** 5962-5969.

Futerman, A.H., and Hannun, Y.A. (2004). The complex life of simple sphingolipids. *EMBO Reports* 5**,** 777-782.

Gault, C.R., Obeid, L.M., and Hannun, Y.A. (2010). An overview of sphingolipid metabolism: from synthesis to breakdown. *Advances in experimental medicine and biology* 688**,** 1-23.

Gorvel, J.-P., Chavrier, P., Zerial, M., and Gruenberg, J. (1991). rab5 controls early endosome fusion in vitro. *Cell* 64**,** 915-925.

Götz, R., Kunz, T.C., Fink, J., Solger, F., Schlegel, J., Seibel, J., Kozjak-Pavlovic, V., Rudel, T., and Sauer, M. (2020). Nanoscale imaging of bacterial infections by sphingolipid expansion microscopy. *Nature Communications* 11**,** 6173.

Grassmé, H., Gulbins, E., Brenner, B., Ferlinz, K., Sandhoff, K., Harzer, K., Lang, F., and Meyer, T.F. (1997). Acidic Sphingomyelinase Mediates Entry of N. gonorrhoeae into Nonphagocytic Cells. *Cell* 91**,** 605-615.

Gulbins, A., Schumacher, F., Becker, K.A., Wilker, B., Soddemann, M., Boldrin, F., Müller, C.P., Edwards, M.J., Goodman, M., Caldwell, C.C., Kleuser, B., Kornhuber, J., Szabo, I., and Gulbins, E. (2018). Antidepressants regulate autophagy by targeting acid sphingomyelinase. *Molecular Psychiatry* 23**,** 2251-2251.

Haas, R., Schwarz, H., and Meyer, T.F. (1987). Release of soluble pilin antigen coupled with gene conversion in Neisseria gonorrhoeae. *Proceedings of the National Academy of Sciences of the United States of America* 84**,** 9079-9083.

Hackstadt, T., Scidmore, M.A., and Rockey, D.D. (1995). Lipid metabolism in Chlamydia trachomatis-infected cells: directed trafficking of Golgi-derived sphingolipids to the chlamydial inclusion. *Proceedings of the National Academy of Sciences of the United States of America* 92**,** 4877-4881.

Hagen, F. (2017). *Sphingolipids in gonococcal infection.* Julius-Maximilians-Universität Würzburg.

Hanada, K. (2005). Sphingolipids in infectious diseases. *Japanese Journal of Infectious Diseases* 58**,** 131-148.

Hatoum, D., Haddadi, N., Lin, Y., Nassif, N.T., and Mcgowan, E.M. (2017). Mammalian sphingosine kinase (SphK) isoenzymes and isoform expression: challenges for SphK as an oncotarget. *Oncotarget* 8**,** 36898-36929.

Hauck, C.R., Grassmé, H., Bock, J., Jendrossek, V., Ferlinz, K., Meyer, T.F., and Gulbins, E. (2000). Acid sphingomyelinase is involved in CEACAM receptor-mediated phagocytosis of Neisseria gonorrhoeae. *FEBS Letters* 478**,** 260-266.

Hauck, C.R., and Meyer, T.F. (2003). 'Small' talk: Opa proteins as mediators of Neisseria-host-cell communication. *Current Opinion in Microbiology* 6**,** 43-49.

Heckels, J.E. (1989). Structure and function of pili of pathogenic Neisseria species. *Clinical Microbiology Reviews* 2 Suppl**,** S66-73.

Hill, S.A., Masters, T.L., and Wachter, J. (2016). Gonorrhea - an evolving disease of the new millennium. *Microbial cell (Graz, Austria)* 3**,** 371-389.

Hinkovska-Galcheva, V., Kjeldsen, L., Mansfield, P.J., Boxer, L.A., Shayman, J.A., and Suchard, S.J. (1998). Activation of a Plasma Membrane–Associated Neutral Sphingomyelinase and Concomitant Ceramide Accumulation During IgG-Dependent Phagocytosis in Human Polymorphonuclear Leukocytes. *Blood* 91**,** 4761-4769.

Hook, E.W., 3rd, and Holmes, K.K. (1985). Gonococcal infections. *Annals of Internal Medicine* 102**,** 229-243.

Hu, Y.-B., Dammer, E.B., Ren, R.-J., and Wang, G. (2015). The endosomal-lysosomal system: from acidification and cargo sorting to neurodegeneration. *Translational neurodegeneration* 4**,** 18-18.

Humbert, M.V., and Christodoulides, M. (2019). Atypical, Yet Not Infrequent, Infections with Neisseria Species. *Pathogens* 9.

Jacobsson, S., Mason, C., Khan, N., Meo, P., and Unemo, M. (2020). High in vitro activity of DIS-73285, a novel antimicrobial with a new mechanism of action, against MDR and XDR Neisseria gonorrhoeae. *The Journal of antimicrobial chemotherapy* 75**,** 3244-3247.

Jarvis, G.A., and Chang, T.L. (2012). Modulation of HIV transmission by Neisseria gonorrhoeae: molecular and immunological aspects. *Current HIV research* 10**,** 211-217.

Jennison, A.V., Whiley, D., Lahra, M.M., Graham, R.M., Cole, M.J., Hughes, G., Fifer, H., Andersson, M., Edwards, A., and Eyre, D. (2019). Genetic relatedness of ceftriaxone-resistant and high-level azithromycin resistant Neisseria gonorrhoeae cases, United Kingdom and Australia, February to April 2018. *Eurosurveillance* 24**,** 1900118.

Jiménez-Rojo, N., Sot, J., Viguera, A.R., Collado, M.I., Torrecillas, A., Gómez-Fernández, J.C., Goñi, F.M., and Alonso, A. (2014). Membrane permeabilization induced by sphingosine: effect of negatively charged lipids. *Biophysical journal* 106**,** 2577-2584.

Johnson, M.B., Ball, L.M., Daily, K.P., Martin, J.N., Columbus, L., and Criss, A.K. (2015). Opa+ Neisseria gonorrhoeae exhibits reduced survival in human neutrophils via Src family kinase-mediated bacterial trafficking into mature phagolysosomes. *Cellular Microbiology* 17**,** 648-665.

Johnson, M.B., and Criss, A.K. (2011). Resistance of Neisseria gonorrhoeae to neutrophils. *Frontiers in microbiology* 2**,** 77-77.

Kalluri, R., and Lebleu, V.S. (2020). The biology, function and biomedical applications of exosomes. *Science* 367**,** eaau6977.

Kirkcaldy, R.D., Weston, E., Segurado, A.C., and Hughes, G. (2019). Epidemiology of gonorrhoea: a global perspective. *Sexual health* 16**,** 401-411.

Kobayashi, S.D., Malachowa, N., and Deleo, F.R. (2018). Neutrophils and Bacterial Immune Evasion. *Journal of Innate Immunity* 10**,** 432-441.

Koch-Edelmann, S., Banhart, S., Saied, E.M., Rose, L., Aeberhard, L., Laue, M., Doellinger, J., Arenz, C., and Heuer, D. (2017). The cellular ceramide transport protein CERT promotes Chlamydia psittaci infection and controls bacterial sphingolipid uptake. *Cellular Microbiology* 19.

Kojima, N., Davey, D.J., and Klausner, J.D. (2016). Pre-exposure prophylaxis for HIV infection and new sexually transmitted infections among men who have sex with men. *Aids* 30**,** 2251-2252.

Kolb, H.C., Finn, M.G., and Sharpless, K.B. (2001). Click Chemistry: Diverse Chemical Function from a Few Good Reactions. *Angewandte Chemie International Edition English* 40**,** 2004-2021.

Kühlewein, C., Rechner, C., Meyer, T.F., and Rudel, T. (2006). Low-phosphate-dependent invasion resembles a general way for Neisseria gonorrhoeae to enter host cells. *Infection and immunity* 74**,** 4266-4273.

Kunz, A.N., Begum, A.A., Wu, H., D'ambrozio, J.A., Robinson, J.M., Shafer, W.M., Bash, M.C., and Jerse, A.E. (2012). Impact of fluoroquinolone resistance mutations on gonococcal fitness and in vivo selection for compensatory mutations. *The Journal of infectious diseases* 205**,** 1821-1829.

Kunz, T.C., Götz, R., Sauer, M., and Rudel, T. (2019). Detection of Chlamydia Developmental Forms and Secreted Effectors by Expansion Microscopy. *Frontiers in Cellular and Infection Microbiology* 9**,** 276.

Kunz, T.C., and Kozjak-Pavlovic, V. (2019). Diverse Facets of Sphingolipid Involvement in Bacterial Infections. *Frontiers in cell and developmental biology* 7**,** 203-203.

Leonard, C.A., Schoborg, R.V., Low, N., Unemo, M., and Borel, N. (2019). Pathogenic Interplay Between Chlamydia trachomatis and Neisseria gonorrhoeae that Influences Management and Control Efforts—More Questions than Answers? *Current Clinical Microbiology Reports* 6**,** 182-191.

Li, C., Wang, A., Wu, Y., Gulbins, E., Grassmé, H., and Zhao, Z. (2019). Acid Sphingomyelinase-Ceramide System in Bacterial Infections. *Cellular Physiology & Biochemistry* 52**,** 280-301.

Li, G., Liu, D., Kimchi, E.T., Kaifi, J.T., Qi, X., Manjunath, Y., Liu, X., Deering, T., Avella, D.M., Fox, T., Rockey, D.C., Schell, T.D., Kester, M., and Staveley-O'carroll, K.F. (2018). Nanoliposome C6-Ceramide Increases the Anti-tumor Immune Response and Slows Growth of Liver Tumors in Mice. *Gastroenterology* 154**,** 1024-1036.e1029.

Lim, Y., Shiver, A.L., Khariton, M., Lane, K.M., Ng, K.M., Bray, S.R., Qin, J., Huang, K.C., and Wang, B. (2019). Mechanically resolved imaging of bacteria using expansion microscopy. *PLoS Biology* 17**,** e3000268.

Lima, S., Milstien, S., and Spiegel, S. (2017). Sphingosine and Sphingosine Kinase 1 Involvement in Endocytic Membrane Trafficking. *Journal of Biological Chemistry* 292**,** 3074-3088.

Liu, H., Sugiura, M., Nava, V.E., Edsall, L.C., Kono, K., Poulton, S., Milstien, S., Kohama, T., and Spiegel, S. (2000). Molecular Cloning and Functional Characterization of a Novel Mammalian Sphingosine Kinase Type 2 Isoform *. *Journal of Biological Chemistry* 275**,** 19513-19520.

Liu, K., Guo, T.L., Hait, N.C., Allegood, J., Parikh, H.I., Xu, W., Kellogg, G.E., Grant, S., Spiegel, S., and Zhang, S. (2013). Biological characterization of 3-(2-amino-ethyl)-5-[3-(4-butoxyl-phenyl)-propylidene]-thiazolidine-2,4-dione (K145) as a selective sphingosine kinase-2 inhibitor and anticancer agent. *PLoS One* 8**,** e56471.

Livak, K.J., and Schmittgen, T.D. (2001). Analysis of relative gene expression data using real-time quantitative PCR and the 2(-Delta Delta C(T)) Method. *Methods* 25**,** 402-408.

Lorenzen, D.R., Günther, D., Pandit, J., Rudel, T., Brandt, E., and Meyer, T.F. (2000). Neisseria gonorrhoeae porin modifies the oxidative burst of human professional phagocytes. *Infection and immunity* 68**,** 6215-6222.

Maceyka, M., Sankala, H., Hait, N.C., Le Stunff, H., Liu, H., Toman, R., Collier, C., Zhang, M., Satin, L.S., Merrill, A.H., Jr., Milstien, S., and Spiegel, S. (2005). SphK1 and SphK2, Sphingosine Kinase Isoenzymes with Opposing Functions in Sphingolipid Metabolism *. *Journal of Biological Chemistry* 280**,** 37118-37129.

Maceyka, M., and Spiegel, S. (2014). Sphingolipid metabolites in inflammatory disease. *Nature* 510**,** 58-67.

Makino, S., Van Putten, J.P., and Meyer, T.F. (1991). Phase variation of the opacity outer membrane protein controls invasion by Neisseria gonorrhoeae into human epithelial cells. *The EMBO journal* 10**,** 1307-1315.

Managò, A., Becker, K.A., Carpinteiro, A., Wilker, B., Soddemann, M., Seitz, A.P., Edwards, M.J., Grassmé, H., Szabò, I., and Gulbins, E. (2015). Pseudomonas aeruginosa pyocyanin induces neutrophil death via mitochondrial reactive oxygen species and mitochondrial acid sphingomyelinase. *Antioxidants & redox signaling* 22**,** 1097-1110.

Meldolesi, J. (2018). Exosomes and Ectosomes in Intercellular Communication. *Current Biology* 28**,** R435-r444.

Mizugishi, K., Yamashita, T., Olivera, A., Miller, G.F., Spiegel, S., and Proia, R.L. (2005). Essential role for sphingosine kinases in neural and vascular development. *Molecular and Cellular Biology* 25**,** 11113-11121.

Morrow, G.L., and Abbott, R.L. (1998). Conjunctivitis. *American Family Physician* 57**,** 735-746.

Morse, S.A., Johnson, S.R., Biddle, J.W., and Roberts, M.C. (1986). High-level tetracycline resistance in Neisseria gonorrhoeae is result of acquisition of streptococcal tetM determinant. *Antimicrobial agents and chemotherapy* 30**,** 664-670.

Mosleh, I.M., Huber, L.A., Steinlein, P., Pasquali, C., Günther, D., and Meyer, T.F. (1998). Neisseria gonorrhoeae porin modulates phagosome maturation. *Journal of Biological Chemistry* 273**,** 35332-35338.

Naser, E., Kadow, S., Schumacher, F., Mohamed, Z.H., Kappe, C., Hessler, G., Pollmeier, B., Kleuser, B., Arenz, C., Becker, K.A., Gulbins, E., and Carpinteiro, A. (2020). Characterization of the small molecule ARC39, a direct and specific inhibitor of acid sphingomyelinase in vitro. *J Lipid Res*.

Neto, A., Sevilha, J., Seabra, D., Oliveira, I., Santos, R.P., Andrade, A., Pinho, P., Costa, P.M., Viana, M., and Pinto, P. (2021). Acute Aortic Regurgitation Due to Endocarditis Caused by Disseminated Gonococcal Infection: A Case Report. *Sexually Transmitted Diseases* 48**,** e48-e50.

Ohta, H., Yatomi, Y., Sweeney, E.A., Hakomori, S., and Igarashi, Y. (1994). A possible role of sphingosine in induction of apoptosis by tumor necrosis factor-alpha in human neutrophils. *FEBS Letters* 355**,** 267-270.

Olayemi, G., Oferczak, M., Elagizi, A., El-Abbassi, I., Eschete, M., and Crowe, J. (2017). Gonococcal Endocarditis: The Gift That Stops Giving! An Uncommon Presentation of a Common Disease. *Journal of the Louisiana State Medical Society* 169**,** 47.

Oliveira, B.L., Guo, Z., and Bernardes, G.J.L. (2017). Inverse electron demand Diels–Alder reactions in chemical biology. *Chemical Society Reviews* 46**,** 4895-4950.

Olivera, A., and Spiegel, S. (1993). Sphingosine-1-phosphate as second messenger in cell proliferation induced by PDGF and FCS mitogens. *Nature* 365**,** 557-560.

Ovcinnikov, N.M., and Delektorskij, V.V. (1971). Electron microscope studies of gonococci in the urethral secretions of patients with gonorrhoea. *The British journal of venereal diseases* 47**,** 419-439.

Palmer, A., and Criss, A.K. (2018). Gonococcal Defenses against Antimicrobial Activities of Neutrophils. *Trends in microbiology* 26**,** 1022-1034.

Peters, S., Kaiser, L., Fink, J., Schumacher, F., Perschin, V., Schlegel, J., Sauer, M., Stigloher, C., Kleuser, B., Seibel, J., and Schubert-Unkmeir, A. (2021). Click-correlative light and electron microscopy (click-AT-CLEM) for imaging and tracking azido-functionalized sphingolipids in bacteria. *Scientific Reports* 11**,** 4300.

Peters, S., Schlegel, J., Becam, J., Avota, E., Sauer, M., and Schubert-Unkmeir, A. (2019). Neisseria meningitidis Type IV Pili Trigger Ca(2+)-Dependent Lysosomal Trafficking of the Acid Sphingomyelinase To Enhance Surface Ceramide Levels. *Infection and immunity* 87**,** e00410-00419.

Pfeffer, S.R. (2013). Rab GTPase regulation of membrane identity. *Current Opinion in Cell Biology* 25**,** 414-419.

Phillips, I. (1976). Beta-lactamase-producing, penicillin-resistant gonococcus. *Lancet* 2**,** 656-657.

Pitson, S.M., Moretti, P.A., Zebol, J.R., Lynn, H.E., Xia, P., Vadas, M.A., and Wattenberg, B.W. (2003). Activation of sphingosine kinase 1 by ERK1/2-mediated phosphorylation. *EMBO Journal* 22**,** 5491-5500.

Poteryaev, D., Datta, S., Ackema, K., Zerial, M., and Spang, A. (2010). Identification of the Switch in Early-to-Late Endosome Transition. *Cell* 141**,** 497-508.

Pralhada Rao, R., Vaidyanathan, N., Rengasamy, M., Mammen Oommen, A., Somaiya, N., and Jagannath, M.R. (2013). Sphingolipid metabolic pathway: an overview of major roles played in human diseases. *Journal of lipids* 2013**,** 178910-178910.

Quillin, S.J., and Seifert, H.S. (2018). Neisseria gonorrhoeae host adaptation and pathogenesis. *Nature reviews. Microbiology* 16**,** 226-240.

Ran, F.A., Hsu, P.D., Wright, J., Agarwala, V., Scott, D.A., and Zhang, F. (2013). Genome engineering using the CRISPR-Cas9 system. *Nat Protoc* 8**,** 2281-2308.

Rechner, C., Kühlewein, C., Müller, A., Schild, H., and Rudel, T. (2007). Host glycoprotein Gp96 and scavenger receptor SREC interact with PorB of disseminating Neisseria gonorrhoeae in an epithelial invasion pathway. *Cell Host & Microbe* 2**,** 393-403.

Rice, P.A. (2005). Gonococcal arthritis (disseminated gonococcal infection). *Infectious Disease Clinics of North America* 19**,** 853-861.

Rink, J., Ghigo, E., Kalaidzidis, Y., and Zerial, M. (2005). Rab Conversion as a Mechanism of Progression from Early to Late Endosomes. *Cell* 122**,** 735-749.

Robertson, D.K., Gu, L., Rowe, R.K., and Beatty, W.L. (2009). Inclusion biogenesis and reactivation of persistent Chlamydia trachomatis requires host cell sphingolipid biosynthesis. *PLoS pathogens* 5**,** e1000664-e1000664.

Rolando, M., and Buchrieser, C. (2019). A Comprehensive Review on the Manipulation of the Sphingolipid Pathway by Pathogenic Bacteria. *Frontiers in cell and developmental biology* 7**,** 168-168.

Rollin-Pinheiro, R., Singh, A., Barreto-Bergter, E., and Del Poeta, M. (2016). Sphingolipids as targets for treatment of fungal infections. *Future medicinal chemistry* 8**,** 1469-1484.

Rouquette-Loughlin, C.E., Reimche, J.L., Balthazar, J.T., Dhulipala, V., Gernert, K.M., Kersh, E.N., Pham, C.D., Pettus, K., Abrams, A.J., Trees, D.L., St Cyr, S., and Shafer, W.M. (2018). Mechanistic Basis for Decreased Antimicrobial Susceptibility in a Clinical Isolate of Neisseria gonorrhoeae Possessing a Mosaic-Like mtr Efflux Pump Locus. *mBio* 9**,** e02281-02218.

Rowley, J., Vander Hoorn, S., Korenromp, E., Low, N., Unemo, M., Abu-Raddad, L.J., Chico, R.M., Smolak, A., Newman, L., Gottlieb, S., Thwin, S.S., Broutet, N., and Taylor, M.M. (2019). Chlamydia, gonorrhoea, trichomoniasis and syphilis: global prevalence and incidence estimates, 2016. *Bulletin of the World Health Organization* 97**,** 548-562P.

Sakamoto, H., Okamoto, K., Aoki, M., Kato, H., Katsume, A., Ohta, A., Tsukuda, T., Shimma, N., Aoki, Y., Arisawa, M., Kohara, M., and Sudoh, M. (2005). Host sphingolipid biosynthesis as a target for hepatitis C virus therapy. *Nature Chemical Biology* 1**,** 333-337.

Sandstrom, E.G., Chen, K.C., and Buchanan, T.M. (1982). Serology of Neisseria gonorrhoeae: coagglutination serogroups WI and WII/III correspond to different outer membrane protein I molecules. *Infection and Immunity* 38**,** 462-470.

Shafer, W.M., and Rest, R.F. (1989). Interactions of gonococci with phagocytic cells. *Annual Review of Microbiology* 43**,** 121-145.

Shaw, J., Costa-Pinheiro, P., Patterson, L., Drews, K., Spiegel, S., and Kester, M. (2018). Novel Sphingolipid-Based Cancer Therapeutics in the Personalized Medicine Era. *Advances in cancer research* 140**,** 327-366.

Shearer, L.J., and Petersen, N.O. (2019). Distribution and Co-localization of endosome markers in cells. *Heliyon* 5**,** e02375.

Shen, H., Giordano, F., Wu, Y., Chan, J., Zhu, C., Milosevic, I., Wu, X., Yao, K., Chen, B., Baumgart, T., Sieburth, D., and De Camilli, P. (2014). Coupling between endocytosis and sphingosine kinase 1 recruitment. *Nature cell biology* 16**,** 652-662.

Simonis, A., Hebling, S., Gulbins, E., Schneider-Schaulies, S., and Schubert-Unkmeir, A. (2014). Differential activation of acid sphingomyelinase and ceramide release determines invasiveness of Neisseria meningitidis into brain endothelial cells. *PLoS pathogens* 10**,** e1004160-e1004160.

Simons, K., and Ikonen, E. (1997). Functional rafts in cell membranes. *Nature* 387**,** 569-572.

Simons, M.P., Nauseef, W.M., and Apicella, M.A. (2005). Interactions of Neisseria gonorrhoeae with adherent polymorphonuclear leukocytes. *Infection and Immunity* 73**,** 1971-1977.

Simons, M.P., Nauseef, W.M., Griffith, T.S., and Apicella, M.A. (2006). Neisseria gonorrhoeae delays the onset of apoptosis in polymorphonuclear leukocytes. *Cellular Microbiology* 8**,** 1780-1790.

Siskind, L.J., Fluss, S., Bui, M., and Colombini, M. (2005). Sphingosine forms channels in membranes that differ greatly from those formed by ceramide. *Journal of Bioenergetics and Biomembranes* 37**,** 227-236.

Solger, F., Kunz, T.C., Fink, J., Paprotka, K., Pfister, P., Hagen, F., Schumacher, F., Kleuser, B., Seibel, J., and Rudel, T. (2020). A Role of Sphingosine in the Intracellular Survival of Neisseria gonorrhoeae. *Frontiers in Cellular and Infection Microbiology* 10.

Song, W., Ma, L., Chen, R., and Stein, D.C. (2000). Role of lipooligosaccharide in Opa-independent invasion of Neisseria gonorrhoeae into human epithelial cells. *The Journal of experimental medicine* 191**,** 949-960.

Spiegel, S., and Milstien, S. (2003). Sphingosine-1-phosphate: an enigmatic signalling lipid. *Nature Reviews Molecular Cell Biology* 4**,** 397-407.

Spiegel, S., and Milstien, S. (2007). Functions of the Multifaceted Family of Sphingosine Kinases and Some Close Relatives *. *Journal of Biological Chemistry* 282**,** 2125-2129.

Stohl, E.A., Dale, E.M., Criss, A.K., and Seifert, H.S. (2013). Neisseria gonorrhoeae metalloprotease NGO1686 is required for full piliation, and piliation is required for resistance to H2O2- and neutrophil-mediated killing. *mBio* 4**,** e00399-00313.

Suay-García, B., and Pérez-Gracia, M.T. (2018). Future Prospects for Neisseria gonorrhoeae Treatment. *Antibiotics (Basel, Switzerland)* 7**,** 49.

Tachida, Y., Kumagai, K., Sakai, S., Ando, S., Yamaji, T., and Hanada, K. (2020). Chlamydia trachomatis-infected human cells convert ceramide to sphingomyelin without sphingomyelin synthases 1 and 2. *FEBS Letters* 594**,** 519-529.

Tapsall, J.W. (2009). Neisseria gonorrhoeae and emerging resistance to extended spectrum cephalosporins. *Current Opinion in Infectious Diseases* 22**,** 87-91.

Trajkovic, K., Hsu, C., Chiantia, S., Rajendran, L., Wenzel, D., Wieland, F., Schwille, P., Brügger, B., and Simons, M. (2008). Ceramide triggers budding of exosome vesicles into multivesicular endosomes. *Science* 319**,** 1244-1247.

Truckenbrodt, S., Maidorn, M., Crzan, D., Wildhagen, H., Kabatas, S., and Rizzoli, S.O. (2018). X10 expansion microscopy enables 25-nm resolution on conventional microscopes. *EMBO reports* 19**,** e45836.

Truckenbrodt, S., Sommer, C., Rizzoli, S.O., and Danzl, J.G. (2019). A practical guide to optimization in X10 expansion microscopy. *Nature Protocols* 14**,** 832-863.

Unemo, M., Seifert, H.S., Hook, E.W., Hawkes, S., Ndowa, F., and Dillon, J.-a.R. (2019). Gonorrhoea. *Nature Reviews Disease Primers* 5**,** 79.

Unemo, M., and Shafer, W.M. (2014). Antimicrobial resistance in Neisseria gonorrhoeae in the 21st century: past, evolution, and future. *Clinical microbiology reviews* 27**,** 587-613.

Van Putten, J.P., Duensing, T.D., and Carlson, J. (1998). Gonococcal invasion of epithelial cells driven by P.IA, a bacterial ion channel with GTP binding properties. *The Journal of experimental medicine* 188**,** 941-952.

Veale, D.R., Goldner, M., Penn, C.W., Ward, J., and Smith, H. (1979). The intracellular survival and growth of gonococci in human phagocytes. *Journal of General Microbiology* 113**,** 383-393.

Venkataraman, K., Thangada, S., Michaud, J., Oo, M.L., Ai, Y., Lee, Y.M., Wu, M., Parikh, N.S., Khan, F., Proia, R.L., and Hla, T. (2006). Extracellular export of sphingosine kinase-1a contributes to the vascular S1P gradient. *Biochemical Journal* 397**,** 461-471.

Verhaegh, R., Becker, K.A., Edwards, M.J., and Gulbins, E. (2020). Sphingosine kills bacteria by binding to cardiolipin. *The Journal of biological chemistry* 295**,** 7686-7696.

Wade, J.J., and Graver, M.A. (2007). A fully defined, clear and protein-free liquid medium permitting dense growth of Neisseria gonorrhoeae from very low inocula. *FEMS Microbiology Letters* 273**,** 35-37.

Wadsworth, C.B., Arnold, B.J., Sater, M.R.A., and Grad, Y.H. (2018). Azithromycin Resistance through Interspecific Acquisition of an Epistasis-Dependent Efflux Pump Component and Transcriptional Regulator in Neisseria gonorrhoeae. *mBio* 9**,** e01419-01418.

Wang, C., Zhao, T., Li, Y., Huang, G., White, M.A., and Gao, J. (2017). Investigation of endosome and lysosome biology by ultra pH-sensitive nanoprobes. *Advanced drug delivery reviews* 113**,** 87-96.

Warner, D.M., Shafer, W.M., and Jerse, A.E. (2008). Clinically relevant mutations that cause derepression of the Neisseria gonorrhoeae MtrC-MtrD-MtrE Efflux pump system confer different levels of antimicrobial resistance and in vivo fitness. *Molecular microbiology* 70**,** 462-478.

Wartosch, L., Bright, N.A., and Luzio, J.P. (2015). Lysosomes. *Current Biology* 25**,** R315-R316.

Wattenberg, B.W. (2010). Role of sphingosine kinase localization in sphingolipid signaling. *World Journal of Biological Chemistry* 1**,** 362-368.

Wertz, P.W. (2018). Lipids and the Permeability and Antimicrobial Barriers of the Skin. *Journal of lipids* 2018**,** 5954034-5954034.

Wigger, D., Gulbins, E., Kleuser, B., and Schumacher, F. (2019). Monitoring the Sphingolipid de novo Synthesis by Stable-Isotope Labeling and Liquid Chromatography-Mass Spectrometry. *Frontiers in Cell and Developmental Biology* 7**,** 210.

Wolf, K., and Hackstadt, T. (2001). Sphingomyelin trafficking in Chlamydia pneumoniae-infected cells. *Cellular Microbiology* 3**,** 145-152.

Wong, L., Tan, S.S., Lam, Y., and Melendez, A.J. (2009). Synthesis and evaluation of sphingosine analogues as inhibitors of sphingosine kinases. *Journal of Medicinal Chemistry* 52**,** 3618-3626.

Wu, Y., Li, C., Riehle, A., Pollmeier, B., Gulbins, E., and Grassmé, H. (2018). Mycobacterial Infection is Promoted by Neutral Sphingomyelinase 2 Regulating a Signaling Cascade Leading to Activation of β1-Integrin. *Cellular Physiology and Biochemistry* 51**,** 1815-1829.

Wu, Y., Liu, Y., Gulbins, E., and Grassmé, H. (2021). The Anti-Infectious Role of Sphingosine in Microbial Diseases. *Cells* 10**,** 1105.

Yang, L., Yatomi, Y., Miura, Y., Satoh, K., and Ozaki, Y. (1999). Metabolism and functional effects of sphingolipids in blood cells. *British Journal of Haematology* 107**,** 282-293.

Young, M.M., Takahashi, Y., Fox, T.E., Yun, J.K., Kester, M., and Wang, H.-G. (2016). Sphingosine Kinase 1 Cooperates with Autophagy to Maintain Endocytic Membrane Trafficking. *Cell reports* 17**,** 1532-1545.

Zemann, B., Urtz, N., Reuschel, R., Mechtcheriakova, D., Bornancin, F., Badegruber, R., Baumruker, T., and Billich, A. (2007). Normal neutrophil functions in sphingosine kinase type 1 and 2 knockout mice. *Immunology Letters* 109**,** 56-63.

Zeng, D., Zeglis, B.M., Lewis, J.S., and Anderson, C.J. (2013). The growing impact of bioorthogonal click chemistry on the development of radiopharmaceuticals. *Journal of nuclear medicine : official publication, Society of Nuclear Medicine* 54**,** 829-832.

Zeth, K., Kozjak-Pavlovic, V., Faulstich, M., Fraunholz, M., Hurwitz, R., Kepp, O., and Rudel, T. (2013). Structure and function of the PorB porin from disseminating Neisseria gonorrhoeae. *Biochemical Journal* 449**,** 631-642.

Zhang, Y., Bi, J., Huang, J., Tang, Y., Du, S., and Li, P. (2020). Exosome: A Review of Its Classification, Isolation Techniques, Storage, Diagnostic and Targeted Therapy Applications. *International journal of nanomedicine* 15**,** 6917-6934.

Zhang, Y., Liu, Y., Liu, H., and Tang, W.H. (2019). Exosomes: biogenesis, biologic function and clinical potential. *Cell & Bioscience* 9**,** 19.

6 Appendix

6.1 Abbreviations

7AAD	7-aminoactinomycin D
α	alpha
µ	micro (10^{-6})
ω	omega
A	ampere
AF	Alexa fluor
AMR	antimicrobial resistance
APC	Allophycocyanin
APS	ammonium persulfate
aSM	acid sphingomyelinase
ATP	adenosine triphosphate
BSA	bovine serum albumin
C.	*Chlamydia*
$CaCl_2$	calcium chloride
Cas	CRISPR-associated
cDNA	complementary DNA
CEACAM	carcinoembryonic antigen cell adhesion molecule
Cer	ceramide
CERT	ceramide transfer protein
CFU	colony forming unit
CID	collision-induced dissociation
cm^2	square centimetre
CO_2	carbon dioxide
CoA	coenzyme A
CRISPR	clustered regularly interspaced short palindromic repeats
Cu	copper
CuAAC	copper(I)-catalyzed azide-alkyne cycloaddition
Cy	cyanin
°C	degree Celsius
d_3	deuterated
DAPI	4',6-diamidino-2-phenylindole
DBCO	diarylcyclooctyne
ddH_2O	double distilled water
DGI	disseminated gonococcal infection
dH_2O	distilled water
DIBO	dibenzocyclooctyne
DMEM	Dulbecco's Modified Eagle's Medium

DMSO	dimethyl sulfoxide
DNA	deoxyribonucleic acid
DNase	deoxyribonuclease
dNTP	deoxyribonucleoside-triphosphate
DPBS	Dulbecco's phosphate buffered saline
DTT	dithiothreitol
ECL	enhanced chemiluminescence
E. coli	*Escherichia coli*
EDTA	ethylenediaminetetraacetate
e.g.	exempli gratia (for example)
ESI+	positive electrospray ionization
et al.	et alii (and others)
EtOH	ethanol
eV	electron Volt
ExM	expansion microscopy
f	femto (10^{-15})
FACS	fluorescence-activated cell sorting
FCS	fetal calf serum
FIASMA	functional inhibitors of acid sphingomyelinase
FITC	fluorescein isothiocyanate
for	forward
FSC	forward scatter
Fwd	forward
g	gram; g-force
GA	glutaraldehyde
GAPDH	glyceraldehyde 3-phosphate dehydrogenase
GFP	green fluorescent protein
gRNA	guideRNA
h	hour
HBSS	Hank's Balanced Salt Solution
HEPES	4-(2-hydroxyethyl)-1-piperazineethanesulfonic acid
HPLC	high performance liquid chromatography
HRP	horseradish peroxidase
i.e.	id est (that is)
IEDDA	inverse electron demand Diels–Alder
IF	immunofluorescence
kb	kilobase
l	litre
LAMP	lysosomal-associated membrane protein
LB	Luria Bertani

LC-HRMS	liquid chromatography high-resolution mass spectrometry
LOS	lipooligosaccharides
m	milli (10^{-3}), metre
M	Molar
MDR	multi drug resistant
MeOH	methanol
$MgCl_2$	magnesium chloride
mm^2	square millimetres
MOI	multiplicity of infection
mRNA	messenger RNA
mtr	multiple transferable resistance
m/z	mass-to-charge ratio
N_3	azide
n	nano (10^{-9})
N.	*Neisseria*
NA	numerical aperture
NAD	nicotinamide adenine dinucleotide
NHS	*N*-hydroxysuccinimide
nSM	neutral sphingomyelinase
OD	optical density
Opa	opacity
p	pico (10^{-12})
P	probability value
PBS	phosphate buffered saline
PCR	polymerase chain reaction
PDL	Poly-D-Lysine
PEG	polyethylene glycol
PFA	paraformaldehyde
pH	pH value
pi	post infection
PI	propidium iodide
PI3K	phosphoinositide 3-kinase
PID	pelvic inflammatory disease
PKD1	protein kinase D1
PLCγ1	phospholipase Cγ1
PMN	polymorphonuclear leukocyte
Por	porin
$PorB_{IA}$	PorB of serotype A
$PorB_{IB}$	PorB of serotype B
ppm	parts per million

PPM	Proteose Peptone medium
PPM+	Proteose Peptone medium supplemented with vitamine mix
PVA	poly(vinyl alcohol)
QTOF MS	quadrupole-time-of-flight mass spectrometer
Rab	Ras-associated binding
RBC	red blood cell
rev	reverse
RFP	red fluorescent protein
RNA	ribonucleic acid
RNase	ribonuclease
rpm	rounds per minute
RPMI	Roswell Park Memorial Institute
RT	reverse transcription
SD	standard deviation
SEM	standard error of mean
sgRNA	single guide RNA
SIM	structured illumination microscope
SiR	silicon-rhodamine
SMS	sphingomyelin synthase
SPAAC	strain-promoted azide-alkyne click chemistry reaction
Sph	sphingosine
SphK	sphingosine kinase
Spg	sphinganine
spp.	species pluralis (multiple species)
SPT	serine palmitoyltransferase
SREC	scavenger receptor expressed on endothelial cells
SRM	selected reaction monitoring
SSC	side scatter
STI	sexually transmitted infection sexually
TAE	tris-acetate-EDTA
TBS	Tris-buffered saline
TEMED	tetramethylethylenediamine
T_m	melting temperature
Tris	tris(hydroxymethyl)aminomethane
U	unit
UV	ultraviolet
V	volt; volume
VAP-A	vesicle-associated membrane protein-associated protein A
vs.	versus
v/v	volume per volume

WT	wildtype
w/v	weight per volume
XDR	extremely drug resistant
YFP	yellow fluorescent protein

6.2 Electronical supplement

Videos are available in the electronical supplement attached to this thesis. The respective video captions are enlisted below.

Video 1: Rapid uptake of intracellular ω-N3-sphingosine
Chang cells were fed with ω-N_3-sphingosine, clicked with DIBO-488 and infected with RFP-N927. Time-lapse imaging demonstrates the rapid uptake of ω-N_3-sphingosine into the neisserial membrane (magenta: RFP-N927, green: ω-N_3-sphingosine, scale bar: 2 µm).

Video 2: Rapid uptake of intracellular 1-N3-sphingosine
Chang cells were fed with 1-N_3-sphingosine, clicked with DIBO-488 and infected with RFP-N927. Time-lapse imaging demonstrates the uptake of 1-N_3-sphingosine into the neisserial membrane (magenta: RFP-N927, green: 1-N_3-sphingosine, scale bar: 5 µm).

Video 3: Formation of ω-N_3-sphingosine vesicles intracellularly
Chang cells were fed with ω-N_3-sphingosine, clicked with DIBO-488 and infected with RFP-N927. Time-lapse imaging shows the formation of a sphingosine vesicle (white arrowhead) over time (magenta: RFP-N927, green: ω-N_3-sphingosine, scale bar: 2 µm).

Video 4: Intracellular ω-N_3-sphingosine vesicle catches escaping *Neisseria*
Chang cells were fed with ω-N_3-sphingosine, clicked with DIBO-488 and infected with RFP-N927. Time-lapse imaging shows ω-N_3-sphingosine vesicle which is attached to gonococci and the formation of a "tentacle" to pull back escaping bacterium (magenta: RFP-N927, green: ω-N_3-sphingosine, scale bar: 2 µm).

Video 5: Long-term infection of Chang cells fed with 1-N_3-sphingosine
Time-lapse imaging of long-time infection with RFP-N927 of Chang cells fed with 1-N_3-sphingosine. Click reaction was performed with DIBO-488 before infection. The formation of extracellular vesicles was observed, which attach to *Neisseria* resulting in the loss of RFP-expression and the accumulation of sphingosine (magenta: RFP-N927, green: sphingosine, scale bar: 10 µm).

Video 6: Long-term infection of Chang cells fed with ω-N_3-sphingosine
Time-lapse imaging of long-time infection with RFP-N927 of Chang cells fed with ω-N_3-sphingosine. Click reaction was performed with DIBO-488 before infection. The formation of extracellular vesicles was observed, which attach to *Neisseria* resulting in the loss of RFP-expression and the accumulation of sphingosine (magenta: RFP-N927, green: sphingosine, scale bar: 10 µm).

Video 7: YFP-LAMP1 Chang cells fed with 1-N_3-sphingosine and infected with N927
Time-lapse imaging of Chang cells expressing YFP-tagged LAMP1, which were fed with 5 µM 1-N_3-sphingosine and clicked with DIBO-594 before infection with stained N927. Intracellular accumulations of LAMP1 were detected but no changes in their localizations. Formation of the already described sphingosine vesicles were observed with their attachment to *Neisseria* (blue: LAMP1, magenta: N927, green: 1-N_3-sphingosine, scale bar: 10 µm).

Video 8: YFP-Rab5 Chang cells fed with 1-N_3-sphingosine and infected with N927
Time-lapse imaging of Chang cells expressing YFP-tagged Rab5, which were fed with 5 µM 1-N_3-sphingosine and clicked with DIBO-594 before infection with stained N927. Here, most of the cells either expressed YFP-tagged Rab5 proteins or took up the sphingosine analogue. Formation of the already described sphingosine vesicles were observed with their attachment to *Neisseria* (blue: Rab5, magenta: N927, green: 1-N_3-sphingosine, scale bar: 10 µm).

Video 9: YFP-Rab7 Chang cells fed with 1-N_3-sphingosine and infected with N927
Time-lapse imaging of Chang cells expressing YFP-tagged Rab7, which were fed with 5 µM 1-N_3-sphingosine and clicked with DIBO-594 before infection with stained N927. Rab7 was expressed only at low detection levels. Another issue was the instability of the used microscope during live cell imaging. Formation of the already described sphingosine vesicles were observed with their attachment to *Neisseria* (blue: Rab7, magenta: N927, green: 1-N_3-sphingosine, scale bar: 10 µm).

Video 10: YFP-LAMP1 Chang cells fed with ω -N_3-sphingosine and infected with N927
Time-lapse imaging of Chang cells expressing YFP-tagged LAMP1, which were fed with 5 µM ω-N_3-sphingosine and clicked with DIBO-594 before infection with stained N927. Intracellular accumulations of LAMP1 were detected but no changes in their localizations. Formation of the already described sphingosine vesicles were observed with their attachment to *Neisseria* (blue: LAMP1, magenta: N927, green: ω-N_3-sphingosine, scale bar: 10 µm).

Video 11: YFP-Rab5 Chang cells fed with ω-N_3-sphingosine and infected with N927
Time-lapse imaging of Chang cells expressing YFP-tagged Rab5, which were fed with 5 µM ω-N_3-sphingosine and clicked with DIBO-594 before infection with stained N927. Here, most of the cells either expressed YFP-tagged Rab5 proteins or took up the sphingosine analogue. Formation of the already described sphingosine vesicles were observed with their attachment to *Neisseria* (blue: Rab5, magenta: N927, green: ω-N_3-sphingosine, scale bar: 10 µm).

Video 12: YFP-Rab7 Chang cells fed with ω-N_3-sphingosine and infected with N927
Time-lapse imaging of Chang cells expressing YFP-tagged Rab7, which were fed with 5 µM ω-N_3-sphingosine and clicked with DIBO-594 before infection with stained N927. Distinct intracellular Rab7 signals were detected, which did not change over time. Formation of the already described sphingosine vesicles were observed with their attachment to *Neisseria*. For none of the vesicles a clear Rab7 signal could have been observed (blue: Rab7, magenta: N927, green: ω-N_3-sphingosine, scale bar: 10 µm).

6.3 List of Figures

6.4 List of Tables

6.5 List of Videos

Video 1: Rapid uptake of intracellular ω-N_3-sphingosine

Video 2: Rapid uptake of intracellular 1-N_3-sphingosine

Video 3: Formation of ω-N_3-sphingosine vesicles intracellularly

Video 4: Intracellular ω-N_3-sphingosine vesicle catches escaping *Neisseria*

Video 5: Long-term infection of Chang cells fed with 1-N_3-sphingosine

Video 6: Long-term infection of Chang cells fed with ω-N_3-sphingosine

Video 7: YFP-LAMP1 Chang cells fed with 1-N_3-sphingosine and infected with N927

Video 8: YFP-Rab5 Chang cells fed with 1-N_3-sphingosine and infected with N927

Video 9: YFP-Rab7 Chang cells fed with 1-N_3-sphingosine and infected with N927

Video 10: YFP-LAMP1 Chang cells fed with ω-N_3-sphingosine and infected with N927

Video 11: YFP-Rab5 Chang cells fed with ω-N_3-sphingosine and infected with N927

Video 12: YFP-Rab7 Chang cells fed with ω-N_3-sphingosine and infected with N927

6.6 Publications and presentations

Publications

Solger, F., Kunz, T. C., Fink, J., Paprotka, K., Pfister, P., Hagen, F., Schumacher, F., Kleuser, B., Seibel, J. & Rudel, T. (2020).
A Role of Sphingosine in the Intracellular Survival of *Neisseria gonorrhoeae*.
Frontiers in cellular and infection microbiology, *10*, 215. doi:10.3389/fcimb.2020.00215

Götz R., Kunz T. C., Fink J., **Solger F**., Schlegel J., Seibel J., Kozjak-Pavlovic V., Rudel T. & Sauer M. (2020).
Nanoscale imaging of bacterial infections by sphingolipid expansion microscopy.
Nature communications. 11(1):6173. doi: 10.1038/s41467-020-19897-1

All listed publications are included in this thesis.

Presentations

Solger F., Heydarian M., Kozjak-Pavlovic V. and Rudel T. (2019) **Sphingosine interferes the survival of invasive *Neisseria gonorrhoeae.*** Retreat FOR2123 with SFB 1039 and GRK 2098, Schloss Rauischholzhausen (talk and poster)

Solger F., Hagen F. and Rudel T. (2018) **Sphingosine interferes the survival of invasive *Neisseria gonorrhoeae.*** Sphingoworkshop FOR2123, Würzburg (poster)

Danksagung

Zuallererst möchte ich mich bei meinem Doktorvater Prof. Dr. Thomas Rudel für die gegebene Möglichkeit und Betreuung der Promotion bedanken. Die motivierenden und inspirierenden Diskussionen waren stets eine große Hilfe. Ein weiterer Dank geht an Prof. Dr. Alexandra Schubert-Unkmeir für die Übernahme des Zweitgutachtens und speziell für die Hilfe die ersten Einblicke in die Click Chemie zu bekommen.

Bei meinen Kollaborationspartnern des SphingoFOR2123 aus der organischen Chemie und der Uni Potsdam bedanke ich mich für eine freundliche, flexible und vor allem erfolgreiche Zusammenarbeit.

Des Weiteren geht ein großer Dank an den gesamten Lehrstuhl für Mikrobiologie für eine sehr schöne Zeit, die ich dort verbracht habe. Speziell möchte ich mich beim MiBi Running Club für den sportlichen Ausgleich bei jedem Wetter bedanken.

Ein ganz besonderer Dank geht an Regi und Kerstin K., die es immer geschafft haben ein Lachen ins Gesicht zu zaubern. Auch bei allen Görlz + und Turbo bedanke ich mich für lustige/laute Mittags-/Kaffeepausen, die Zusammenarbeit, den Teamgeist und immer eine helfende Hand in allen Lebenslagen. Danke dafür!

Auch möchte ich bei den ehemaligen Kollegen Dani und Max bedanken, die während der gemeinsamen Zeit zu Freunden wurden. An diesem Punkt möchte ich auch Sonnenschein Adriana, Nadine und Kathrin nennen, die immer ein offenes Ohr für mich hatten.

Außerhalb des Lehrstuhls gebührt zum einen ein großer Dank meinem Mentor und Shihan Dr. Frank-Dieter Hörner für Ratschläge und Denkanstöße nicht nur Karate betreffend.
Zum anderen sollen Ann-Kris und Frau Lein an dieser Stelle nicht vergessen werden. Danke euch für die zauberhaften Ablenkungen!

Natürlich gebührt der größte Dank meiner Familie (Mama, Opa und Laura), die immer für mich da waren und da sein werden. Vielen Dank für alles! Speziell bei Patrick möchte ich mich bedanken, der in allen Phasen der Doktorarbeit und darüber hinaus immer für mich da war. Danke dir!

Affirmation

Eidesstattliche Erklärungen nach §7 Abs. 2 Satz 3, 4, 5 der Promotionsordnung der Fakultät für Biologie

Eidesstattliche Erklärung

Hiermit erkläre ich an Eides statt, die Dissertation: „Die zentrale Rolle von Sphingolipiden auf das intrazelluläre Überleben von *Neisseria gonorrhoeae* in Epithelzellen“, eigenständig, d. h. insbesondere selbständig und ohne Hilfe eines kommerziellen Promotionsberaters, angefertigt und keine anderen, als die von mir angegebenen Quellen und Hilfsmittel verwendet zu haben.

Ich erkläre außerdem, dass die Dissertation weder in gleicher noch in ähnlicher Form bereits in einem anderen Prüfungsverfahren vorgelegen hat.

Weiterhin erkläre ich, dass bei allen Abbildungen und Texten bei denen die Verwertungsrechte (Copyright) nicht bei mir liegen, diese von den Rechtsinhabern eingeholt wurden und die Textstellen bzw. Abbildungen entsprechend den rechtlichen Vorgaben gekennzeichnet sind sowie bei Abbildungen, die dem Internet entnommen wurden, der entsprechende Hypertextlink angegeben wurde.

Affidavit

I hereby declare that my thesis entitled: „Central role of sphingolipids on the intracellular survival of *Neisseria gonorrhoeae* in epithelial cells“ is the result of my own work. I did not receive any help or support from commercial consultants. All sources and / or materials applied are listed and specified in the thesis.

Furthermore, I verify that the thesis has not been submitted as part of another examination process neither in identical nor in similar form.

Besides I declare that if I do not hold the copyright for figures and paragraphs, I obtained it from the rights holder and that paragraphs and figures have been marked according to law or for figures taken from the internet the hyperlink has been added accordingly.

Würzburg, den